Pyrite in the Pepegoona, Pepegoona West and Pannikan uranium deposits, Lake Eyre Basin, S.A.: implications for regional uranium exploration

Thesis submitted in accordance with the requirements of the University of Adelaide for an Honours Degree in Geology

Edwina Ingham

November 2012

THE UNIVERSITY of ADELAIDE

TITLE

Pyrite in the Pepegoona, Pepegoona West and Pannikan uranium deposits, Lake Eyre Basin, S.A.: implications for regional uranium exploration

RUNNING TITLE

Pyrite Geochemistry at Beverley North

ABSTRACT

The common sulphide mineral pyrite is abundant throughout sedimentary uranium systems at Pepegoona, Pepegoona West and Pannikan, South Australia. No in-depth geochemical and textural characterisation of this important mineral has previously been conducted. Multiple micro-analytical techniques have successfully constrained textural and chemical patterns within the pyrite. Results point to variation in fluid composition, sulphur source and precipitation conditions during a protracted mineralisation event.

In-situ micron-scale sulphur isotope analysis of pyrite demonstrated broad-scale isotopic heterogeneity ($\delta^{34}S$= -43.9 to +32.4‰$_{CDT}$), indicative of complex, multi-faceted pyrite evolution and sulphur derived from two or more sources. Preserved textures support this assertion and indicate a genetic model involving more than one phase of pyrite formation. Authigenic, pre-ore pyrite underwent prolonged evolution and recrystallisation, evidenced by a genetic relationship between archetypal framboidal aggregates and pyrite euhedra. Secondary hydrothermal pyrite commonly displayed hyperenrichment of several trace elements (Mn, Co, Ni, As, Se, Mo, Sb, W and Tl) in ore-bearing horizons. Hydrothermal fluids of magmatic and meteoric origin supplied metals to the system but the geochemical signature of pyrite suggests a dominant granitic source and influence of mafic lithologies. Irregular variation in $\delta^{34}S$, coupled with oscillatory trace element zonation in secondary pyrite, is interpreted in terms of continuous variations in fluid composition and possible cycles of diagenetic recrystallisation. A late-stage oxidising fluid, which mobilised selenium from pre-existing pyrite, caused ongoing pyrite re-crystallisation and precipitation of native selenium.

These results provide the first qualitative constraints on the formation mechanisms of the uranium deposits at Beverley North. Insight into depositional conditions and sources of both sulphide and uranium mineralisation allow for a preliminary paragenetic scheme for the ore systems. This new understanding of pyrite geochemistry can also underpin an effective vector for uranium exploration, not only at Beverley North, but throughout the sedimentary systems of the Lake Eyre Basin.

KEYWORDS

Pyrite, Beverley North, uranium exploration, sulphur isotopes, trace elements, Eyre Formation

TABLE OF CONTENTS

LIST OF TABLES AND FIGURES

INTRODUCTION

Constraining the nature of sulphide mineralisation in the context of epigenetic uranium mineralisation and the host sedimentary basin evolution is fundamental in understanding the processes of uranium ore formation (Clark *et al.* 2004). The resistate mineral pyrite, is the most common sulphide mineral, and provided that complete recrystallisation does not occur, is able to record its evolution by preserving patterns of intra-crystal morphological and chemical zonation (Cook *et al.* 2009).

The interpretation of geochemical variations within pyrite in terms of its depositional and post-depositional history has significant implications, not only for the understanding of depositional conditions, fluid composition and the source of uranium, but also for regional basin evolution (Abraitis *et al.* 2004, Clark *et al.* 2004, Barrie *et al.* 2009). The ability to use the properties of pyrite as a tool for uranium exploration would likely have significant economic impacts; however this potential vector remains undeveloped particularly in the context of sedimentary basins.

Pyrite is a common constituent of the uranium ores in the hydrothermal systems at the Beverley uranium deposit and throughout the sedimentary systems of the Lake Eyre Basin (Brugger *et al.* 2005, Skirrow 2009, Wülser *et al.* 2011). To date, the textural and chemical signatures of pyrite at Pepegoona, Pepegoona West and Pannikan, to the north of the Beverley deposit, have not been characterised in any detail.

The aim of this study is to define the first qualitative constraints on the depositional conditions and sources of both economic uranium mineralisation and the associated pyrite at Beverley North. Distinct styles of pyrite mineralisation within the system will be characterised using new textural and trace element data; the interpretation of which

will undoubtedly give major insight into mineral paragenesis and the controls on ore formation within the sandstone-hosted uranium systems. Unique, high-resolution sulphur isotope data, specific to Beverley North will be obtained, which will give unparalleled insight into likely sulphur sources. Furthermore, the possibility of the mixing of sulphur from distinct sources within these seemingly simple sedimentary systems will be explored.

The overarching purpose of this study remains to use this new information to define the controls on pyrite genesis and its subsequent effect on uranium mineralisation, to define as to what extent pyrite may act as an effective exploration tool for uranium, not only at Beverley North but also throughout the sedimentary systems of the Lake Eyre Basin.

GEOLOGICAL SETTING

The sandstone-hosted uranium deposits of Pepegoona, Pepegoona West and Pannikan (Beverley North) (Figure 1 and 2) were discovered in 2009 and lie approximately 8 km NNE of the Beverley uranium deposit operated by Heathgate Resources (Heathgate Resources 2012, Märten *et al.* 2012). In order to better delineate their genesis and make optimal use of new pyrite data, it is important to understand the position of the mineralisation within the context of regional geology.

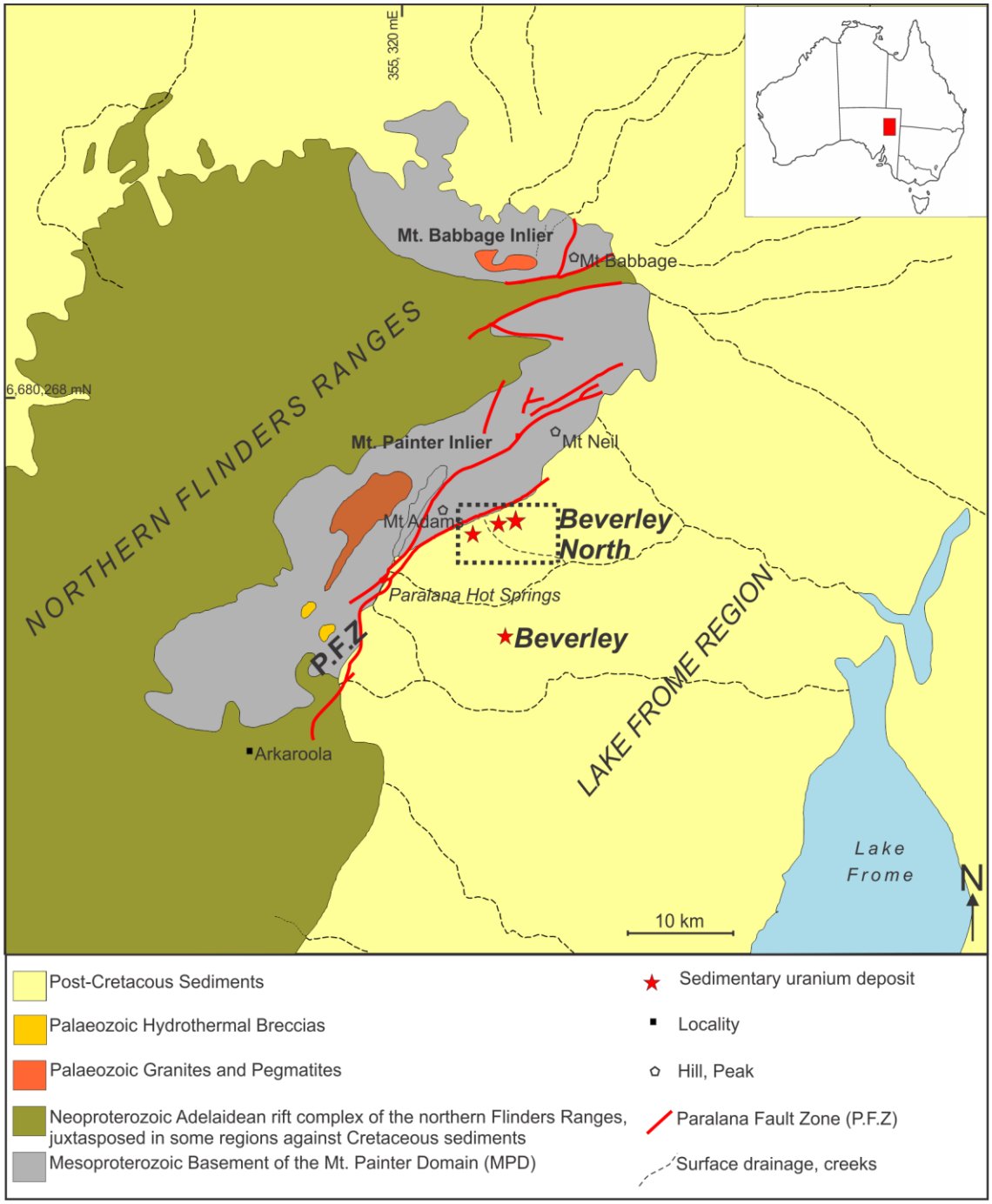

Figure 1: The location of the Beverley North uranium deposits in the context of the regional geology. The Lake Frome Region (also commonly described as the Frome Embayment) is broadly recognised as the area of the Callabonna sub-basin, proximal to the Beverley and Beverley North deposits. The Lake Frome region is bound to the west by the Mount Painter Domain and the Paralana Fault Zone. The Beverley North uranium deposits, outlined in the dashed box are outlined in more detail by Figure 2. Adapted from Wülser *et al.* (2011).

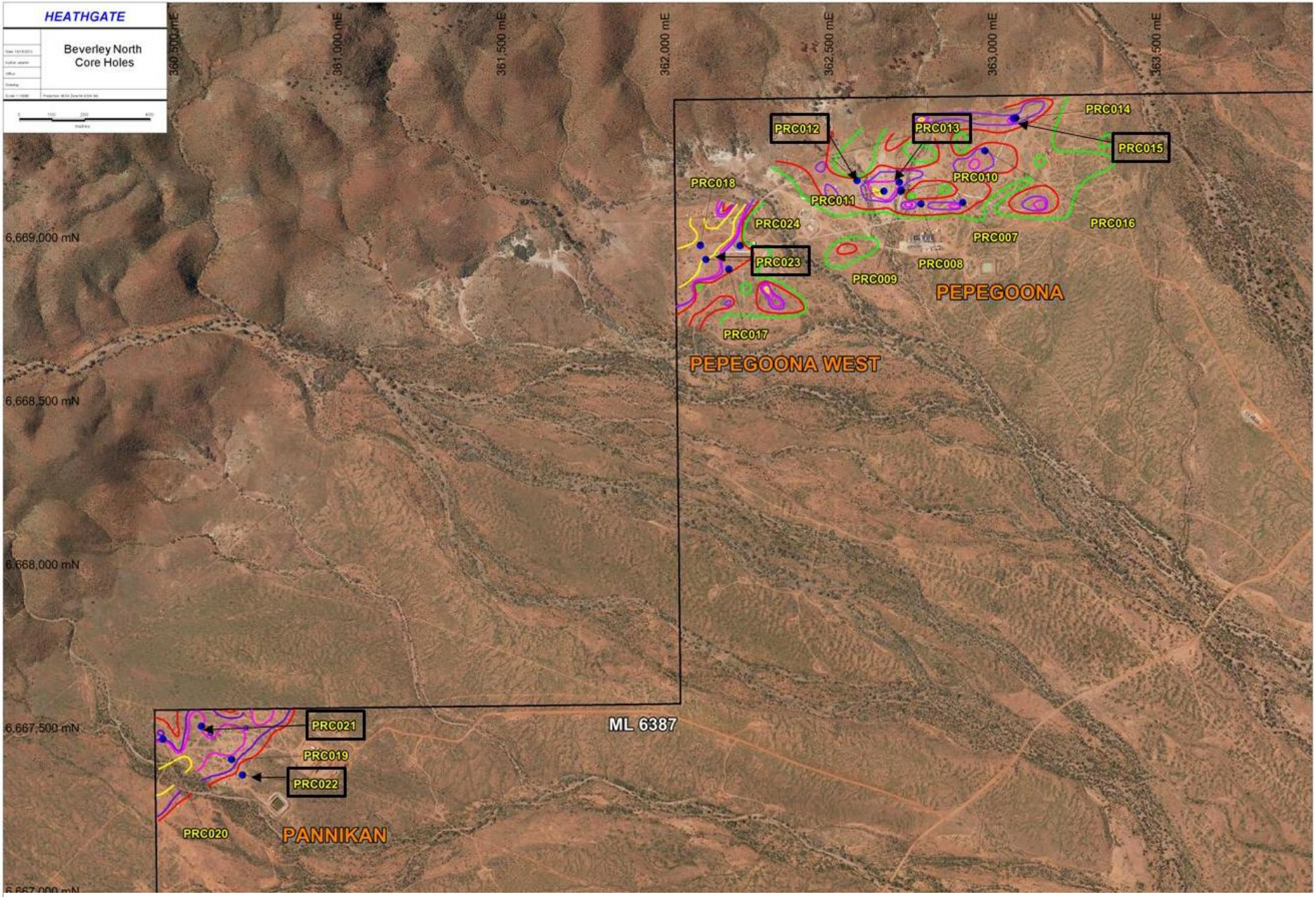

Figure 2: The Beverley North uranium deposits of Pepegoona, Pepegoona West and Pannikan on Mining Lease 6387. Heathgate Resources surface interpretation is outlined on the satellite image as a roll-front deposit at Pannikan, and tabular, stacked lenses of uranium mineralisation at Pepegoona and Pepegoona West. Core numbers outlined in black represent cores from which samples were taken. Image courtesy of Heathgate Resources (2012).

Stratigraphy and tectonic evolution

The Beverley North uranium deposits are hosted by the organic-rich terrestrial sands of the Eocene Eyre Formation (outlined in stratigraphic context in Table 1) and sit approximately 500 m from the eastern escarpment of the northern Flinders Ranges at a depth of ca. 200-260 m (Walker 1999, Lambert *et al.* 2005, Jaireth *et al.* 2008, Hill & Hore 2011, Märten *et al.* 2012).

The formation was deposited as the basal unit of the Lake Eyre Basin, unconformably overlying the Frome Embayment; the broad area around Beverley North where the southernmost portion of the Cretaceous Eromanga Basin unconformably on-laps the Proterozoic basement (Table 1). A ~30-50 Ma hiatus in deposition at the end of the Cretaceous, associated with extensive weathering resulted in widespread disconformities between the basins (Skirrow 2009, Wülser *et al.* 2011). The depositional age of the host Eocene Eyre Formation constrains the maximum age of uranium mineralisation to $\leq$55 Ma (Skirrow 2009). Sedimentation continued in the interior non-marine Lake Eyre Basin until the late Oligocene when widespread gentle folding caused uplift and division into sub-basins. The Beverley North region is encompassed by the Callabonna Sub-basin, broadly known as the Lake Frome region and bound to the west by the northern Flinders Ranges and the Paralana Fault Zone (PFZ) (Figure 1, Skirrow 2009).

The uplift and division of basins resulted from the establishment of a regional E-W compressional regime in the early Palaeozoic. The regime caused basement uplift and initiation of a regional fault network, in which the broadly NE-SW trending, W-dipping

Table 1: The stratigraphy of the Lake Frome region

Cenozoic	**Quaternary**	**Lake Eyre Basin (Callabonna Sub-basin)**	**Present-day regolith**	Terrestrial aeolian and alluvial erosion of the uplifted areas of the northern Flinders ranges, is currently depositing sediments in a variety of environments such as; claypans, dunes, playas, and alluvial fans. Deposition extends from the ranges to the shores of Lake Frome to the east.
			Willawortina Fm	Deposited during the main uplift and exposure of the Mount Painter Domain (late Cenozoic to Plio-Pleistoce). Palaeosoils define an age older than 780 Ka. The Willawortina Fm may reach 100 m in thickness. Contains coarse siliciclastics from braided fans and fine sands and clays from lacustrine settings.
	Miocene		**Namba Fm**	Deposited in Miocene lacustrine, alluvial and other low relief environments, the Namba Fm unconformably overlies the Eyre Fm. It is characterised by angular immature sands and silts with minor conglomerates, black carbonaceous clays and grey, green and white clays with some Mg-rich clays, dolomites and some lignite. The Namba Fm is commonly capped by silcrete in the Lake Frome area which contains kaolinite, alunite and gypsum as a result of weathering processes of late Pliocene.
	Late Palaeocene - Eocene		**Eyre Fm**	Deposition of this basal unit of the Lake Eyre Basin commenced as a result of tectonic subsidence in the late Palaeocene and continued until middle Eocene. The basin was subject to episodic fluvial and lacustrine sedimentation and sediments commonly formed in braided rivers. Two major stages of deposition occurred (~55-49 Ma and ~45 –37 Ma) resulting from the basin subsidence caused by the uplift of the northern Flinders Ranges to the west. The Eyre Fm has been recognised in S-N palaeochannels throughout the region, which commonly incise the underlying units of the Eromanga Basin and Proterozoic basement. Characterised by pyritic carbonaceous mature sands of very fine to pebble grain size, the Eyre Fm is regionally capped by silcrete developed from widespread oxidation and weathering conditions post-deposition.
Mesozoic	**Cretaceous**	**Eromanga Basin (Frome Embayment)**	**Bulldog Shale**	Deposited during the late Cretaceous, in a non-marine setting as the uppermost unit of the Eromanga Basin. The Bulldog Shale is a blue-gray silty, bioturbated clay mudstone with abundant organic matter which unconformably overlies the Proterozoic basement at Beverley North.
			Cadna-owie Fm	The Cretaceous Cadna-owie formation is the lowest unit of the Eromanga Basin but is absent in the stratigraphy at Beverley North. It represents a transitional depositional environment from terrestrial to marine conditions.
Proterozoic Basement				

Summarised from Skirrow (2009), Hill & Hore (2010, 2011), Wülser *et al*. (2011).

structures, extend to the surface from the basement (Brugger *et al.* 2011, Wülser *et al.* 2011, Märten *et al.* 2012). The fault network has been active since the late Miocene and is currently active as a cluster of reverse faults (Wülser *et al.* 2011). The continuing uplift of the Proterozoic basement associated with episodic fault reactivation in the intra-continental compressional regime, has caused the 100-200 m of relief on the eastern escarpment of the northern Flinders Ranges today (Hore & Hill 2010, Wülser *et al.* 2011).

The northern Flinders Ranges adjacent to the study area are largely comprised of the metamorphic inliers of the Mount Painter Domain (MPD, Figure 1). The MPD, and in particular Mount Painter Inlier contain high concentrations of heat producing granites and uplifted Proterozoic basement rocks (~1590 Ma) of metasedimentary, granitic and metabasaltic origin (Stoian 2010, Brugger *et al.* 2011, Wülser *et al.* 2011). The MPD was pervasively deformed and metamorphosed up to amphibolite facies during the Delamerian Orogeny (~514-490 Ma), evidenced by widespread pegmatitic and leucogranitic intrusions (Foden *et al.* 2006, Wülser *et al.* 2011). A second period of felsic magmatism occurred at the end of the Delamerian (~440 Ma) and resulted in the emplacement of granites with localised U and Th enrichment, reaching up to ~110 ppm U in some localities (Neumann *et al.* 2000, Elburg *et al.* 2003, Wülser *et al.* 2011). This uranium is believed to be the source of the secondary uranium mineralisation in the adjacent Lake Frome Region (Hore & Hill 2010, Brugger *et al.* 2011, Wülser *et al.* 2011).

The Paralana Fault Zone also hosts the Paralana Hot Springs (PHS); a heat flow regime which has been active since the late Palaeozoic. The regime is controlled by the hydrothermal circulation of meteoric water through U-enriched radiogenic basement rocks of the MPD which are undergoing contemporaneous rapid uplift (Neumann *et al.* 2000, McLaren *et al.* 2002, Skirrow 2009, Brugger *et al.* 2011). Low-temperature epithermal activity, limited by

low rainfall continues in the PHS and the current shallow groundwater is considered a relic of the palaeo-water responsible for major mineralisation in the region (Brugger *et al.* 2005, Skirrow 2009, Brugger *et al.* 2011)

Uranium mineralisation in context of regional geology

The location of the Beverley North deposits in intracratonic sedimentary basins, adjacent to highly deformed igneous and metamorphic terrains, indicates a complex and multi-faceted evolution. The geometry of epigenetic deposits such as at Beverley North, are primarily controlled by the permeability of strata and the distribution of chemical traps for the dissolved uranium (Hobday & Galloway 1999). The sandstone-hosted uranium deposits of Pepegoona and Pepegoona West have been characterised as stacked tabular formations whilst the Pannikan deposit is a roll-front deposit capped with silcrete lenses (Figure 3) (Märten *et al.* 2012). Due to the relatively recent discovery of these deposits, the full geometry of the uranium forming systems at Beverley North is undergoing continued reinterpretation. In the context of this study, it is important to recognise that both deposit models form under similar conditions from migrating oxidising fluids (Hobday & Galloway 1999).

Sandstone-hosted roll-front deposits reflect down-dip fluid flow of oxidised groundwater carrying dissolved uranium, within a confined sandstone aquifer (see Gross (1956), Galloway (1978), Min *et al* (2005a) and Jaireth *et al* (2008)). The uranium-bearing minerals precipitate at redox fronts where reducing agents such as organic matter and pre-ore pyrite are present. Similarly, tabular uranium represent the flow of U-bearing fluids into the host sandstone from the edges of a sedimentary basin, generally as a result of less rapid fluid migration than roll-front formation (Min *et al.* 2005a).

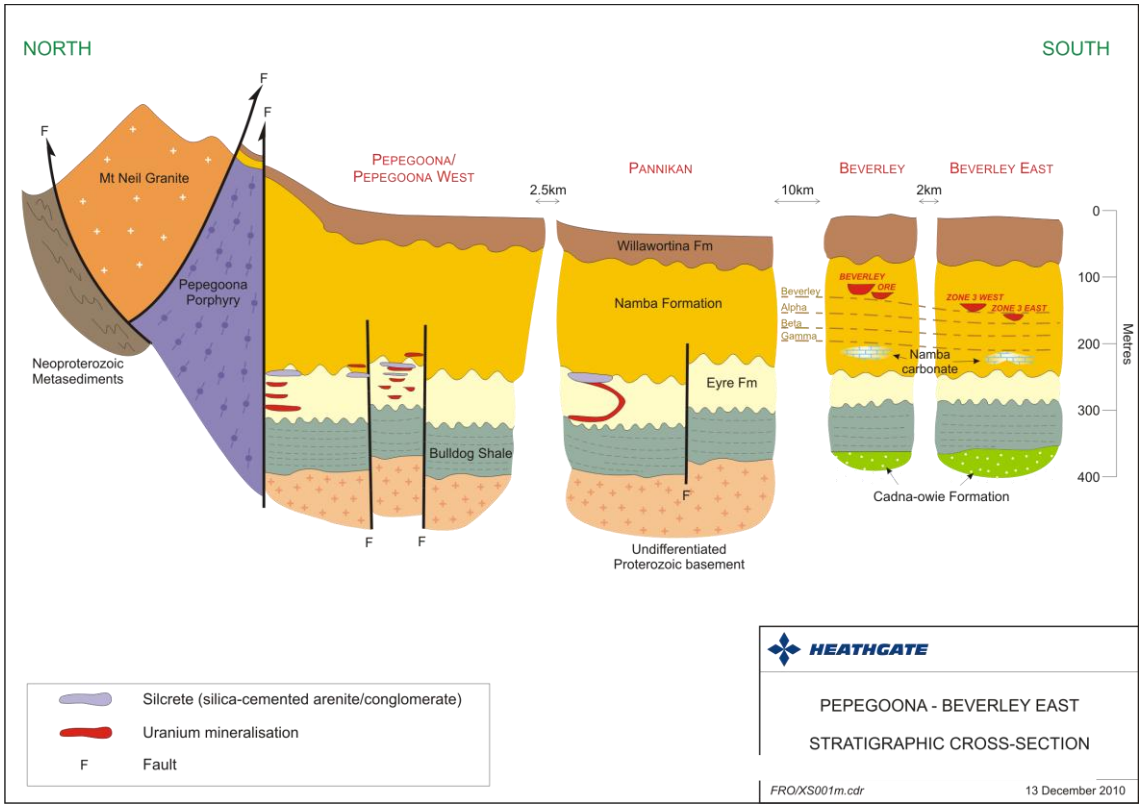

Figure 3: Schematic cross-section of the stratigraphy of the Lake Frome region hosting the sandstone-hosted uranium deposits of Pepegoona, Pepegoona West and Pannikan. The deposits are hosted by the Eocene Eyre Fm, and hence their genetic relationship with the Miocene Namba Fm-hosted Beverley deposit is limited. Pepegoona and Pepegoona West are broadly interpreted as stacked tabular lenses of uranium mineralisation, whilst the Pannikan deposit hosts roll-front mineralisation. All deposits are associated with lenses of silcrete formation. Model courtesy of Heathgate Resources (2012).

Primary uranium dissolution and the subsequent transport and deposition from its source in the Mt Painter Inlier, was likely by low-temperature, slightly acidic and oxidising groundwater (Hill & Hore 2010, Brugger *et al.* 2011, Wülser *et al.* 2011). Aquifer sources such as the PHS provided oxidised groundwater which precipitated uranium into the stratigraphic column where sufficiently low redox conditions existed, until anomalous U-concentrations accumulated in the environment (Pirlo & Giblin 2004). Coeval mineralisation of ore-stage pyrite and other reduced minerals occurred as a result of repeated dissolution and precipitation of pre-ore minerals during groundwater flow down aquifer gradients (Pirlo & Giblin 2004, Wülser *et al.* 2011).

Many of the known Eyre Fm hosted deposits (e.g. Four Mile and Honeymoon) in the Lake Frome Region are associated with palaeochannels, and are characterised by carbonaceous and pyritic sands intercalated with clays and gravels (Skirrow 2009). The accumulation of organic matter in the bends of low-energy meandering stream systems, act as reductants precipitating uranium at these locations (Landais 1996, Skirrow 2009).

CONTROLS ON PYRITE CHEMISTRY

Sulphides are important components of the geochemical systems of sandstone-hosted uranium deposits as they are common reductants (Granger & Warren 1969, Jaireth *et al.* 2008). Pyrite associated with U-mineralisation is generally considered to have been derived from the reduction of sulphates in ore-bearing solutions (Granger & Warren 1969). However, all models for the genesis of U-deposits require the presence of pyrite in the host-rock prior to mineralisation (Granger & Warren 1969, Min *et al.* 2005a).

Pyrite is abundant in the reduced zones of ore-bearing systems and commonly displays geochemical zonation (Jaireth *et al.* 2008). The precipitation of pyrite over its polymorph, marcasite in sandstone hosted U-deposits is favoured by certain physiochemical conditions such as elevated pH and an abundance of polysulphide species (Goldhaber & Kaplan 1980, Reynolds & Goldhaber 1983, Min *et al.* 2005a). The amount of pyrite formed in a sediment is limited by the supply of organic matter, dissolved sulphates and reactive detrital iron minerals (Berner 1984).

Authigenic pyrite is broadly interpreted to have formed indirectly via iron monosulphides, during biogenic sulphate reduction, in the absence of oxygen. Other pyrite phases may precipitate abiotically, directly from solution (Berner 1984, Sawlowicz 1993, Min *et al.* 2005b). This sedimentary pyrite commonly occurs as euhedral grains or clustered framboids, a morphology indicative of biogenic influences during formation (Wilkin *et al.* 1996).

In sedimentary settings, pyrite is generally considered to form syngenetically and during early diagenesis (Sawlowicz 1993, Folk 2005); indicative of shallow and relatively low temperature settings (e.g. <200 ºC) (Wilkin & Barnes 1997, Butler et al. 2000, Scott et al. 2009).

Sulphur Isotopes

The presence of sulphur in nearly all natural environments established sulphur isotopes as effective geochemical tracers of past geological and environmental processes (Bendall *et al.* 2006). The two most abundant isotopes of sulphur (^{32}S and ^{34}S) make up 99.2% of all naturally occurring sulphur and these, along with less common isotopes (^{33}S and ^{36}S) are used to provide information on sulphur source and precipitation mechanisms (Warren 1972, Johnston 2011). Moreover, *in-situ* analytical techniques, allow high-resolution analysis of the smallest areas within complex pyrite crystals and give insight into the complex biological and chemical interplay that occurs in sediments during sulphide precipitation (Kohn *et al.* 1998).

Sulphur isotope fractionation occurs when one unstable sulphur species is decomposed to produce two or more new sulphur species. The heavier isotope generally accumulates in species with strong chemical bonds, such as sulphates causing later sulphides from the same system to become relatively depleted (Granger & Warren 1969).

Sulphur isotopic composition is commonly expressed in terms of $\delta^{34}S$ (a ratio of $^{34}S/^{32}S$) (Bendall *et al.* 2006). Depletion or enrichment of the heavy sulphur isotopes (^{34}S and ^{36}S) reveals information about biogeochemical processes, hydrothermal fluid sources and sediment diagenesis (Butler *et al.* 2004, Ono *et al.* 2006, Johnston 2011). Major changes in sulphur isotope ratios during the deposition of ore and gangue minerals indicate a systematic change in the redox conditions of the fluid during ore deposition (Fleming & Bekken 1995).

These chemical variations make it possible to trace out processes of transport, concentration and local precipitation during ore genesis (Fleming & Bekken 1995, Hoefs 2009).

Isotope studies of sedimentary sulphur have focused primarily on the sulphur isotopic composition of iron sulphide minerals and, in particular pyrite (Butler *et al.* 2004). Studies of these isotopic ratios have been instrumental in elucidating the role of microorganisms in the precipitation of minerals and may be used to argue for the influence of specific sulphur sources (Thode *et al.* 1953, Kohn *et al.* 1998). In sedimentary environments, sulphur isotope fractionation is commonly caused by sulphate-reducing bacteria (Butler *et al.* 2004).

METHODS

A total of 37 core samples were collected from the Beverley North deposits (Appendix A). These samples were selected to be representative of the deposit, redox system and host formation, whilst optimising pyrite content where possible. The samples were set in epoxy resin and prepared as one-inch polished blocks for mineralogical and petrographic analysis. A range of methods was applied to the samples (detailed in Appendix B), in order to build a dataset for the characterisation of pyrite at Beverley North.

Optical and Scanning Electron Microscopy (SEM) in Back-Scattered Electron mode (BSE) were used to characterise pyrite morphologies, document significant textures and mineralogical relationships, and identify U-bearing minerals and Fe-(Ti)-oxides present. The SEM (Philips XL-30) was equipped with energy-dispersive X-ray spectrometer to aid mineral characterisation.

Pyrite, U-bearing minerals and Fe-(Ti)-oxides in selected representative samples were analysed by Electron Probe Microanalysis (EPMA) to determine their major and minor

element compositions. Details of count times, standards and minimum detection limited are outlined in Appendix B.

Laser-Ablation Inductively-Coupled Mass Spectrometry (LA-ICP-MS) (Ridley & Lichte 1998) was subsequently used on selected samples to provide trace element concentrations on pyrites from varied localities and horizons as well as distinct morphological types. Generally the phases analysed by LA-ICP-MS were coarse-grained and whenever possible free from visible inclusions of other minerals. The sulphide standard MASS-1 (Wilson *et al.* 2002) was used as a calibration standard (Appendix B).

LA-ICP-MS element mapping of approximately 0.5 cm^2 sized areas of pyrite focussed on areas of zonation to gain two-dimensional images of trace element partitioning within grains. This new generation laser system (Appendix B) permits high spatial resolution matched by sensitivity of low (sub-ppm) element concentrations.

In-situ sulphur isotope analysis by Secondary-Ion-Mass-Spectrometry (SIMS) (Appendix B) was carried out on selected pyrite grains from 7 samples taken across from the deposits to test for variations in ^{34}S and analyse the distinct pyrite morphologies for characteristic signatures. Variations in the trace element concentration and sulphur isotopes were used to identify possible geochemical trends which may enhance understanding of ore genesis and allow insight into the paragenetic sequencing of the minerals.

OBSERVATIONS & RESULTS

Pyrite morphology and textural observations

Throughout the Beverley North mineralised systems, visible coarse-grained pyrite in the sandstone matrix is limited. Intercalation of oxidised and reduced sandstones with silcrete and clay-rich siltstones is prevalent throughout cores. Both pyrite and uranium-bearing minerals were found to be ubiquitous proximal to reduced and organic rich zones, a result of the morphology of the uranium deposits. Pervasive hydrocarbon staining, evident in hand samples was observed across these reduced zones a likely result of the proximity of the porous host sandstone to the hydrocarbon-rich Eromanga Basin.

Samples are prediminately medium to coarse-grained, matrix supported, sub-rounded quartz sandstones with accessory minerals prevalent throughout the matrix. A consistent mineral assemblage is observable across all pyrite-bearing samples (EI1-20B), with their assemblage largely made up of quartz ($\geq$50%), pyrite ($\geq$30%), $\pm$ U-bearing minerals ($\leq$10%), $\pm$ ilmenite ($\leq$5%), $\pm$ rutile ($\leq$ 5%) $\pm$ minor zircon, hematite and sphalerite. Samples containing negligible pyrite (EI21-37) are predominantly quartz ($\geq$ 80%), ilmenite ($\leq$ 15%) and rutile ($\leq$5%) $\pm$ pyrite $\pm$ hematite.

Pyrites displayed varying morphologies and for the purposes of this study were categorised as framboidal, euhedral and cubic, cement or veined, infill and overgrowth. Specific morphologies do not appear exclusive to any particular deposit, horizon or sample type.

Framboidal pyrite is the most common and diverse pyrite morphology observed throughout the sample suite (Figure 4). Small framboids (~ $\leq$10 µm) are dominated by densely packed, spherical aggregates of sub-micron sized pyrite crystals, commonly found in clusters of up to several hundred framboids. Idiomorphic microcrystals within framboids are highly uniform

in both size and shape (Figure 4a). Some evidence of three dimensional aggregations was observed (Figure 4b).

Framboidal aggregates throughout the samples are comparable with those defined by Wilkin & Barnes (1997), however we extend this definition to include a range of pyrite aggregates whose morphologies likely share similar formation processes (Figure 4d-f). Hypidiomorphic framboids preserve a somewhat spherical nature but lack the porosity associated with microcrystal aggregations in classic framboidal pyrite. This secondary range of framboidal pyrites is typically found in isolated clusters and infrequently coexists with archetypal framboids (Figure 4d). No framboid morphologies were observed exclusive to any sample type, horizon or deposit but are frequently observed intergrown with other pyrite morphologies (Figure 4g).

Cubic and euhedral pyrites observed across the sample suite are commonly found clustered together or intergrown with crystalline pyrite cement (Figure 5). In some instances the euhedral cubic grains appear to be associated with framboidal growth; identifiable by the appearance of porous microcrystals within the centre of the grains (Figs. 4f and 5c). Texturally massive pyrite euhedra often display distinct multi-phase growth patterns. Anhedral pyrite grains are common in samples where massive pyrites are observed; but also coexist with idiomorphic cubic pyrites or as singular grains within the matrix. Similar to other pyrite morphologies, anhedral pyrite grains were observed intergrown with cemented pyrite. Porous xenomorphic pyrite overgrowth is commonly observed around both cubic and anhedral pyrite grains (Figure 5f).

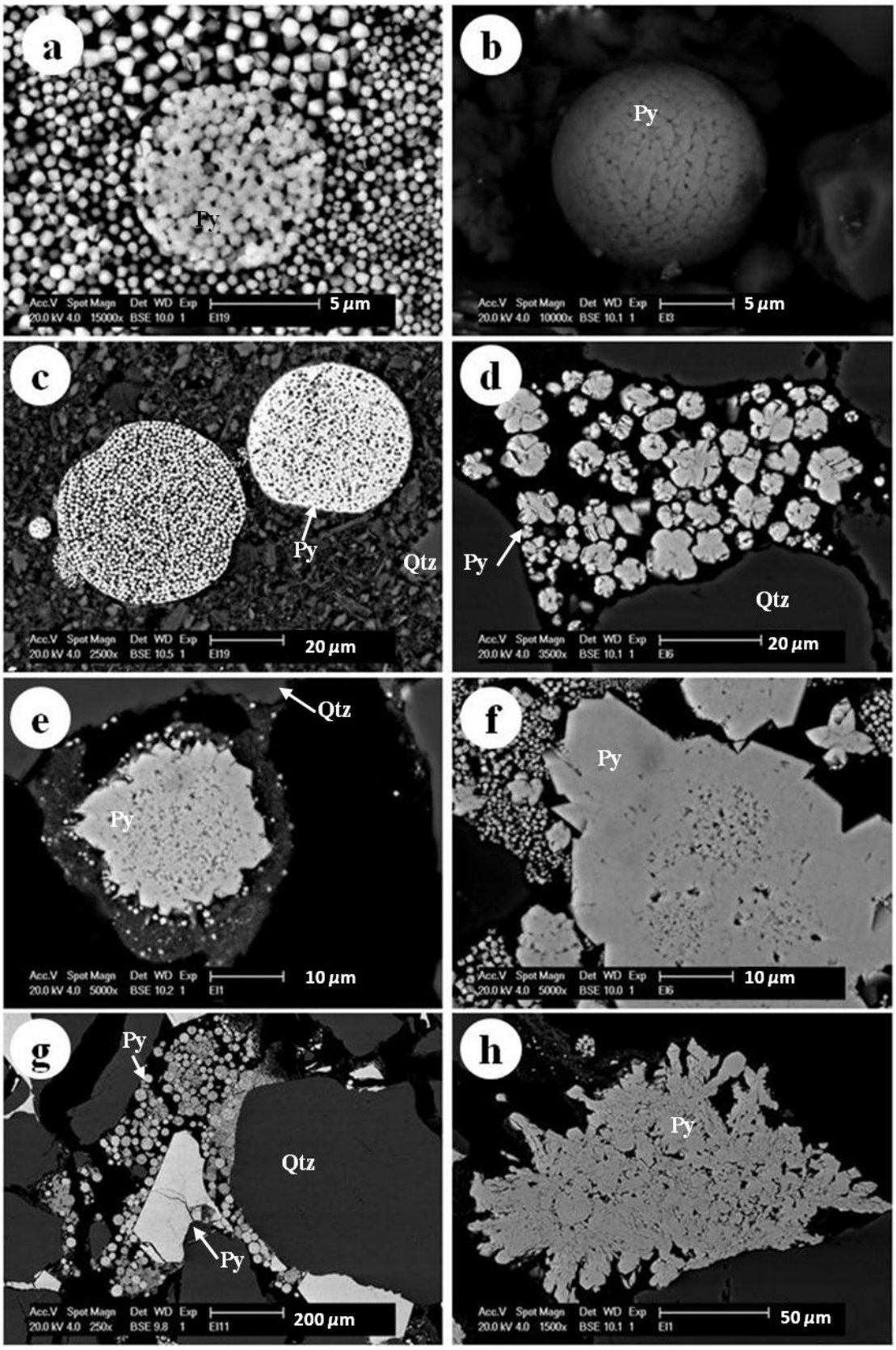

Figure 4: BSE images of varied framboidal pyrite (Py) morphologies; a) Spherical aggregate of sub-micron sized pyrite crystals surrounded by un-ordered micro-crystals of similar provenance; b) Three-dimensional framboidal aggregate evidencing spherical nature of framboids; c) Framboidal aggregates in quartz (Qtz) matrix; d) Hypidiomorphic framboidal aggregates are irregular but retain a spherical shape; e) & f) display porous framboidal pyrite overgrown by euhedral pyrite; g) Clusters of both classic and hypidiomorphic framboidal pyrite coexisting in the matrix with homogenous pyrite cement; h) Framboidal pyrite intergrown with anhedral pyrite.

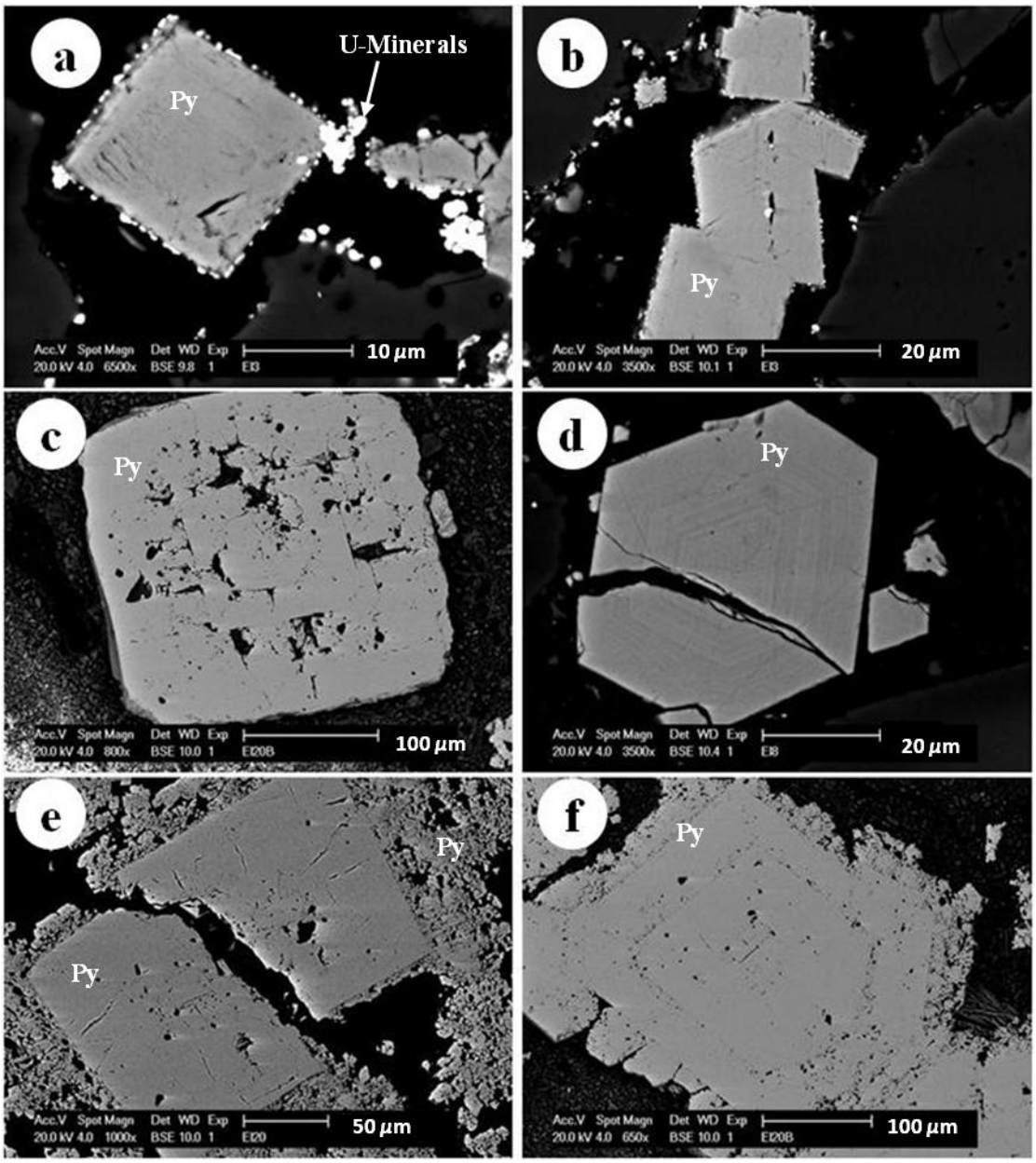

Figure 5: BSE images of euhedral and cubic pyrite (Py) grains found present throughout the sample suite. Grains commonly display forms of compositional and textural zonation; a) Cubic pyrite with associated U-nodules at grain edges; b) Intergrowths of cubic and euhedral pyrites, with U-minerals also present at grain edges; c) Porous cubic pyrite demonstrating progressive stages of growth around a spheroidal nucleus; d) Compositionally zoned euhedral pyrite grain which has undergone post-depositional micro-fracturing; e) Porous cubic pyrite demonstrating internal textural variance, overgrown by xenomorphic pyrite cement and pervasively fractured; f) Texturally zoned euhedral pyrite with porous xenomorphic growth apparent at grain edges and between phases of pyrite growth.

Pyrite cement is a dominant pyrite morphology throughout the sample suite and occurs primarily as the cemented matrix common in sandstone-host rocks. The appearance and growth of pyrite cement appears varied, with petrographic and SEM analysis showing texturally homogenous, crystalline and xenomorphic cement growth present (Figure 6). A limited number of samples display compositional zonation throughout pyrite cement on both optical and BSE images (Figure 6b). Varied porosities within pyritic cements affect their textural homogeneity. Little association exists between oscillatory zonation or porosity and sample depth, location or horizon.

Veined and infill textures are also a common pyrite type (Figure 6). This phase of pyrite formation is commonly seen fracturing and overprinting other pyrite types, quartz and the Fe-(Ti)-oxide accessory minerals. Pervasive micro-fracturing of quartz grains by pyrite commonly follows grain edge boundaries (Figure 6f); although larger-scale fractures through grain centres is not uncommon (Figure 6e).Consistent fracturing and overprinting of pyrite across the sample suite indicates more than one generation of pyrite formation and defines fluid flow as a likely mechanism of sulphide precipitation.

Micro-fracturing and overprinting of quartz grains and texturally homogenous pyrite cement by hematite and native selenium was observed in sample EI11 (PRC015, Pepegoona) (Figure 7). The zone of oxidised sandstone from which this sample was taken, displayed prevalent visible yellow sulphur staining on the core. The secondary overprinting minerals are pervasive throughout the sample, and appear to be genetically linked. Hematite is precipitated within fracture zones and displays massive infill morphology, commonly juxtaposed against porous acicular native selenium growth (Figure 7a). Native selenium was also observed as an accumulation of porous feathery and bladed grains (Figure 7b). Both secondary minerals

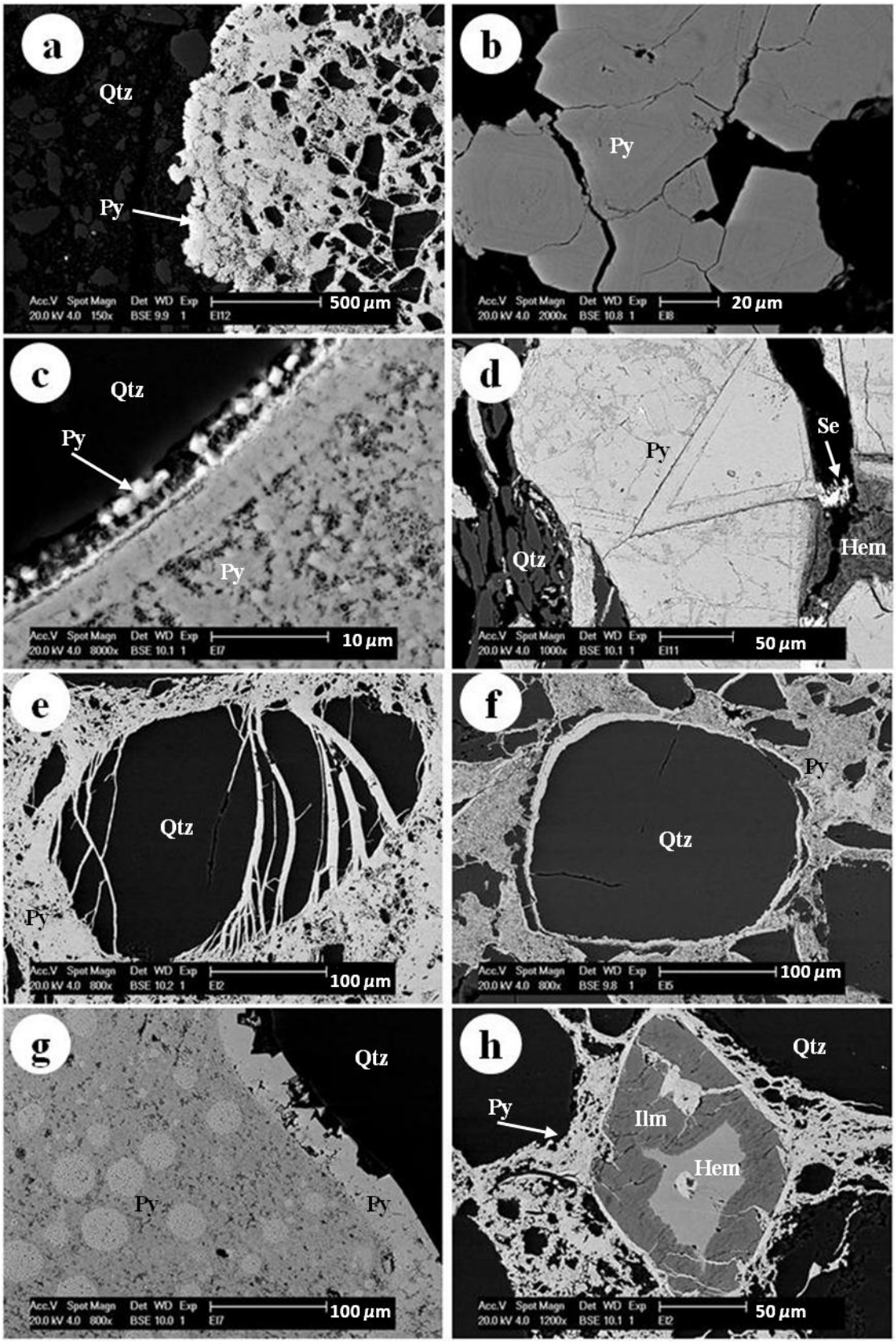

Figure 6: BSE images of cement, veined and infill pyrite (Py) morphologies. Pyrite ranges from highly porous intergrown to crystalline and compositionally zoned; a) Porous, xenomorphic pyrite cement precipitated in the matrix of coarse-grained sub-rounded quartz (Qtz) sandstone; b) Compositionally-zoned, crystalline pyrite cement; c) Porous pyrite cement, bordered by homogenous coherent pyrite veins and associated with micron-scale cubic pyrite crystal growth in porous space; d) Massive pyrite cement displays deterioration and replacement by pervasive late-stage hematite (Hem) and native selenium (Se); e) & f) Pervasive infill pyrite fractured sub-rounded quartz grains; g) Framboidal pyrite is overgrown by porous pyrite cement, which is likely intergrown with other minerals. Veined pyrite with cubic growth overprints the porous cement; h) Veined and infill pyrite fills porous space and pervasively fractures euhedral ilmenite (Ilm) grains coexisting with hematite.

form septian textures (Schwartz 1951) which appear as oscillatory deterioration patterns within the otherwise texturally homogenous pyrite cements (Figure 7c).

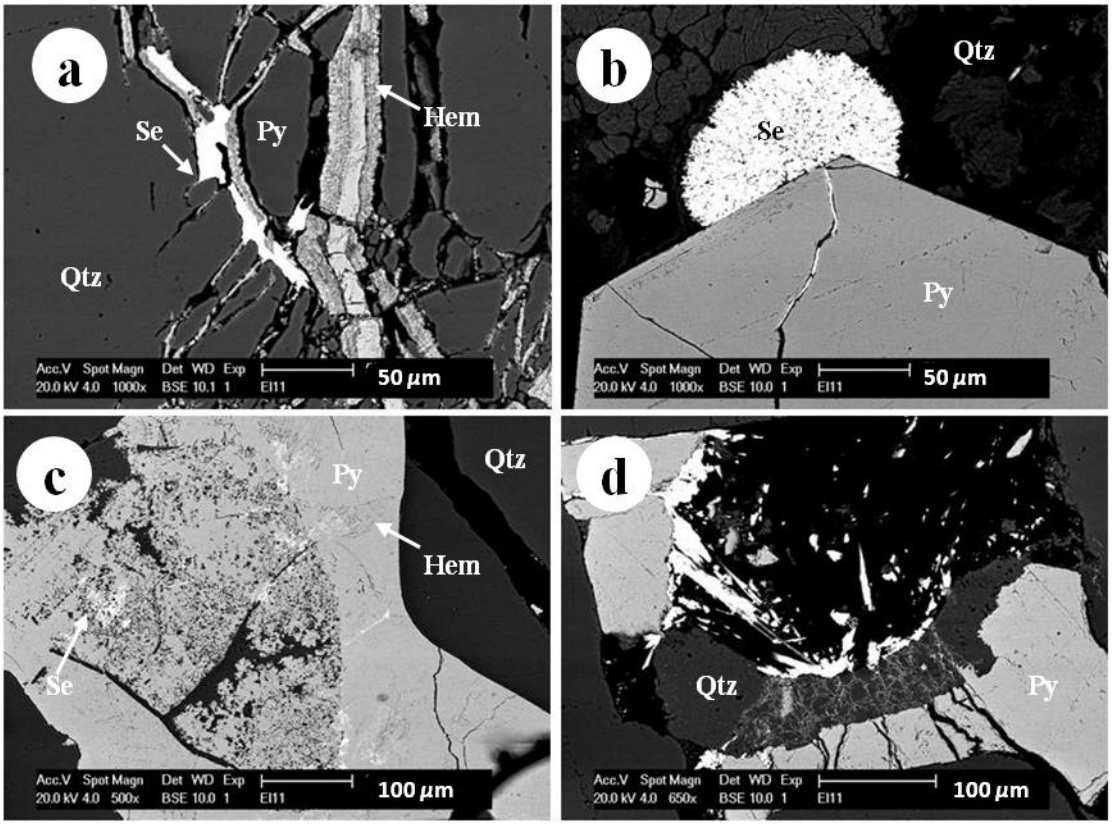

Figure 7: BSE images displaying pervasive precipitation of late-stage native selenium (Se) and hematite (Hem) throughout sample EI11, a) infilling micro-fractures in quartz (Qtz) and pyrite (Py) associated with hematite; b) crystalline native selenium growth in porous sandstone; c) associated with hematite septial replacement textures in homogenous pyrite cement and d) as bladed fragments associated with quartz and pyrite fracturing.

Uranium occurs primarily as uraninite, with minor coffinite and brannerite as confirmed by EPMA analysis. These U-bearing minerals are abundant in samples taken from mineralised horizons and commonly occur as extremely fine-grained, nodule-like minerals overgrowing framboidal pyrite, or as cement-like textures intergrown with porous pyritic cement (Figure 8). Lignite is also found predominantly in the presence of pervasive uranium mineralisation and framboidal pyrite (Figure 8b & 8c).

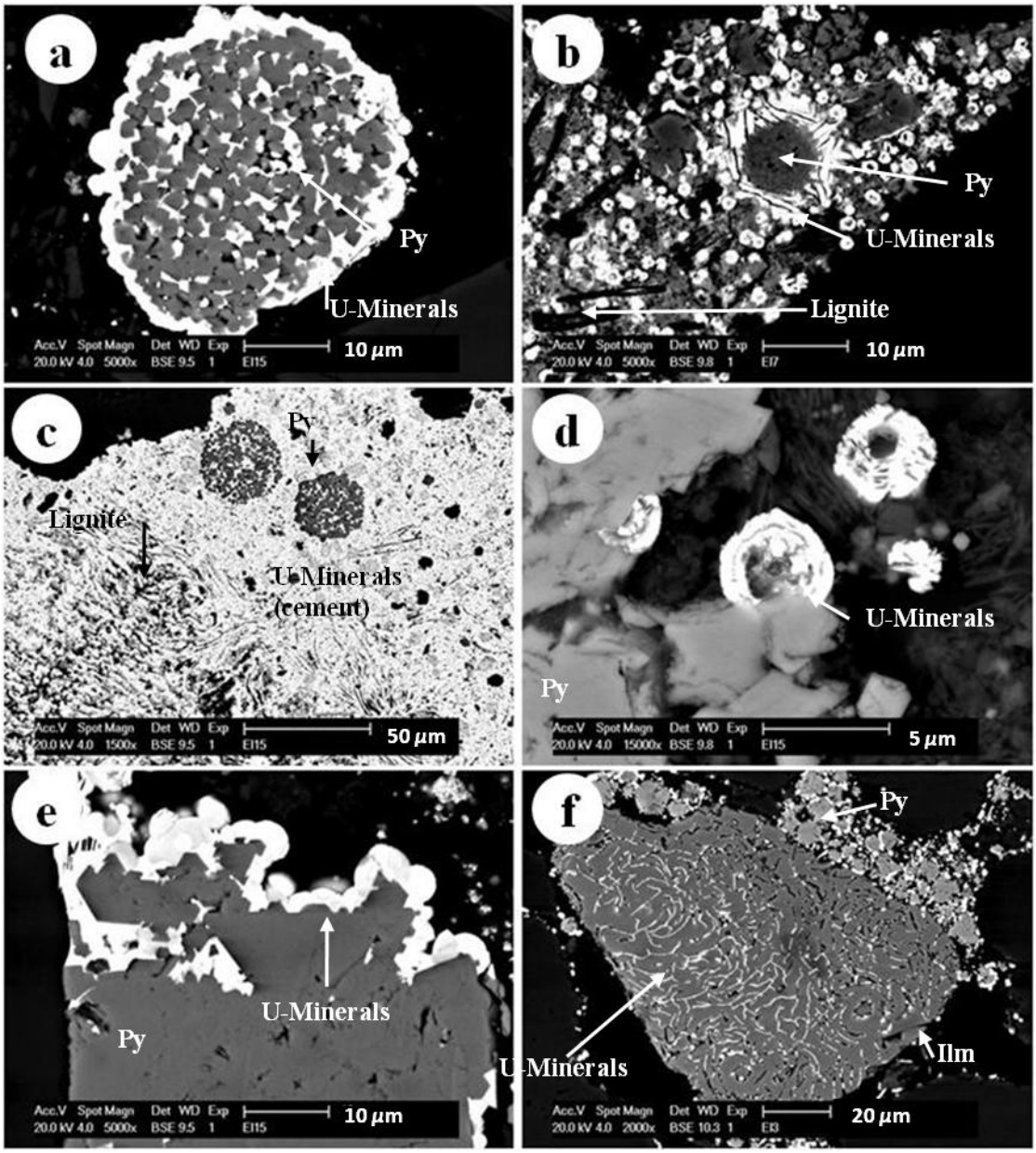

Figure 8: BSE images of fine-grained uranium minerals, predominantly coffinite and uraninite existing as; a) intergrowths with porous framboidal pyrites; b) small nodules associated with the presence of lignite and framboidal pyrite; c) porous cement intergrown with pyrite, quartz and lignite; d) nodules with inclusions of pyrite; e) overgrown at pyrite grain edges and f) infilling porous space in coarse anhedral ilmenite grain, indicative of contemporaneous precipitation of both minerals.

Titanium-bearing minerals; ilmenite and rutile are common throughout all samples (Figure 9). They are most prevalent in samples from oxidised zones and samples containing negligible pyrite. Coarse sub- and euhedral ilmenite and rutile appear to have undergone significant deterioration, fracturing and breakdown and linear and boxwork textures and pyrite infill of fractures are common (Figure 9a & 9b). Hematite with relic framboidal textures was observed in oxidised sandstones (Figure 9c) and limited coexistence of ilmenite intergrown with hematite was also observed (Figure 9d).

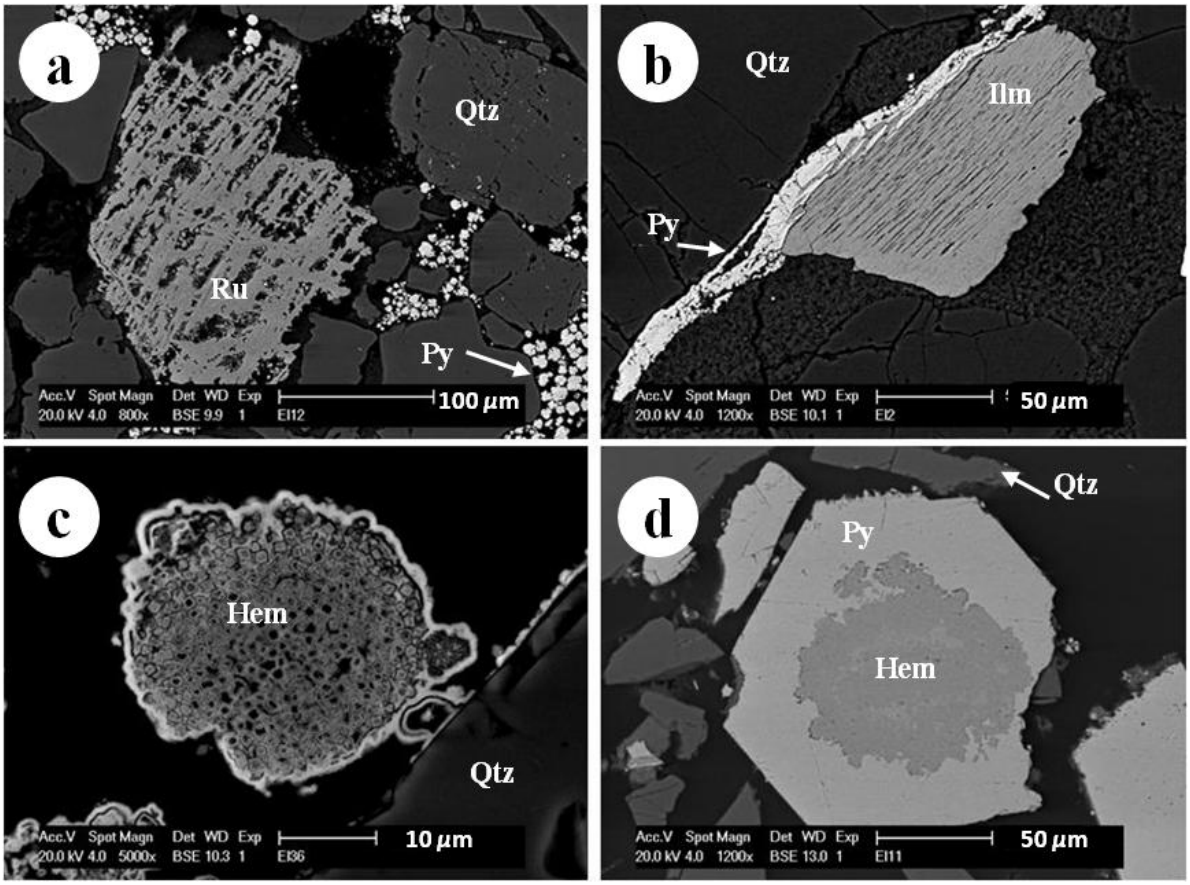

Figure 9:BSE images showing accessory minerals present throughout the sample suite; a) Rutile displaying boxwork deterioration patterns, adjacent to unaltered framboidal pyrite; b) Ilmenite with linear alteration patterns intergrown with pyrite; c) Hematite with relic framboidal textures present in oxidised sandstones and d) Hematite coexisting in euhedral pyrite grains.

Minor and trace elements in pyrite

LA-ICP-MS analysis indicated a broad variation in trace element composition of pyrite across 19 samples. Significant non-uniform elevations of V, Cr, Mn, Co, Ni, As, Se, Mo, Sb, Ba, W and Tl were observed throughout the sample suite and are summarised by Table 2.

Table 2: Summary table of LA-ICP-MS trace element data for pyrite (ppm).

		V	*Cr*	*Mn*	*Co*	*Ni*	*As*	*Se*	*Mo*	*Sb*	*Ba*	*W*	*Tl*
Pepegoona	**EI1 (**216.3m)												
	Min	8.4	3.5	97	5.8	13	276	33	25	3.9	271	10	154
	Max	2082	1317	434	835	1401	1054	285	435	83	16517	2568	243
	Mean	446	275	240	238	352	553	126	111	31	4116	560	204
	Std Dev	915	582	129	344	591	309	100	181	34	6990	1123	39
	EI2 (247.1m)												
	Min	0.98	bdl	4.7	bdl	bdl	4.7	bdl	0.64	0.28	133	1.6	0.59
	Max	19	7.2	27	4.8	7.3	571	2.4	15	5.4	329	41	25
	Mean	8.4	3.0	13	1.1	2.5	139	1.4	4.4	1.6	232	17	6.3
	Std Dev	7.5	2.6	7.7	1.5	2.6	171	0.60	4.2	1.4	69	15	7.5
	EI3 (201.7m)												
	Min	32	bdl	3.7	159	75	2773	191	107	241	15	15	186
	Max	3853	1308	180	635	780	16903	944	351	869	3429	3300	1337
	Mean	1566	211	72	342	409	12091	461	225	563	1113	1370	895
	Std Dev	1184	428	63	170	237	4957	259	64	165	1018	1028	400
	EI4 (204.0m)												
	Min	37	bdl	13	66	24	176	18	11	1.9	81	16	24
	Max	533	437	335	269	344	333	103	90	10	14473	761	43
	Mean	170	104	88	153	115	274	44	37	4.9	5684	230	35
	Std Dev	206	187	138	86	131	59	35	31	3.2	7131	305	9.1
	EI6 (203.9m)												
	Min	3.1	bdl	2.0	11	20	298	42	15	1.6	8.4	1.5	11
	Max	221	375	8.2	181	350	1259	319	123	29	447	50	62
	Mean	73	86	3.7	139	90	992	101	39	7.0	206	13	36
	Std Dev	72	125	2.0	54	93	276	86	33	8.2	179	16	13
	EI7 (219.2m)												
	Min	23	1.8	23	400	229	659	bdl	10	3.9	170	0.67	130
	Max	15230	454	8228	12085	12122	57295	482	2576	12523	30589	12520	1521
	Mean †	429	4.0	49	1129	803	4240	23	46	166	401	248	326
	Std Dev	53697	159	2892	3986	4065	19101	163	895	4373	10676	44179	443
	EI8 (222.6m)												
	Min	1.2	bdl	4.2	0.6	6.4	140	bdl	16	0.33	6.3	0.24	3.5
	Max	229	31	32	291	253	1921	7.5	488	15	1625	8.2	57
	Mean	39	7.5	9.9	52	71	580	3.5	122	4.1	151	2.1	15
	Std Dev	65	8.4	7.2	75	66	542	1.7	127	4.2	397	2.2	14
	EI9 (231.3m)												
	Min	0.34	bdl	2.6	bdl	0.40	2.1	bdl	4.0	0.32	8.9	0.32	0.02
	Max	3.2	4.1	141	125	153	1953	51	293	126	230	3.4	130
	Mean	1.3	1.1	15	27	56	292	9.4	122	19	128	1.9	29
	Std Dev	0.7	0.9	35	39	51	532	14	84	40	80	1	42

		V	*Cr*	*Mn*	*Co*	*Ni*	*As*	*Se*	*Mo*	*Sb*	*Ba*	*W*	*Tl*
Pepegoona West	**EI11 (**253.0m)												
	Min	0.36	bdl	1.4	0.34	bdl	22	8.7	2.6	0.45	13	2.5	1.0
	Max	487	5.8	14	410	51	1301	36432	935	688	288	466	136
	Mean	77	1.3	7.2	70	12	407	2663	270	63	88	65	29
	Stdev	106	1.4	3.3	96	15	329	7620	222	133	50	98	34
	EI12 (257.2m)												
	Min	0.08	bdl	10	3.0	5.3	24	bdl	0.59	2.7	12	0.22	1.7
	Max	5.7	2.4	187	262	699	450	12	43	103	388	2.4	94
	Mean	2	1.1	73	107	207	184	3.5	17	31	224	1.6	44
	Stdev	1.6	0.7	60	98	210	118	4	14	31	151	0.7	31
	EI13 (269.1m)												
	Min	0.56	bdl	1.2	0.23	1.2	25	1.9	1.4	0.11	12	0.02	4.3
	Max	11	5	32	79	141	602	3.2	25	2.8	1468	1.3	297
	Mean	1.8	1.1	6.3	25	40	214	2.2	7.8	1.1	184	0.4	46
	Stdev	3.2	1.4	9.6	26	42	167	0.4	7.5	1	452	0.4	90
Pannikan	**EI14** (222.5m)												
	Min	43	bdl	15	48	35	86	bdl	26	1.9	290	101	18
	Max	640	285	140	281	1566	359	914	667	15	23443	788	53
	Mean	144	95	47	133	290	221	167	119	5.4	6524	342	31
	Stdev	204	106	43	79	523	82	305	222	4.5	8225	259	12
	EI15 (260.4m)												
	Min	0.81	bdl	15	2.8	37	25	bdl	0.32	0.09	57	0.09	285
	Max	94	3.9	27	3949	3233	550	58	59	4.2	170	227	529
	Mean	12	1.1	21	569	532	165	8	12	0.7	95	35	415
	Std Dev	29	1.1	4.2	1219	988	162	18	23	1.3	33	73	81
	EI16 (228.1m)												
	Min	0.99	bdl	12	2.2	1.3	12	bdl	4.8	0.21	39	1.6	11
	Max	59	128	170	174	106	51	28	225	3.1	610	49	140
	Mean	20	20	60	39	27	27	8.7	54	1.2	191	16	55
	Std Dev	19	44	55	62	36	12	10	70	1.1	192	16	44
	EI17 (244.2m)												
	Min	1.45	bdl	700	0.21	1.3	156	984	52	0.40	45	0.56	11
	Max	37	30	1356	100	503	496	1736	109	4.2	234	11	232
	Mean	11	9	982	38	123	281	1291	75	1.6	134	3.3	85
	Std Dev	15	13	267	42	214	137	348	21	1.5	86	4.4	90
	EI18 (263.6m)												
	Min	0.48	bdl	4.9	0.11	0.35	0.51	bdl	bdl	bdl	8.2	0.27	0.16
	Max	44	109	151	8.3	52	87	6.5	3.9	1.3	236	28	6.1
	Mean	12	17	36	2	10	38	1.7	1.5	0.3	99	8	2.1
	Std Dev	15	34	48	2.7	16	37	1.7	1.6	0.4	93	10	2.5
	EI19 (265.4m)												
	Min	bdl	bdl	2.5	1.1	6.3	238	2.4	4.9	3.8	5.1	bdl	6.1
	Max	5.5	237	47	6.5	34	608	23	16	17	627	0.73	50
	Mean	1.5	27	10	3.1	16	353	7.3	8.0	6.6	152	0.1	14
	Std Dev	2.0	74	13	1.9	9.7	138	6.2	3.0	4.2	188	0.2	13
	EI20 (264.4m)												
	Min	0.71	bdl	11	0.7	0.38	1.1	bdl	bdl	bdl	18	1.9	0.29
	Max	33	11	161	38	108	140	3.2	40	0.72	461	13	4.3
	Mean	6.7	2.6	57	4.9	17	49	1.9	7.8	0.2	101	4.3	1
	Std Dev	9.7	3.1	55	12	33	44	0.5	13	0.2	129	3.5	1.3
	EI20B(264.4m)												
	Min	0.87	bdl	4.5	0.14	0.51	bdl	bdl	bdl	bdl	35	1.6	0.1
	Max	4.7	1.2	34	4.5	11	26	bdl	2.3	0.91	128	3.1	1.5
	Mean	2.7	0.7	18	1.7	4.1	9.3	1.8	0.6	0.2	68	2.4	0.4
	Std Dev	1.7	0.4	13	1.8	4.4	11	0.2	0.9	0.3	38	0.6	0.5

Ore-bearing horizons (shaded grey) show hyper enrichment of a range of elements and moderate elevations are observed in samples taken proximal (<2 m) from ore zones (striped grey). 'bdl' represents values below detection limites and practices outlined by Winderbaum *et al*. (2012) were followed. The <mdl values preserved in Appendix C were halved to facilitate their inclusion in statistical calculations so as to approximate the correct spread of data; they not however make any significant changes to inter-element correlations.

† The mean of EI7 was recalculated without extreme outlier values to show a more representative value of the dataset.

EPMA data for 140 pyrite grains within 16 samples (Appendix D) indicates limited enrichment of common pyrite minor elements as evidenced by their mean concentrations in Table 3. Despite higher minimum detection limits of EPMA, there is a strong association between concentrations measured by the two analysis techniques. The analyses also indicate a general trend towards stoichiometric pyrite with consistent Fe:S ratios (Appendix D).

Table 3: Minor elements show limited enrichment in pyrite from 16 samples from EPMA analysis. Mean values are given in weight percent of the total pyrite (wt%).

	As	Co	Ni	Se	Mo
Mean $_{(wt\%)}$	0.18	0.02	0.03	0.29	0.65

Arsenic is broadly enriched in pyrite, found at elevated levels in 15 of the 19 samples analysed by LA-ICP-MS methods. Whilst typically present at ~500-600 ppm, As reaches 16,000 ppm in pyrite in some samples. Strong positive correlations exist between As and Co, Sb and Tl when data is transformed on a logarithmic scale (Table 4).

Table 4: Pearsons Coeffiecients of the LA-ICP-MS Trace Element data for pyrite (n=194) after logarithmic transformation

	V	Cr	Mn	Co	Ni	As	Se	Mo	Sb	Ba	W	Tl
Cr	0.5											
Mn	0.34	0.26										
Co	0.63	0.38	0.23									
Ni	0.49	0.41	0.35	0.88								
As	0.56	0.37	0.11	0.70	0.64							
Se	0.59	0.27	0.20	0.54	0.30	0.54						
Mo	0.49	0.27	0.07	0.55	0.38	0.59	0.60					
Sb	0.56	0.29	0.18	0.68	0.55	0.82	0.63	0.67				
Ba	0.63	0.51	0.47	0.44	0.45	0.32	0.31	0.35	0.41			
W	0.89	0.46	0.37	0.52	0.35	0.41	0.57	0.46	0.51	0.67		
Tl	0.45	0.26	0.33	0.72	0.71	0.76	0.42	0.42	0.67	0.35	0.34	

Note: For this table, values <mdl are taken as 50% of the respective mdl value. Data in red and pink are coeffiecients indicating recognisable very strong or strong positive correlation respectively.

The correlation coefficients between Co and Ni, V and W and As and Sb (Figure 10) are the highest of the dataset, with Pearson's r values of 0.88, 0.89 and 0.82, respectively. The r values represent the strength of the linear relationship of the datasets from the log transformed data (Table 4) and the strong inter-element concentrations evidence a common source of the trace elements.

The correlation of As and Sb displays trace element variability relative to sample location (Figure 10c). This inter-deposit trend is typified by higher trace element concentrations in the Pepegoona and Pepegoona West deposits relative to the Pannikan deposit. Data from the Pepegoona and Pepegoona West deposits show a range of trace element concentrations across five orders of magnitude, and whilst some low values are comparable with those from the Pannikan deposit, their median concentrations exceed those in the latter deposit.

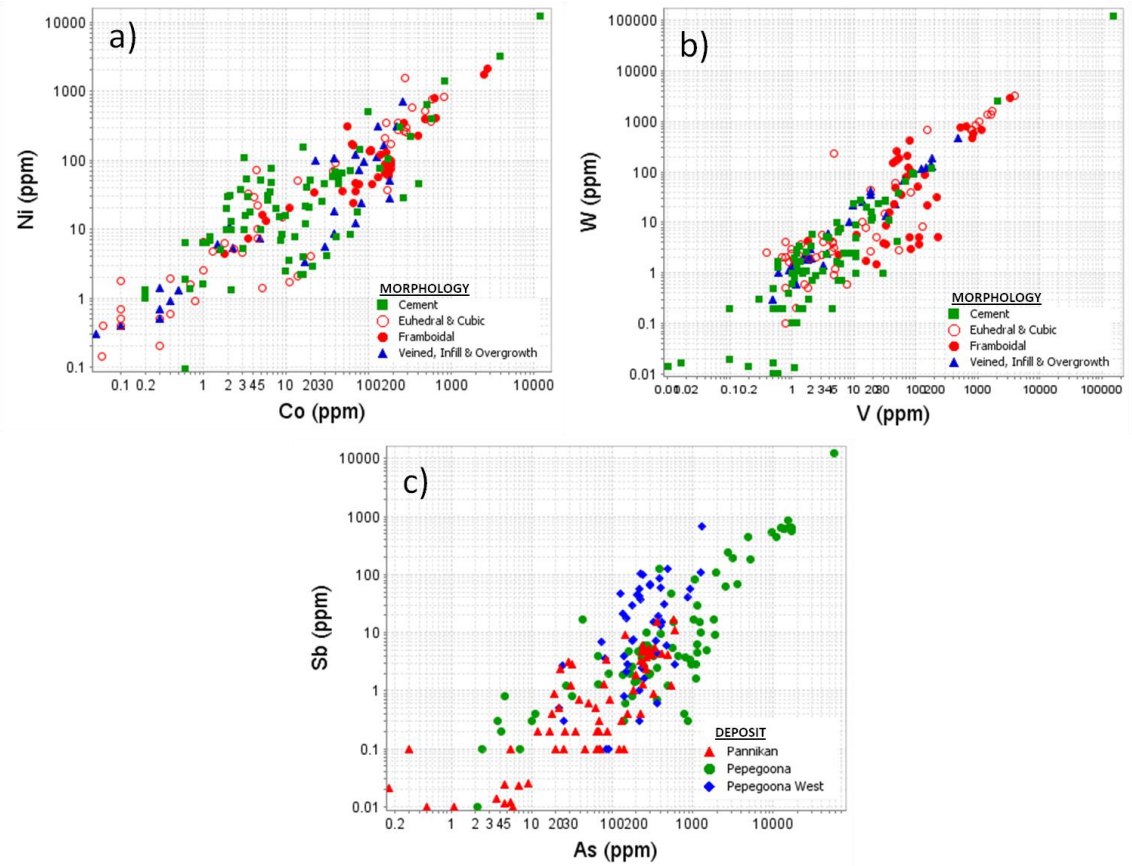

Figure 10: Inter-element plots display strong positive correlations between trace elements Co & Ni (a), V & W (b) and As & Sb (c) within pyrites from across the dataset. Plots a) and b) demonstrate that these correlations appear independent of pyrite morphology. Plot c) demonstrates a trend of greater trace element enrichment in pyrites from Pepegoona and Pepegoona West relative to Pannikan.

Within the Pannikan deposit, variation in trace element concentration in pyrite is observed. Trace elements, and in particular As, Co and Ni are elevated in pyrite from core PRC021 relative to those from PRC022 (Figure 11). This trend appears to be representative of core sample location relative to the oxidised front of the roll-front deposit. Samples taken from closer to the dominant mineralised zone are consistently more enriched in trace elements than their more distant counterparts.

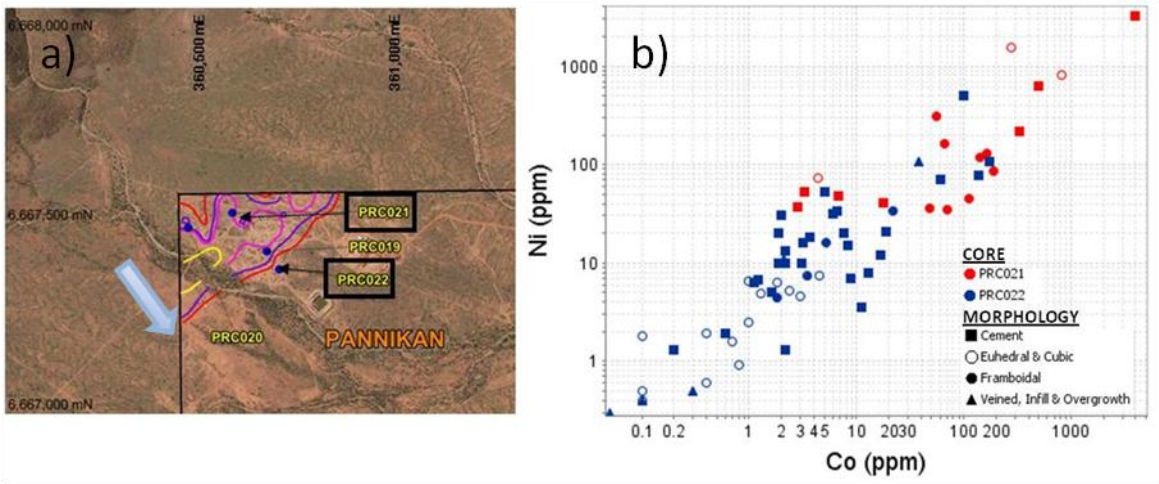

Figure 11: Inter-element plot of Co and Ni demonstrates that pyrites from core PRC021 are consistently more enriched in trace elements than pyrites from core PRC022, irrespective of morphology or horizon. Core PRC021 is shown on the deposit model to be from within the roll-front system whilst PRC022 is taken from in front of the oxidising system (blue arrow demonstrating the approximate direction of the roll movement). This supports the hypothesis that trace element enrichment is primarily associated with hydrothermal fluids which supplied uranium to the system.

Corresponding patterns are observed when the dataset is analysed in terms of uranium mineralised horizons throughout the broad deposits of Beverley North. Pyrites within samples taken from zones hosting uranium mineralisation are consistently more enriched in trace elements than pyrites hosted by other stratigraphic horizons (Figure 12).

This trend is most prevalent for Tl (Figure 12a), which rarely exceeds background concentrations (≤50 ppm) in samples from outside of the mineralised horizons but

systematically attains concentrations of ~500-1,300 ppm in pyrite associated with uranium mineralisation (Table 2).

Nickel, and to some extent Co, which are strongly correlated across all horizons, show additional enrichments in samples from mineralised horizons (Figure 12b). Both commonly reach ~800-2,000 ppm in ore bearing horizons but average only ~150 ppm in the U-barren zones. To a limited extent As, V, Sb and W which display broad trace element enrichment, display hyper enrichment in pyrite from zones of uranium mineralisation (Figure 12c).

Minor and limited trace element enrichment is also observable in pyrite in samples taken proximal (<2 vertical metres) from zones of U-mineralisation (Table 2). These elevations are not uniform across the LA-ICP-MS dataset however; As, V, Co, Ni, Mo and Sb display moderate enrichments in the proximal zones (Figure 12).

The apparent exception to these trends is sample EI11 taken from within the roll-front at Pepegoona West, which contains abundant hematite and native selenium (Figure 12d). Pyrite in this sample is enriched in As, Se, Mo, Sb and W but is not associated with a stratigraphic horizon proximal or within a zone bearing uranium mineralisation. Enrichment in Se (~2663 ppm) appears somewhat unusual as Se is commonly limited in other samples.

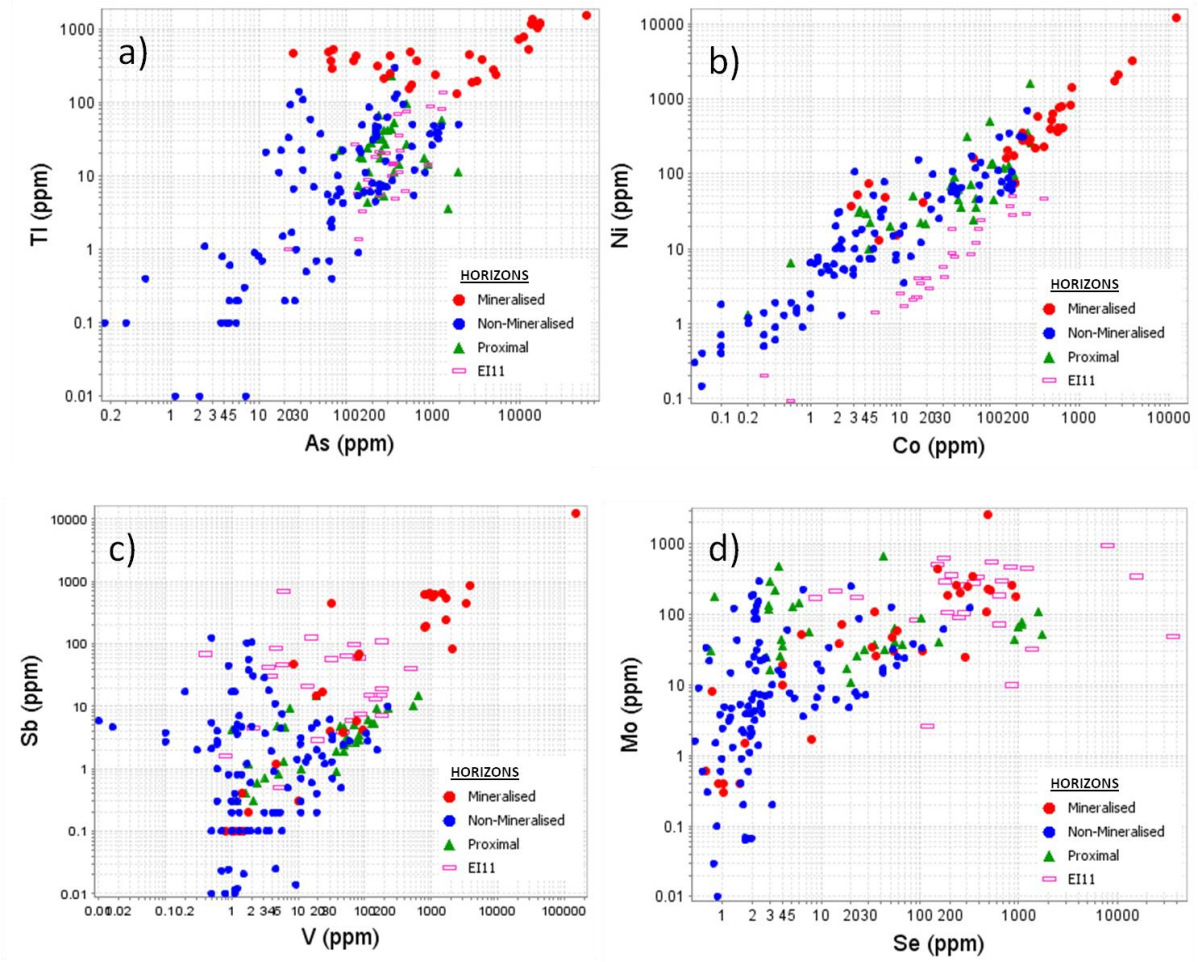

Figure 12: Inter-element plots As v Tl, Co v Ni and V and Sb (a to c, respectively) demonstrate consistent trace element enrichment in pyrites from ore-bearing horizons relative to their non-mineralised counterparts. Consistently, pyrites from zones proximal to ore-bearing horizons display moderate enrichment generally just below levels seen in mineralised horizons. Sample EI11 appears as the exception to these trends. For samples taken proximal to mineralised horizons, moderate enrichment occurs in most elements (e.g. 12a and 12b) however in plot c) and d) pyrite shows significant enrichment in samples from proximal to mineralised horizons. d) The plot of Se against Mo further supports this exception to the trend. The samples from EI11 are significantly more enriched in both elements and this is interpreted in terms of a late-stage oxidising fluid and consequent precipitation of native Se and hematite into the sandstone.

LA-ICP-MS element mapping of pyrite from 3 samples (EI7, EI8, EI11) demonstrated irregular trace element enrichment across all pyrite morphologies consistent with previous observations. The map of pyrite from sample EI7 demonstrates distinct variation in trace element concentrations between pyrite morphologies (Figure 13). Consistent with LA-ICP-MS spot analysis, framboids host limited trace element concentrations relative to other pyrite morphologies; in this case being depleted in As, Co, Ni, Mn, Sb, Tl and V. Limited element zonation of As, Co and Ni at framboid edges was apparent. In contrast, porous pyrite cement was enriched in these elements and we additionally note decreased Fe throughout this phase. The late-stage veined pyrite was enriched in terms of Mo and As, whilst the region of cubic infill which displayed visible zonation on BSE images (Figure 6e), was highly enriched in Mo and V.

The second map (EI8; Appendix E) contains pyrite cement which displayed visible oscillatory zonation on BSE images (Figure 6b), however reveals only weak chemical zonation expressed by As, Co, Ni, Mo and Sb enrichment at grain margins and Mn and Tl enrichment at grain cores.

The pyrite cement of sample EI11 (Figure 14) shows distinct oscillatory zoning with respect to As, Mo, Sb, and Tl. The septial deterioration zone visible in the reflected light image (Figure 14a) is highly enriched in Co, Ni, As, Se, Mo, Tl, V and W and trace element enrichment in the surrounding pyrite appears focused around this “nucleic” zone. Se, which pervasively overprints the pyrite as native selenium is limited throughout the cement of this sample, appearing only highly enriched in the aforementioned zone. A strong crystalline nature of the pyrite cement is evident which was not apparent from prior study of the massive pyrite cement.

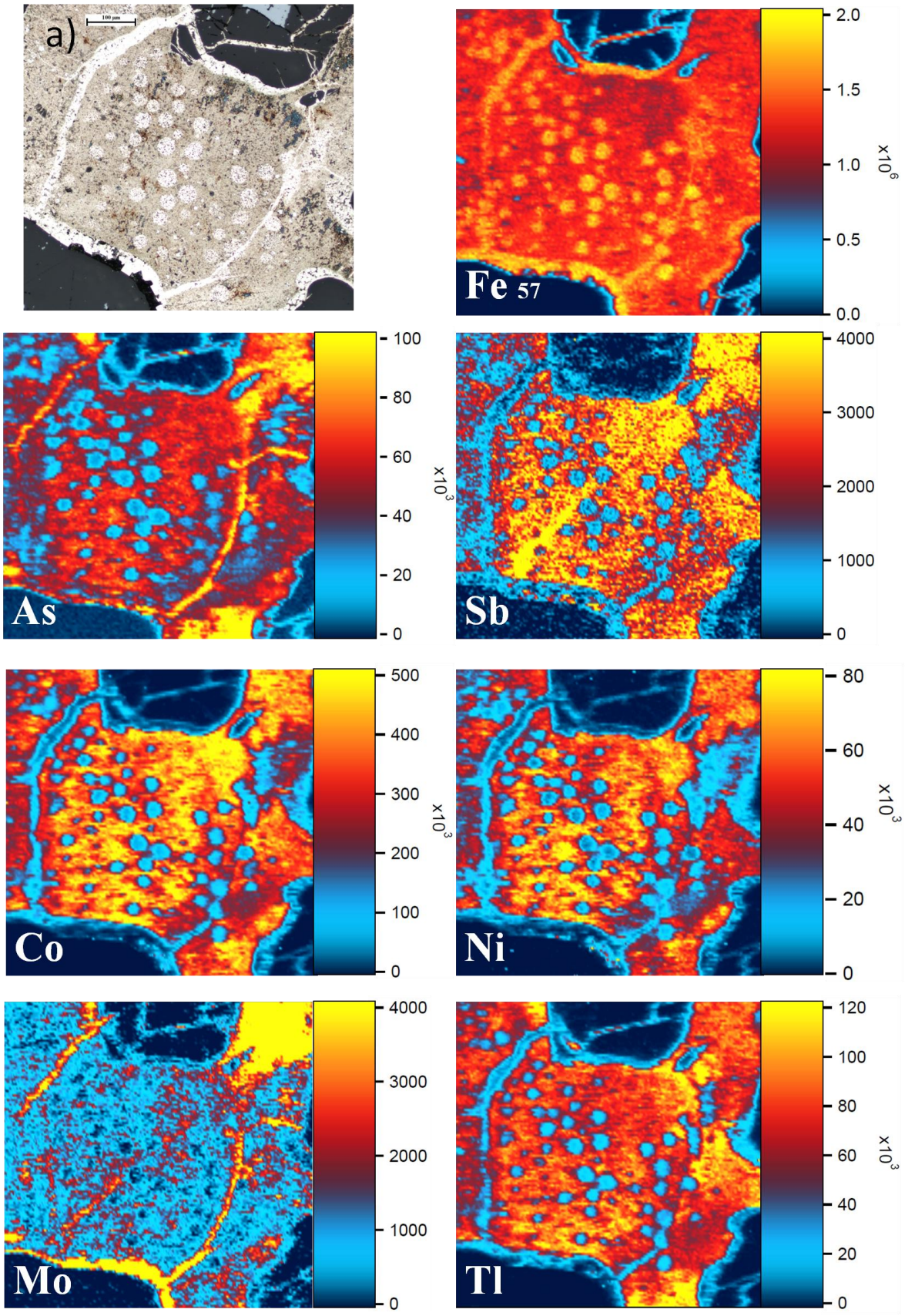

Figure 13: LA-ICP-MS elements maps of an intergrowth of cement, framboidal and veining pyrite from sample EI7 (PRC015, Pepegoona) (a) petrographic image of ablated pyrite displaying authigenic framboids, overgrown by porous pyrite which is subsequently overprinted by veined and cubic pyrite. Throughout the element maps framboids show limited enrichment of As, Sb, Co, Ni and Tl relative to the adjacent veined and cement morphologies. Minor zonation is observable within As and Ni. Porous cement is enriched in As, Sb, Co, Ni and Tl. The late-stage veined pyrite is enriched in As, Mo and intra-vein zonation is apparent on the Co, Ni and Tl maps. The resolution of pyrite mapping was not sufficient to delineate any zonation patterns within cubic infill which displayed compositional zonation on BSE images.

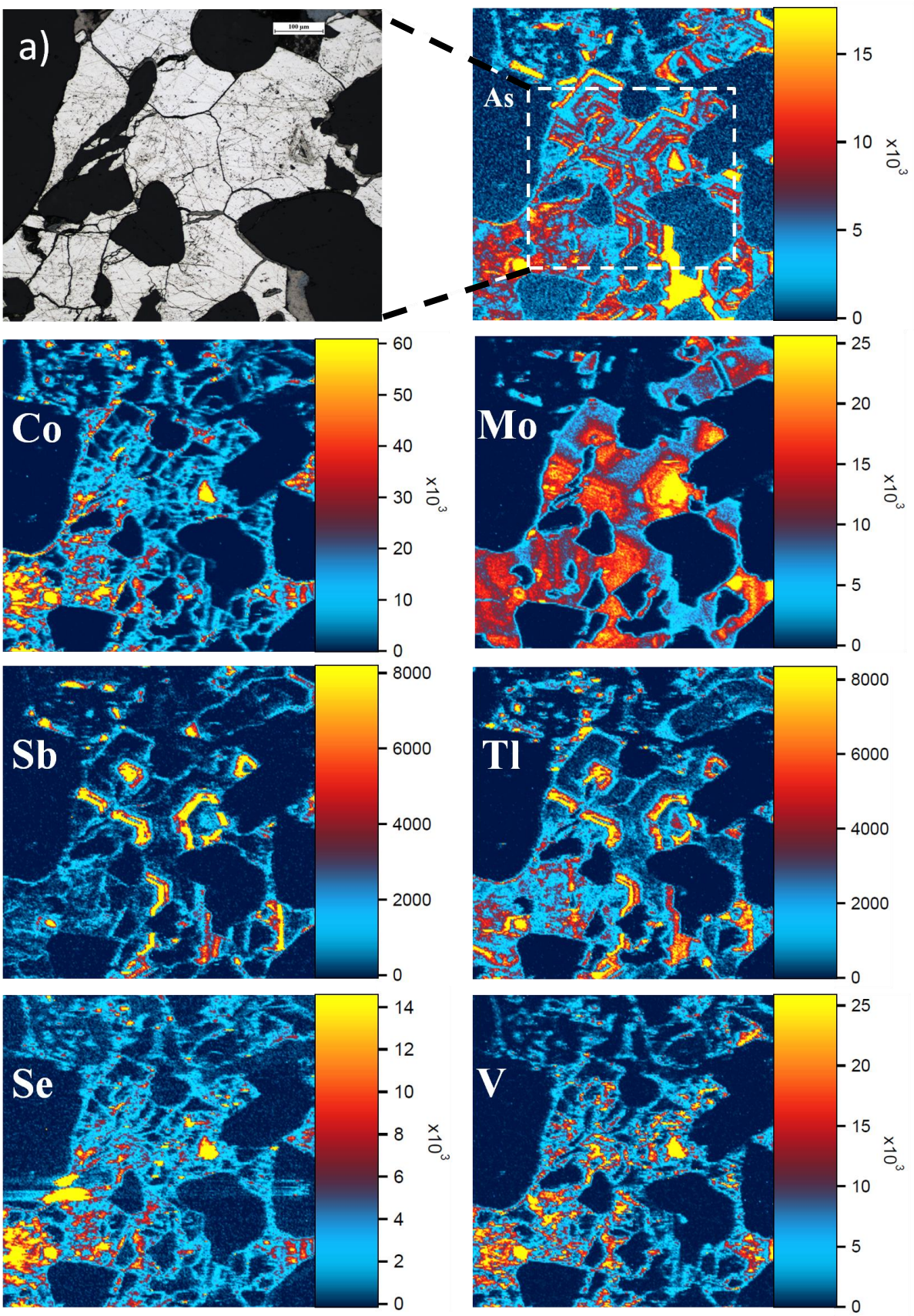

Figure 14: LA-ICP-MS element maps of sample EI11 (PRC023, Pepegoona West) displaying a highly crystalline nature of cement; a) petrographic image of massive pyrite cement on which the analysis was conducted. Cement displays some septian textures associated with hematite replacement. These patterns appears to be nucleic zones for trace element portioning as they are highly enriched in As, Co, Mo, Tl, Se and V. Arsenic displays strong zonation, which correlates with an enrichment in Sb and Tl. Molybdenum displays a gradient of enrichment centred around the nucleic zones. Cobalt, V and Se (and Ni and W not shown) show similar patterns of trace element enrichment.

Electron probe microanalysis of U-bearing minerals aimed to identify any compositional variation present (Appendix D). Analysis was plagued by the porous character of the phases, and the highly inter-grown nature of pyrites and U-bearing phases. This resulted in analytical totals that generally fell well short of 100 % for the mineral likely to be uraninite from textural characterisation and previous studies at Beverley (Wülser *et al.* 2011). Although we cannot rule out the presence of hydrated U-species (of which schoepite, $(UO_2)_8O_2(OH)_{12}.12H_2O$, is the most common) we nevertheless attribute these probe data to uraninite. Minor elements present in the 'better' analyses (totals ~90-93 wt%) include, Ca, Y, La, Ce, K, Fe, Ti, Mg, Si, Al and P, but significantly neither Th nor Pb (Appendix D). The presence of LREE, P and S is suggestive of either limited solid solution, or of sub-micron to nano-scale inclusions of minerals containing these elements. The EPMA study also confirmed the presence of brannerite (U, Ca, Ce)$(Ti, Fe)_2O_6$ (Table 3) and what appears to be a U-Al-bearing silicate (Table 5).

Table 5: EPMA analysis confirming the presence of Brannerite

	wt.%
CaO	2.81
Y_2O_3	0.22
Nd_2O_3	0.27
Sm_2O_3	*0.06
Gd_2O_3	*0.11
Tb_2O_3	*0.15
Er_2O_3	*0.13
Lu_2O_3	*0.07
Nb_2O_5	*0.04
K_2O	*0.18
UO_2	48.73
Fe_2O_3	1.07
TiO_2	43.44
MgO	*0.04
SiO_2	0.48
P_2O_5	0.34
F	1.46
Total	99.59

(* indicates value is below minimum detection limit)

Sulphur isotopic composition

In-situ sulphur isotope analysis was performed on pyrites from across all deposits and results are summarised by Table 6. The $\delta^{34}S$ compositions are broadly heterogeneous, ranging from -43.8 to +32.4‰.

Table 6: Summary of data obtained during *in-situ* sulphur isotope analysis. Despite the limited number of analyses per sample a large variation in sulphur isotopic composition was recorded (Appendix E)

	Sample No.	Pyrite Morpholoy		δ^{33}_{CDT}	Uncertainty	2s	δ^{34}_{CDT}	Uncertainty	2s
Pepegoona	EI3	Framboidal	Min	**-22.72**	0.09	0.19	**-43.87**	0.11	0.21
			Max	**-21.80**	0.15	0.29	**-42.17**	0.16	0.32
			Mean (n=10)	**-22.14**	0.11	0.23	**-42.88**	0.13	0.26
			Std Dev	**0.32**	0.02	0.04	**0.64**	0.02	0.04
	EI7	Framboidal	Min	**-17.47**	0.12	0.23	**-34.11**	0.08	0.16
			Max	**-15.36**	0.17	0.34	**-29.87**	0.21	0.41
			Mean (n=4)	**-16.40**	0.15	0.30	**-31.88**	0.15	0.30
			Std Dev	**0.86**	0.03	0.05	**1.74**	0.06	0.12
Pepegoona West	EI11 (assoc with native Se)	Cement	Min	**13.46**	0.08	0.16	**25.97**	0.07	0.14
			Max	**16.67**	0.18	0.37	**32.40**	0.27	0.53
			Mean (n=16)	**15.16**	0.12	0.24	**29.45**	0.14	0.28
			Std Dev	**0.95**	0.03	0.06	**1.84**	0.05	0.09
	EI12	Porous Cement	Min	**-7.55**	0.09	0.17	**-14.96**	0.12	0.23
			Max	**13.86**	0.15	0.30	**27.01**	0.18	0.36
			Mean (n=20)	**5.64**	0.12	0.25	**10.73**	0.13	0.27
			Std Dev	**7.30**	0.02	0.03	**14.29**	0.01	0.03
Pannikan	EI15	Cement, Anhedral & Framboidal	Min	**-20.72**	0.09	0.18	**-40.18**	0.08	0.15
			Max	**13.66**	0.21	0.43	**26.28**	0.34	0.68
			Mean (n=10)	**-3.27**	0.12	0.25	**-6.74**	0.16	0.31
			Std Dev	**11.22**	0.04	0.08	**21.81**	0.07	0.14
	EI19	Massive Cement	Min	**-2.50**	0.07	0.14	**-5.07**	0.10	0.21
			Max	**-1.68**	0.12	0.24	**-3.68**	0.12	0.25
			Mean (n=14)	**-2.26**	-1.26	-0.26	**-4.54**	1.74	2.74
			Std Dev	**0.21**	0.02	0.03	**0.36**	0.01	0.01
	EI20	Cubic, Euhedral & Overgrowth	Min	**-5.82**	0.07	0.15	**-11.62**	0.05	0.11
			Max	**11.46**	0.22	0.44	**22.19**	0.27	0.53
			Mean (n=20)	**6.89**	0.11	0.22	**13.18**	0.12	0.24
			Std Dev	**4.64**	0.04	0.07	**9.08**	0.06	0.11

δ ratios represent a per mil deviation from the universal standard; *trolilite* from the Canyon Diablo Meteorite (CDT) (0.00‰) (Farquhar & Wing 2003).

Within this unusually broad range of values, distinct populations may nevertheless be recognised (Figure 15). These correlate to some extent, although never exclusively with pyrite morphology. Figure 15, in which $\delta^{34}S$ is plotted against $\delta^{33}S$, displays a large variation is isotopic values both within and among grains and this information may be used to extract information about source and precipitation mechanisms of the sulphur. The S-isotope compositions of the morphologically-distinct framboidal pyrite population (samples EI3 & EI7) show discrete depleted populations in relatively tight clusters. The spread of all framboid $\delta^{34}S$ data ranges between -43.8 and -18.3‰.

Data recorded from other pyrite morphologies, commonly cement, cubic and porous overgrowth (Table 6) display a rather broader spectrum of values. The internal datasets for some samples are commonly highly variable (EI12, EI15 & EI20), while others are tightly clustered (EI11 & EI19). Despite this isotopic complexity, and the large Δ34S of 65.0‰, these S-isotope compositions are enriched relative to framboidal pyrite.

The analyses from homogeneous pyritic cement of sample EI11, from which BSE images showed secondary, overprinting of hematite and elemental Selenium, plot as a tight cluster of highly $\delta^{34}S$-enriched points (Standard deviation of 0.04).
The massive pyrite of sample EI19 which lacked any significant trace element enrichment (Table 2) demonstrated minor (~$\delta^{34}S$ -3.68‰) depletion in $\delta^{34}S$.

Within and among grains from both the visibly homogenous pyrite cement of sample EI15 and the porous pyrite matrix of EI12, variations in $\delta^{34}S$ are largely irregular. These isotopically heterogeneous pyrite types appear to have negligible systematic isotopic variation associated with grain habit, margins or analysis location (Appendix F).

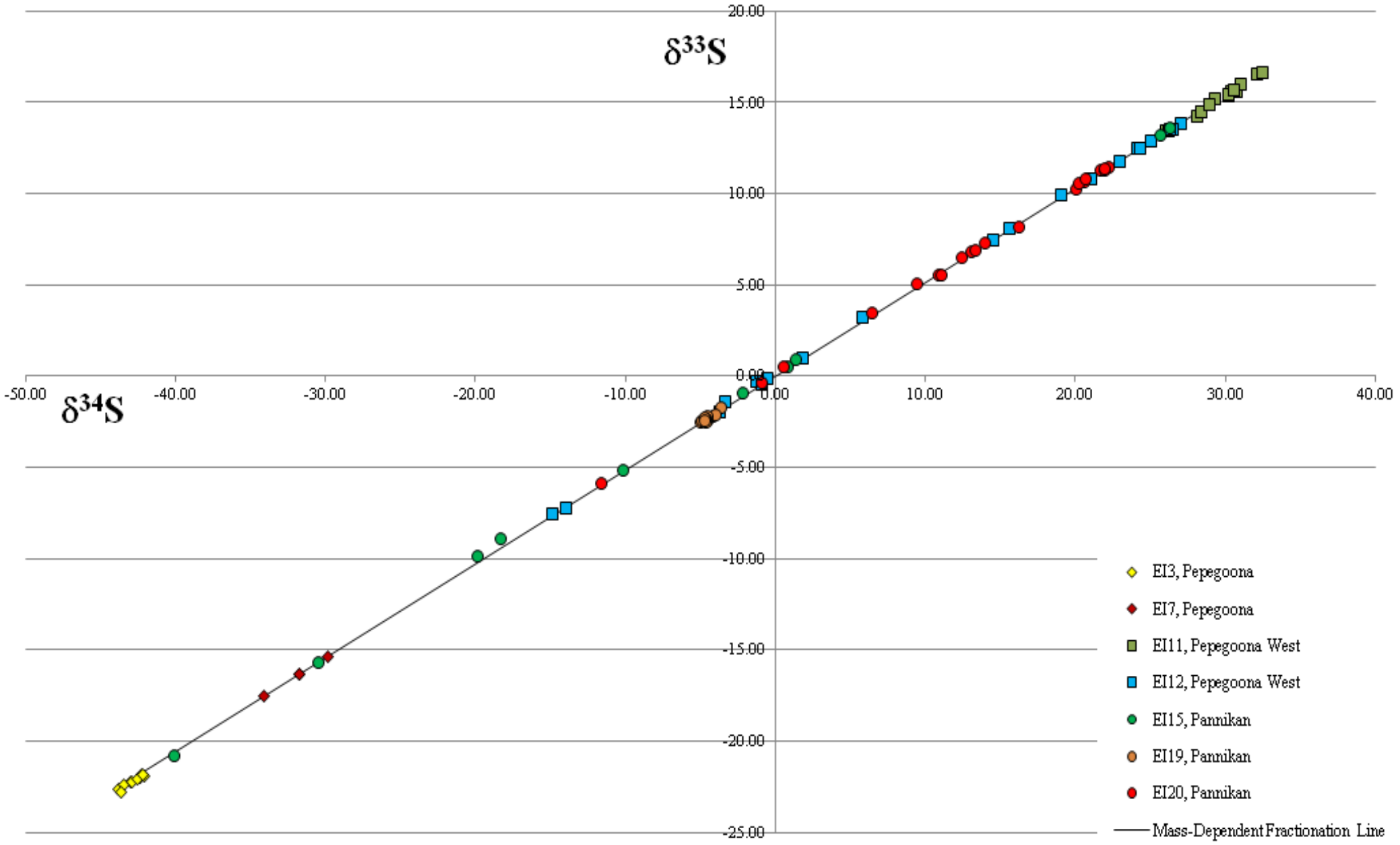

Figure 15: Recorded $\delta^{34}S$ values are displayed against $\delta^{33}S$ values for each individual analysis. Analyses are displayed by sample type and display an association with pyrite morphology (Appendix F). The information displayed by this plot can be used to extract information about the source of the sulphur and the formation processes that affected the pyrite. Despite the limited number of analyses per sample, a large variation of sulphur isotope compositions was recorded. Fit to the MDFL line indicates that all sulphur isotope fractionation was carried out by Mass-Dependent Fractionation processes (Ono *et al.* 2006).

DISCUSSION

The uranium-bearing ore systems of Pepegoona, Pepegoona West and Pannikan are the products of prolonged and evolving hydrothermal flow of uranium enriched fluids in the Lake Frome Region that is likely continuing to the present day (Skirrow 2009, Wülser *et al.* 2011).

The mineralogy and geochemistry of the ores reflect a superposition of a succession of hydrothermal fluids onto an already lithologically-varied sequence of sedimentary rocks. The location of U-mineralisation is controlled by the interplay between sediment permeability, palaeochannel architecture and the proportion of reducing components such as carbonaceous matter and sulphides in the host rock (Skirrow 2009).

Given this complexity, many factors likely influenced the pyrite morphology, trace element geochemistry and isotopic signatures of pyrite across the deposits. The practicability of any vectoring approach to exploration using the trace element chemistry of pyrite depends on understanding both the cause and expression of this variation at a range of scales. The data generated in this study is intended to expand the volume of published data on U-mineralisation at Beverley. The ability to draw new comparisons between the established hydrothermal systems of Beverley and the relatively uncharacterised deposits at Beverley North has positive implications for the understanding of the controls on ore genesis in the regional sedimentary basins. Most importantly, the dataset was obtained using site-specific methods, allowing information to be correlated not only with geological position but also with textures and grain morphology observed at microscopic scale.

Sulphur Sources

New sulphur isotope data for pyrites of the sedimentary uranium systems at Beverley North was obtained with a view toward gaining insights into chemical and physical controls on regional pyrite precipitation.

The $\delta^{34}S$ compositions of the dataset are highly variable (-43.8 to +32.4‰, Figure 15, Table 6). Heterogeneity within datasets is a common feature of sulphur isotope compositions obtained from sedimentary pyrite (e.g. Kohn *et al* (1998)) as sulphur isotope fractionation and the consequent partitioning of light stable isotopes in mineral forming systems is driven by temperature, bacterial reduction, pH and reservoir effects (Fleming & Bekken 1995, Ohmoto & Goldhaber 1997, Ulrich *et al.* 2011). The overall discordance of the data at the regional scale, suggests that multiple mineralisation episodes, with at least two sources of sulphur were involved in pyrite formation (Fleming & Bekken 1995).

The distinct populations observable within the broad dataset correlate to some extent, although not exclusively with pyrite morphology and mineral paragenesis. Where different phases of sulphides occur in close petrographic context, *in-situ* sulphur isotope analysis is capable of sufficient spatial resolution to address these textural variations (Ulrich *et al.* 2011).

Isotopic ratios from morphologically-distinct framboidal pyrites display discrete and largely depleted $\delta^{34}S$ populations (-43.8 to -18.3‰). This depletion in framboidal pyrites is characteristic of a biogenic sulphur source (Schwarcz & Burnie 1973, Raiswell 1982, Seal 2006) with minor differences in the clustered isotopic ratios from different samples reflecting diversity of the reduction processes (Schwarcz & Burnie

1973, Seal 2006). Sulphate-reducing bacteria preferentially select sulphate with light sulphur (Chambers & Trudinger 1979), and organic material in the sedimentary system supplies energy for sulphate reduction (Warren 1972, Beier & Feldman 1991).

Relative to framboidal pyrite, the remaining highly heterogeneous dataset, which represents a range of pyrite morphologies, displays significant $\delta^{34}S$ enrichment. These values are indicative of pyrite mineralisation, developed in disequilibrium in an open system (Seal 2006) and point primarily towards a hydrothermal sulphur source (Thode *et al.* 1953, Kohn *et al.* 1998).

Progressive $\delta^{34}S$ enrichment due to the preferential uptake of lighter sulphur isotopes by pyrite and the mixing of two or more major sources of sulphur during late-stage diagenesis appear likely mechanisms to produce the broad range of $\delta^{34}S$ values observed in the hydrothermal pyrites (Warren 1972, Beier & Feldman 1991). In this case the mixing of sulphur from discrete sources was likely carried out by an interaction between the intrusive rocks of the nearby Mt Painter Domain granites (displaying $\delta^{34}S$ values close to zero) and sediments containing ^{34}S-rich sulphur such as evaporites throughout the Lake Eyre Basin (Ohmoto & Goldhaber 1997, Wülser *et al.* 2011). Migrating hydrothermal fluids of meteoric and magmatic origin likely facilitated these interaction processes.

In addition, these hydrothermal pyrites often appear to be texturally homogenous, with only minor variations in alteration patterns and porosity; however intragranular isotopic variations are common throughout the dataset (e.g. EI12 & EI15). These irregular ratios show no systematic variation by grain habit or morphology, and without in-depth

mapping of the heterogeneous sulphur isotope ratios, they are considered relic of the varied sulphur composition of hydrothermal fluids which underwent mixing processes.

Comparable sulphur isotope data for the Lake Frome Region is limited to large-scale depletions of $\delta^{34}S$ in sulphides observed in the Beverley uranium deposit (Wülser *et al.* 2011). These depletions were interpreted to indicate origin via bacterially-mediated sulphate reduction, possibly in an early diagenetic lacustrine setting (Wülser *et al.* 2011). Whilst analogous data was obtained in the present study, primarily associated with framboidal pyrites; the new expanded set of S-isotopes evidences a more complex evolution of ore-stage sulphides than has previously been proposed. Evidence for multiple sulphur sources with a late hydrothermal component, reinforces the importance of understanding the controls on all stages of pyrite mineralisation in the context of the uranium deposits at Beverley North.

Deposit-scale variations in trace element concentration of pyrite

The non-uniform enrichment of 12 trace elements in pyrite occurs across the uranium deposits of Pepegoona, Pepegoona West and Pannikan. The large standard deviations of individual trace element datasets, as outlined by Table 2 reflect variability in pyrite textural homogeneity, porosity and possible inclusion development.

Arsenic is broadly enriched relative to background levels, across all pyrite morphologies and deposits. Due to its chemical properties it is commonly included into the pyrite lattice by substitution for sulphur (Savage *et al.* 2000, Lowers *et al.* 2007). Other elements such as Co, Ni and Se, present in trace concentrations may also be included into pyrite via similar substitution processes for Fe or S.

The enrichment of trace elements (Fig 10c) in the Pepegoona and Pepegoona West deposits relative to the Pannikan deposit is likely an influence of fluid flow through sandstone horizons and the geometry of both active and palaeoaquifers within the regional sedimentary systems. Fluid properties and flow directions are controlled by the general S-N trend of the Eocene palaeochannels and the distance of each deposit from the U-rich source rocks of the Mt Painter Inlier (Skirrow 2009). These influences on hydrothermal fluid properties are a likely a partial cause of the inter-deposit variations; however such an interpretation does not consider the wide range of extraneous factors which may have influenced enrichment of trace elements in pyrite at a broader scale.

The intra-deposit variation at Pannikan, evidenced by the correlation between As, Co and Ni is associated with the location of the drillhole intersections in the roll-front deposit. Interpretation of deposit models (Figure 11a) and roll-front morphology shows that core PRC021 intersects the roll-front system whilst core PRC022 is located in front of the oxidising system, where hydrothermal fluids have not extensively penetrated. Hence, the relatively barren pyrite observed in samples from PRC022 is a result of the lack of protracted hydrothermal flow at that location. More in-depth modelling of the deposit system is required to make absolute conclusions.

Horizon-scale observations

The enrichment of a mix of trace elements (e.g. Co, Ni, W, Mo, Sb, Tl, Se, As, and V) in pyrite from ore-bearing horizons is likely a result of input into the mineralising hydrothermal fluids from multiple sources.

Cobalt and nickel are commonly associated with fluids derived from a mafic source or have leached a source rock containing these elements (Goldschmidt 1958, Clark *et al.* 2004, Pohl 2011). Likewise, W and Mo are commonly enriched in fluids from a granitic source (Blevin *et al.* 1996), and Sb, Tl, As and V are representative of an influence from organic-rich black shales (Brumsack 2006). Within the geological setting of the Beverley North deposits, all three components are present.

On the same note, broad-scale enrichment of Co, Ni and As across the dataset indicates that these elements were likely sourced by different morphologies from different sources. Their limited enrichment in authigenic pyrites indicates leaching from the host lithologies, whilst their hyper enrichment in hydrothermal pyrite of ore-bearing horizons is indicative of continued compositional variation of the hydrothermal fluids during the progressive evolution of the deposits (Figure 13).

Given these trends, it is interesting to note an apparent negligible relationship between $\delta^{34}S$ values and samples from mineralised horizons. Of the samples analysed from ore-bearing horizons two showed significant $\delta^{34}S$ depletion, which was interpreted as a result of the presence of morphologically-distinct framboidal pyrites in the samples. Analyses made on the third-ore bearing sample, comprised a range of pyrite morphologies and displayed a significantly wider variance in $\delta^{34}S$ values (-40.8 to +26.3‰), with the analysis of a framboidal pyrite aggregate from this sample representing the largest $\delta^{34}S$ depletion.

Comparable, $\delta^{34}S$ heterogeneous but enriched ratios derived from samples taken from non-mineralised horizons would indicate an almost null relationship existing between $\delta^{34}S$ isotopic composition and U-mineralisation. Conversely, it appears that a more consistent relationship between pyrite morphology and sulphur source exists.

Further to this conclusion, we infer that the elevated levels in trace elements as observed across the sample set are independent of the sulphur source (i.e. most metals were derived from a range of different sources). In such a scenario, it is likely that the trace element enrichment in the pyrites of mineralised horizons was inherited from both the (epigenetic) fluid transporting uranium into the basin and proximal sedimentary lithologies.

Pyrite Morphology and Textures

Textural characterisation led to the recognition of four broad morphological groups of pyrite.

Framboidal pyrite is observed throughout the sample suite and is comparable with the distinct aggregates described by Wilkin & Barnes (1997). The widespread preservation of framboidal pyrite throughout the samples is dependent on two factors; isolation of framboids from the influence of the external diagenetic environment and the interruption of the supply of at least one essential compound in the mineralising fluid (Fe and/or H_2S) (Sawlowicz 1993).

Both LA-ICP-MS spot analysis and element mapping display limited enrichment of trace elements in framboidal pyrite relative to other pyrite morphologies (Figure 13). This limited enrichment and some minor zonation in As, Co and Ni at aggregate edges indicate that trace elements were supplied to the system during authigenic growth by the sandstone host lithology. The presence of iron oxide minerals with relic framboidal textures in oxidised sandstones and the lack of rounded pyrite morphologies makes it unlikely that detrital deposition of pyrite into the host sandstone occurred.

Repeated observations of framboidal pyrite overgrown by hydrothermal pyrite cements and U-bearing minerals, as well as the depleted $\delta^{34}S$ values and limited trace element enrichment, permits the interpretation of this authigenic pyrite as initial pre-ore pyrite.

Sawlowicz (1993) commented on a possible genetic relationship between framboidal and euhedral pyrite. The author considers framboidal pyrite to exist in a metastable state on which different mechanisms may act to result in the homogenisation of framboids into euhedral crystals. This process of transformation is a result of a trend to minimise surface energy (Sawlowicz 1993). Observance of different phases of framboidal pyrite in the present study (Figure 4e & f) is considered indirect evidence for such a hypothesis. The new pyrite may show variations in chemical properties resulting from inherited trace element and isotopic signatures. The massive cubic pyrites with porous centres (Figure 5c) are seemingly consistent with this hypothesis and show negligible trace element enrichment and mixed sulphur isotopic data possibly as a result of diagenetic recrystallisation processes during the transformation of framboids to euhedra.

Protracted ore-stage hydrothermal pyrite precipitation, and possible late-stage diagenetic recrystallisation is evident from the element maps of EI7 and EI11 (Figure 13 & 14). Examples of compositional zonation demonstrate an evolution of hydrothermal fluid composition and/or variation in physiochemical conditions of sulphide precipitation throughout formation of ore-stage pyrite (Belcher *et al.* 2004). The resolution of element mapping does not allow delineation as to what extent this compositional zonation is associated with the oscillatory zonation patterns observed in multiple samples by BSE images.

Limited Fe enrichment in zones commonly observed intergrown with U-minerals indicates the likelihood of the porous pyrite cement hosting other, possibly ore-bearing minerals (Figure 13). Despite this lack of pyrite purity, these observations support earlier conclusions that the majority of trace element enrichment resulted from the penetration of the U-bearing hydrothermal fluids into the sedimentary systems. Furthermore, widespread titanium minerals (Figure 9a & b), the presence of brannerite and the negligible enrichment of titanium as a trace element in pyrite indicates that the authigenic Ti-oxides (ilmenite and rutile) supplied Ti to the system.

Native selenium

The observation of native selenium at Beverley North provides insight into late-stage mineralisation processes (Figure 7). Native selenium is a rare mineral only recognised in a dozen or so localities around the world, many of them sandstone-hosted U-bearing ore systems (Simon *et al.* 1997, Zhu *et al.* 2012). Its presence at Pepegoona West is probably the first recorded observance in Australia. The mobility and bioavailability of selenium in the environment is strongly dependent on redox transformations, and it may be mobilised into fluids at very-low temperatures (Johnson *et al.* 1999, Zhu *et al.* 2004, Chen *et al.* 2006, Zhu *et al.* 2012).

In this instance, the ubiquitous siderophile minerals of the Beverley North system, such as pyrite and Fe-(Ti)-oxides are considered the likely source for the selenium. Both minerals are known for their capacity to control the geochemical behaviour and occurrence of selenium in both reducing and oxidising environments (Howard 1977). Additionally, selenium is commonly incorporated into sulphides as a stoichiometric substitution for sulphur (Howard 1977).

It is considered that the localised occurrence of native Se is a result of oxidation of Se-bearing pyrites, followed by mobilisation and subsequent reduction of Se oxy-anions (selenate and selenite) by microorganisms in the presence of Fe^{2+}-bearing minerals such as Fe-oxides or pyrite (Garbisu *et al.* 1996, Zhu *et al.* 2004, Chen *et al.* 2006, Zhu *et al.* 2012).

The oxidation of the pyrite cements and subsequent reprecipitation likely caused the significant compositional zonation observed in terms of trace element enrichment (Figure 14). Trace element enrichment appears to nucleate from distinct zones of hematitic alteration, with Se almost exclusively enriched in these areas. Marked enrichment also occurs in As, Co, Ni, V, Mo, Sb and W; all of which were likely introduced to the system by protracted stages of hydrothermal mineralisation. It is interesting to note that Co, Ni, V and W, the enrichment of which is almost exclusive to the hematitic alteration zones, are also minor constituents of hematite.

Precipitation of native selenium and associated hematite is a late-stage event in the genesis of the Beverley North deposits. The inflow of Se-rich hydrothermal fluids facilitated by the porosity of the sandstone, pervasively micro-fractured pre-existing mineral assemblages and precipitated the native selenium into the zones of deformation. Sulphur isotopic compositions taken from associated pyrite cement displayed a tight cluster of $\delta^{34}S$ (~ +29.5‰) values, the highest of the dataset (Figure 15). This clustering provides further evidence for the final-stage character of the oxidising fluids associated with secondary mineral precipitation.

It is conceivable that the oxidising fluid had some effect on inherited $\delta^{34}S$ values either as a result of primary in-homogeneity in the pyrite or due to fractionation during dissolution and preferential incorporation of the heavier isotopes (^{34}S) during diagenetic recrystallisation.

Representivity of the dataset

Compositional, textural and chemical heterogeneity occurs throughout the ore-bearing system at every scale. This was evident in the analytical datasets which display broad morphological variation, non-uniform trace element enrichment and a large range of sulphur isotopic compositions. Such high variance may reduce the usefulness of the mean values in characterising the population (Dawson & Sinclair 1974, Ryall 1977).

The relatively small size of the sample set influences its value for petrogenetic interpretation and raises questions about its effectiveness as a representation of the mineralised systems (e.g. Winderbaum *et al* (2012)).While this is likely one factor contributing to the apparent variance across the datasets, the inherent variability within the open system which has undergone protracted mineralisation must be taken into account.

The complexities of the patterns recognised in the acquired data and the lack of supporting data for the region, places limitations on the interpretations which can be drawn from this study. Further detailed study to support the data acquired by this project is required before more specific conclusions about the implications of deposit genesis for uranium exploration can be fully understood.

CONCLUSIONS

Outcomes of this study provide the basis for the following preliminary paragenetic scheme of the sandstone-hosted uranium deposits of Pepegoona, Pepegoona West and Pannikan. This new genetic model is based on data obtained by multiple analytical techniques considered in the context of archetypal sandstone-hosted uranium deposits and known mineralisation models for the proximal Beverley uranium deposit.

Fine-grained pre-ore pyrite is ubiquitous throughout sedimentary ore-bearing systems at Beverley North. Widespread framboidal pyrite aggregates of authigenic provenance display strongly-depleted $\delta^{34}S$ signatures indicative of a discrete biogenic sulphur source, consistent with the accepted biogenic mechanisms of syn-sedimentary pyrite formation (Wilkin & Barnes 1997). Progressive phases of aggregate growth observed throughout the sample suite evidence a genetic relationship between framboidal and euhedral pyrites and surrounding host lithologies acted as a geochemical source during authigenic growth. Diagenetic recrystallisation during continued pyrite growth is a likely factor in the limited trace element concentrations of these pyrites.

Protracted flow of low-temperature hydrothermal fluids into the basin introduced uranium and other trace elements. These fluids of both meteoric and magmatic origin evolved over time from a variety of sources (mafic and granitic influences within the Mt. Painter Domain) and became progressively ^{34}S-enriched due to preferential uptake of lighter sulphur isotopes during ore-stage pyrite precipitation. Interaction of these fluids with pre-existing pyrite occurred as they moved down-dip along palaeochannels and aquifers led to extensive mixing, remobilisation and cycles of overprinting,

expressed in the sample suite as oscillatory trace element zonation and non-systematic variation in S-isotope signature.

The final stage saw inflow of highly ^{34}S enriched oxidising fluids, causing replacement and recrystallisation of pre-existing pyrite, mobilisation of selenium and precipitation of hematite and native selenium within porous sandstone.

The results of this study strongly suggest that the trace element composition of pyrite can represent the basis of a future vectoring approach to exploration. The definition of multiple sources of sulphur in the ore-bearing systems at Beverley North, combined with recognition that uranium transportation takes place solely by trace element enriched hydrothermal fluids (with both granitic and mafic influence), represents a major step towards an integrated genetic model for the deposits.

ACKNOWLEDGMENTS

I sincerely thank my supervisor A/Professor Nigel Cook, for his guidance and enthusiasm throughout the year. His continued advice and ideas on the interpretation of data, direction of the project made the outcomes of this project possible.
I would also like to thank Heathgate Resources for their sponsorship. I particularly thank Adam Huddleston, Horst Märten and Andrea Marsland-Smith for their ongoing interest and support in the outcomes of this project.
Analytical work was made possible by Ben Wade, Angus Netting and the staff at Adelaide Microscopy. Their training, advice and ongoing help with analytical interpretation are greatly appreciated.
Guidance and laboratory access for sulphur isotope analysis was kindly given my John Cliff, Centre for Microscopy, Characterisation & Analysis, UWA.
Pontifex & associates are thanked for their careful and timely preparation of samples.
I would finally like to thank Carla Zammit for her assistance in the field, Katie Howard for advice on all aspects of the project and members of the honours cohort for their helpful peer reviewing.

REFERENCES

ABRAITIS P. K., PATTRICK R. A. D. & VAUGHAN D. J. 2004. Variations in the compositional, textural and electrical properties of natural pyrite: a review. *International Journal of Mineral Processing* **74**, 41-59.

BARRIE C. D., BOYCE A. J., BOYLE A. P., WILLIAMS P. J., BLAKE K., OGAWARA T., AKAI J. & PRIOR D. J. 2009. Growth controls in colloform pyrite. *American Mineralogist* **94**, 415-429.

BEIER J. A. & FELDMAN H. R. 1991. Sulfur isotopes and paragenesis of sulfide minerals in the Silurian Waldron Shale, southern Indiana. *Geology* **19**, 389-392.

BELCHER R. W., ROZENDAAL A. & PRZYBYLOWICZ W. J. 2004. Trace element zoning in pyrite determined by PIXE elemental mapping: evidence for varying ore–fluid composition and electrochemical precipitation of gold at the Spitskop deposit, Saldania Belt, South Africa. *X-Ray Spectrometry* **33**, 174-180.

BENDALL C., LAHAYE Y., FIEBIG J., WEYER S. & BREY G. P. 2006. In situ sulfur isotope analysis by laser ablation MC-ICPMS. *Applied Geochemistry* **21**, 782-787.

BERNER R. A. 1984. Sedimentary pyrite formation: An update. *Geochimica et Cosmochimica Acta* **48**, 605-615.

BLEVIN P. L., CHAPPELL B. W. & ALLEN C. M. 1996. Intrusive metallogenic provinces in eastern Australia based on granite source and composition. *Earth and Environmental Science Transactions of the Royal Society of Edinburgh* **87**, 281-290.

BRUGGER J., LONG N., MCPHAIL D. C. & PLIMER I. 2005. An active amagmatic hydrothermal system: The Paralana hot springs, Northern Flinders Ranges, South Australia. *Chemical Geology* **222**, 35-64.

BRUGGER J., WULSER P. A. & FODEN J. 2011. Genesis and Preservation of a Uranium-Rich Paleozoic Epithermal System with a Surface Expression (Northern Flinders Ranges, South Australia): Radiogenic Heat Driving Regional Hydrothermal Circulation over Geological Timescales. *Astrobiology* **11**, 499-508.

BRUMSACK H.-J. 2006. The trace metal content of recent organic carbon-rich sediments: Implications for Cretaceous black shale formation. *Palaeogeography, Palaeoclimatology, Palaeoecology* **232**, 344-361.

BUTLER I. B., BÖTTCHER M. E., RICKARD D. & OLDROYD A. 2004. Sulfur isotope partitioning during experimental formation of pyrite via the polysulfide and hydrogen sulfide pathways: implications for the interpretation of sedimentary and hydrothermal pyrite isotope records. *Earth and Planetary Science Letters* **228**, 495-509.

BUTLER I. B., RICKARD D. & GRIMES S. 2000. Framboidal Pyrite: Self Organisation in the Fe-S System. *Journal of Conference Abstracts* **5**, 276-277.

CHAMBERS L. A. & TRUDINGER P. A. 1979. Microbiological fractionation of stable sulfur isotopes; a review and critique. *Geomicrobiology Journal* **1**, 249-293.

CHEN Y.-W., LI L., D'ULIVO A. & BELZILE N. 2006. Extraction and determination of elemental selenium in sediments—A comparative study. *Analytica Chimica Acta* **577**, 126-133.

CLARK C., GRGURIC B. & MUMM A. S. 2004. Genetic implications of pyrite chemistry from the Palaeoproterozoic Olary Domain and overlying Neoproterozoic Adelaidean sequences, northeastern South Australia. *Ore Geology Reviews* **25**, 237-257.

COOK N. J., CIOBANU C. L. & MAO J. 2009. Textural control on gold distribution in As-free pyrite from the Dongping, Huangtuliang and Hougou gold deposits, North China Craton (Hebei Province, China). *Chemical Geology* **264**, 101-121.

DAWSON K. M. & SINCLAIR A. J. 1974. Factor Analysis of Minor Element Data for Pyrites, Endako Molybdenum Mine, British Columbia, Canada. *Economic Geology* **69**, 404-411.

ELBURG M. A., BONS P. D., FODEN J. & BRUGGER J. 2003. A newly defined Late Ordovician magmatic-thermal event in the Mt Painter Province, Northern Flinders Ranges, South Australia. *Australian Journal of Earth Sciences* **50**, 611-631.

FARQUHAR J. & WING B. A. 2003. Multiple sulfur isotopes and the evolution of the atmosphere. *Earth and Planetary Science Letters* **213**, 1-13.

FLEMING R. H. & BEKKEN B. M. 1995. Isotope ratio and trace element imaging of pyrite grains in gold ores. *International Journal of Mass Spectrometry and Ion Processes* **143**, 213-224.

FODEN J., ELBURG MARLINA A., JON D. P. & BURTT A. 2006. The Timing and Duration of the Delamerian Orogeny: Correlation with the Ross Orogen and Implications for Gondwana Assembly. *The Journal of Geology* **114**, 189-210.

FOLK R. L. 2005. Nannobacteria and the formation of framboidal pyrite: Textural evidence. *Journal of Earth System Science* **114**, 369-374.

GALLOWAY W. E. 1978. Uranium mineralization in a coastal-plain fluvial aquifer system; Catahoula Formation, Texas. *Economic Geology* **73**, 1655-1676.

GARBISU C., ISHII T., LEIGHTON T. & BUCHANAN B. B. 1996. Bacterial reduction of selenite to elemental selenium. *Chemical Geology* **132**, 199-204.

GOLDHABER M. B. & KAPLAN I. R. 1980. Mechanisms of sulfur incorporation and isotope fractionation during early diagenesis in sediments of the gulf of California. *Marine Chemistry* **9**, 95-143.

GOLDSCHMIDT V. M. 1958. *Geochemistry*. The Clarendon Press, UK.

GRANGER H. C. & WARREN C. G. 1969. Unstable sulfur compounds and the origin of roll-type uranium deposits. *Economic Geology* **64**, 160-171.

GROSS E. B. 1956. Mineralogy and paragensis of the uranium ore, Mi Vida Mine, San Juan County, Utah. *Economic Geology* **51**, 632-648.

HEATHGATE RESOURCES 2012. Heathgate Resources: The Beverley Mine <http://www.heathgate.com.au/thebeverleymine.html>. (retrieved 02 September 2012).

HILL S. M. & HORE S. B. 2010. Overview of Regolith and Landscape Evolution of the Arkaroola Wilderness Sanctuary, northern Flinders Ranges, South Australia. First Australian Regolith Geoscientists Conference, Arkaroola, South Australia (unpubl.).

HILL S. M. & HORE S. B. 2011. Key insights into range-front mineral system expression and evolution from regolith and long-term landscape history, NE Flinders Ranges. *MESA Journal* **63**, 20-31.

HOBDAY D. K. & GALLOWAY W. E. 1999. Groundwater processes and sedimentary uranium deposits. *Hydrogeology Journal* **7**, 127-138.

HOEFS J. 2009. *Stable Isotope Geochemistry* (Sixth ed. edition). Springer-Verlag, Berlin, Heidelberg. .

HORE S. B. & HILL S. M. 2010. Overview of the Geological history of the Arkaroola Wilderness Sanctuary, northern Flinders Ranges, South Australia. First Australian Regolith Geoscientists Conference, Arkaroola, South Australia (unpubl.).

HOWARD J. H. 1977. Geochemistry of selenium: formation of ferroselite and selenium behavior in the vicinity of oxidizing sulfide and uranium deposits. *Geochimica et Cosmochimica Acta* **41**, 1665-1678.

JAIRETH S., MCKAY A. & LAMBERT I. 2008. Association of large sandstone uranium deposits with hydrocarbons; The geology of uranium deposits in Kazakhstan points to similar deposits in Australia. *AUSGEO News*, 1-6.

JOHNSON T. M., HERBEL M. J., BULLEN T. D. & ZAWISLANSKI P. T. 1999. Selenium isotope ratios as indicators of selenium sources and oxyanion reduction. *Geochimica et Cosmochimica Acta* **63**, 2775-2783.

JOHNSTON D. T. 2011. Multiple sulfur isotopes and the evolution of Earth's surface sulfur cycle. *Earth-Science Reviews* **106**, 161-183.

KOHN M. J., RICIPUTI L. R., STAKES D. & ORANGE D. L. 1998. Sulfur isotope variability in biogenic pyrite; reflections of heterogeneous bacterial colonization? *American Mineralogist* **83**, 1454-1468.

LAMBERT I., JAIRETH S., MCKAY A. & MIEZITIS Y. 2005. Australia's uranium endowment: Metallogeny, exploration and potential

Mineral Deposit Research: Meeting the Global Challenge. *In:* Mao J. & Bierlein F. P. eds., pp 281-284, Springer Berlin Heidelberg.

LANDAIS P. 1996. Organic geochemistry of sedimentary uranium ore deposits. *Ore Geology Reviews* **11**, 33-51.

LOWERS H. A., BREIT G. N., FOSTER A. L., WHITNEY J., YOUNT J., UDDIN M. N. & MUNEEM A. A. 2007. Arsenic incorporation into authigenic pyrite, Bengal Basin sediment, Bangladesh. *Geochimica et Cosmochimica Acta* **71**, 2699-2717.

MÄRTEN H., PHILLIPS R. & WOODS P. 2012. New Uranium ISR Satellites at Beverley North, South Australia

The New Uranium Mining Boom. *In:* Merkel B. & Schipek M. eds., pp 23-30, Springer Berlin Heidelberg.

MCLAREN S., DUNLAP W. J., SANDIFORD M. & MCDOUGALL I. 2002. Thermochronology of high heat-producing crust at Mount Painter, South Australia: Implications for tectonic reactivation of continental interiors. *Tectonics* **21**.

MIN M., CHEN J., WANG J., WEI G. & FAYEK M. 2005a. Mineral paragenesis and textures associated with sandstone-hosted roll-front uranium deposits, NW China. *Ore Geology Reviews* **26**, 51-69.

MIN M., XU H., CHEN J. & FAYEK M. 2005b. Evidence of uranium biomineralization in sandstone-hosted roll-front uranium deposits, northwestern China. *Ore Geology Reviews* **26**, 198-206.

NEUMANN N., SANDIFORD M. & FODEN J. 2000. Regional geochemistry and continental heat flow: implications for the origin of the South Australian heat flow anomaly. *Earth and Planetary Science Letters* **183**, 107-120.

OHMOTO H. & GOLDHABER M. B. 1997. Applications of sulfur and carbon isotopes in ore deposit research, *in* Barnes, H.L., ed., Geochemistry of hydrothermal ore deposits (third edition): New York, John Wiley & Sons. p. 517-611.

ONO S., WING B., JOHNSTON D., FARQUHAR J. & RUMBLE D. 2006. Mass-dependent fractionation of quadruple stable sulfur isotope system as a new tracer of sulfur biogeochemical cycles. *Geochimica et Cosmochimica Acta* **70**, 2238-2252.

PIRLO M. C. & GIBLIN A. M. 2004. Application of groundwater–mineral equilibrium calculationsto geochemical exploration for sediment-hosted uranium:observations from the Frome Embayment,South Australia. *Geochemistry: Exploration, Environment, Analysis* **4**, 113-127.

POHL W. L. 2011. *Economic Geology: Principles and Practice*. Wiley-Blackwell, West Sussex, UK.

RAISWELL R. 1982. Pyrite texture, isotopic composition and the availability of iron. *American Journal of Science* **82**, 1244-1263.

REYNOLDS R. L. & GOLDHABER M. B. 1983. Iron disulfide minerals and the genesis of roll-type uranium deposits. *Economic Geology* **78**, 105-120.

RIDLEY W. I. & LICHTE E. E. (Editors) 1998. *Major, trace and ultratrace element analysis by laser ablstaion ICP-MS.* (Reviews in Economic Geology, Vol. 7).

RYALL W. R. 1977. Anomalous trace elements in pyrite in the vicinity of mineralized zones at Woodlawn, N.S.W., Australia. *Journal of Geochemical Exploration* **8**, 73-83.

SAVAGE K. S., TINGLE T. N., O'DAY P. A., WAYCHUNAS G. A. & BIRD D. K. 2000. Arsenic speciation in pyrite and secondary weathering phases, Mother Lode gold district, Tuolumne County, California. *Applied Geochemistry* **15**, 1219-1244.

SAWLOWICZ Z. 1993. Pyrite framboids and their development: a new conceptual mechanism. *Geologische Rundschau* **82**, 148-156.

SCHWARCZ H. P. & BURNIE S. W. 1973. Influence of sedimentary environments on sulfur isotope ratios in clastic rocks: a review. *Mineralium Deposita* **8**, 264-277.

SCHWARTZ G. M. 1951. Classification and definitions of textures and mineral structures in ores. *Economic Geology* **46**, 578-591.

SCOTT R. J., MEFFRE S., WOODHEAD J., GILBERT S. E., BERRY R. F. & EMSBO P. 2009. Development of Framboidal Pyrite During Diagenesis, Low-Grade Regional Metamorphism, and Hydrothermal Alteration. *Economic Geology* **104**, 1143-1168.

SEAL R. R. 2006. Sulfur Isotope Geochemistry of Sulfide Minerals. *Reviews in Mineralogy and Geochemistry* **61**, 633-677.

SIMON G., KESLER S. E. & ESSENE E. J. 1997. Phase relations among selenides, tellurides, and oxides; II, Applications to selenide-bearing ore deposits. *Economic Geology* **92**, 468-484.

SKIRROW R. G. 2009. *Uranium ore-forming systems of the Lake Frome region, South Australia: Regional spatial controls and exploration criteria*. Australia G. **2009/040**. Geoscience Australia.

STOIAN L. M. 2010. Palynology of Mesozoic and Cenozoic sediments of the Eromanga and Lake Eyre basins: results from recent drilling in the northwest Frome Embayment. *MESA Journal* **57**, 27-35.

THODE H. G., MACNAMARA J. & FLEMING W. H. 1953. Sulphur isotope fractionation in nature and geological and biological time scales. *Geochimica et Cosmochimica Acta* **3**, 235-243.

ULRICH T., LONG D. G. F., KAMBER B. S. & WHITEHOUSE M. J. 2011. In Situ Trace Element and Sulfur Isotope Analysis of Pyrite in a Paleoproterozoic Gold Placer Deposit, Pardo and Clement Townships, Ontario, Canada. *Economic Geology* **106**, 667-686.

WALKER S. 1999. Beverley uranium project - in situ mining approved. *MESA Journal* **13**, 8-10.

WARREN C. G. 1972. Sulfur Isotopes as a Clue to the Genetic Geochemistry of a Roll-Type Uranium Deposit. *Economic Geology* **67**, 759-767.

WILKIN R. T. & BARNES H. L. 1997. Formation processes of framboidal pyrite. *Geochimica et Cosmochimica Acta* **61**, 323-339.

WILKIN R. T., BARNES H. L. & BRANTLEY S. L. 1996. The size distribution of framboidal pyrite in modern sediments: An indicator of redox conditions. *Geochimica et Cosmochimica Acta* **60**, 3897-3912.

WILSON S. A., RIDLEY W. I. & KOENIG A. E. 2002. Development of sulfide calibration standards for the laser ablation inductively-coupled plasma mass spectrometry technique. *Journal of Analytical Atomic Spectrometry* **17**, 406-409.

WINDERBAUM L., CIOBANU C., COOK N., PAUL M., METCALFE A. & GILBERT S. 2012. Multivariate Analysis of an LA-ICP-MS Trace Element Dataset for Pyrite. *Mathematical Geosciences* **44**, 823-842.

WÜLSER P.-A., BRUGGER J., FODEN J. & PFEIFER H.-R. 2011. The Sandstone-Hosted Beverley Uranium Deposit, Lake Frome Basin, South Australia: Mineralogy, Geochemistry, and a Time-Constrained Model for Its Genesis. *Economic Geology* **106**, 835-867.

ZHU J.-M., JOHNSON T. M., FINKELMAN R. B., ZHENG B.-S., SÝKOROVÁ I. & PEŠEK J. 2012. The occurrence and origin of selenium minerals in Se-rich stone coals, spoils and their adjacent soils in Yutangba, China. *Chemical Geology* **330–331**, 27-38.

ZHU J., ZUO W., LIANG X., LI S. & ZHENG B. 2004. Occurrence of native selenium in Yutangba and its environmental implications. *Applied Geochemistry* **19**, 461-467.

APPENDIX A: SAMPLE LOCATIONS

Sample Number	Location	Depth	Description
EI 1	EI12.4 Pepegoona PRC012	216.3	Light grey to brown, medium grained quartz sandstone, with distinct colour boundaries across sample, some angular blocky pyrite dispersed throughout
EI 2	EI12.5 Pepegoona PRC012	247.02	Medium grey, fine to very fine grained, clay rich siltstone, large amounts of fine grained pyrite in matrix
EI 3	EI13.3 Pepegoona PRC013	201.7	Dark grey, fine to very fine grained quartz rich sandstone, well sorted medium grained pyrite throughout entire sample
EI 4	EI13.4 Pepegoona PRC013	204	Light grey to brown coarse grained quartz rich clast supported sandstone, with few >5mm lithic inclusions, minimal fine – very fine grained pyrite poorly sorted throughout silty matrix
EI 5	EI13.5 Pepegoona PRC013	206.21	Dark grey quartz sandstone, matrix supported, abundant fine grained pyrite in silty matrix
EI 6	EI15.1 Pepegoona PRC015	203.9	Coarse grained, quartz rich sandstone, light grey/white, angular blocky pyrite
EI 7	EI15.3 Pepegoona PRC015	219.2	Coarse grained, quartz sandstone, fine grained pyrite throughout, some sulphur alteration
EI 8	EI15.5 Pepegoona PRC015	222.6	Large amounts of visible medium grained pyrite in dark grey coarse grained, quartz sandstone
EI 9	EI15.6 Pepegoona PRC015	231.25	Dark grey quartz rich sandstone, fine grained well sorted abundant pyrite, some pyrite veins up to 1mm wide
EI 10	EI23.2 Pepegoona West PRC023	241.14	Light to medium grey fine grained siltstone, with pockets of unconsolidated sands, small amount of very fine grained pyrite throughout
EI 11	EI23.4 Pepegoona West PRC023	253	Coarse grained quartz sandstone, some dark grey brown silty matrix, well sorted blocky angular medium pyrite grains throughout, some sulphur staining (not associated with pyrite)
EI 12	EI23.5 Pepegoona West PRC023	257.2	Minimal, very fine grained pyrite, commonly associated with lignite and reduced areas
EI 13	EI23.6 Pepegoona West PRC023	269.1	Large amounts of medium grained pyrite between coarse grained quartz clasts of the sandstone
EI 14	EI21.2 Pannikan PRC021	222.5	Medium grey to brown, fine to medium grained, clast supported quartz sandstone, with minimal fine grained angular blocky pyrite poorly sorted
EI 15	EI21.6	260.4	Light grey coarse quartz sandstone, silty matrix supported,

	Pannikan PRC021		small amounts of fine grained pyrite, bordered by dark grey matrix supported sandstone with abundant fine to medium grained angular blocky pyrite along the contact
EI 16	EI22.1 Pannikan PRC022	228.1	Coarse grained quartz sandstone, some silty matrix, clast supported, fine grained pyrite veining up to 5mm in width
EI 17	EI22.3 Pannikan PRC022	244.18	Light grey, silica rich siltstone, small 1mm dark veins are very fine grained pyrite, some platey fine grained muscovite
EI 18	EI22.4 Pannikan PRC022	263.55	Transition zone from light grey clay siltstone to dark grey quartz sandstone, lithic inclusions and large pyrite grains (in siltstone), fine grained pyrite associated with grain and transition boundaries
EI 19	EI22.5 Pannikan PRC022	265.4	Large pyrite grains in light grey clay rich silstone
EI 20	EI22.6 Pannikan PRC022	264.4	Large dark grey lithic inclusion, approx 2.5cm in diameter with medium to coarse grained angular blocky pyrite grains, set in quartz rich clay siltstone, with large angular blocky pyrite grains associated with boundaries

Sample Number	**Location**	**Depth**	**Description**
EI21	EI12.1 Pepegoona PRC012	191.09 m	Namba/Eyre Unconformity, fine to medium grained, light whitish cream, quartz rich sandstone, clast supported, well sorted
EI22	EI12.2 Pepegoona PRC012	204.4 m	Dark grey to black, fine to medium grained, unconsolidated, sub to well rounded, hydrocarbon stained quartz rich sands, well sorted
EI23	EI12.3 Pepegoona PRC012	213.3 m	Coal pet, dark grey brown, very fine grained hydrocarbon stained, siltsone/mudstone, inclusions of lignites and organic content, blocky black shiny organic inclusions
EI24	EI12.6 Pepegoona PRC012	247.04 m	Light grey, very fine silty clay mudstone, some small pockets of coarse grained, subrounded quartz rich unconsolidated sands in silty grey matrix, top of Bulldog Shale. Very fine black dispersed throughout – perhaps organic matter
EI25	EI13.1 Pepegoona PRC013	200.301 m	Consolidated, light brown to grey coarse grained sandstone, quartz rich, subangular to sub rounded grains, sulphur stained, Mu rich and somewhat glassy, clast supported, light reddish brown silty matrix
EI26	EI13.2 Pepegoona PRC013	199.8 m	Silcrete, consolidated, light grey, fine grained, quartz rich with some zones of darker more mafic/organic minerals, some potential pyrite associated with darker areas
EI27	EI13.6 Pepegoona PRC013	210.5 m	Medium to coarse grained, sub rounded, well sorted, light cream and grey, quartz rich sandstone, some black well sorted inclusions (organic content?)
EI28	EI15.2 Pepegoona PRC015	216.2 m	Light pinkish, brown, silica cemented sands, with oxidised areas, clast supported, sub angular to sub rounded sandstone, almost 100% quartz, some yellow sulphur alteration, some black minerals present
EI29	EI15.4 Pepegoona PRC015	221.5 m	Below ferricrete band, yellow uranophane present, some coarser grained quartz rich nodules, light grey to black hydrocarbon stained coarse grained, sub angular to sub rounded, well sorted sandstone, clast supported

EI30	No Sample Number – Lignites Between Soft Sands Pepegoona PRC015	230.38 m	Sample of Lignite from Depth. Unconsolidated small, 0.5-1cm (length) pieces, dark brown in colour, containing fine grained pyrite,
EI31	EI23.1 Pepegoona West PRC023	233.9 m	Fine to medium grained, well sorted, clast supported, hydrocarbon stained, dark grey, sub rounded sandstone. Lignite layers in close proximity to sandstone
EI32	EI23.3 Pepegoona West PRC023	248 m	Light pink and grey, oxidised coarse grained, well sorted, medium to coarse grained sandstone, relatively unconsolidated, sub angular to sub rounded
EI33	EI21.1 Pannikan PRC021	219.74 m	Silcrete in Namba formation, consolidated, matrix supported, sub rounded quartz clasts, light grey in colour, some pinkish zones, some zones of very coarse grained, black minerals or organic matter
EI34	EI21.3 Pannikan PRC021	233.75 m	White, very fine grained, well sorted, clay siltstone, with some pockets of sulphur stained, yellow and white coarse grained quartz rich, sub rounded unconsolidated sands, some well sorted medium grained muscovite
EI35	EI21.4 Pannikan PRC021	237.55 m	Light pinkish, orange brown, coarse to very coarse grained, moderately sorted, sub angular to sub rounded quartz rich sandstone, clast supported
EI36	EI21.5 Pannikan PRC021	256.1 m	Reddish brown, medium grained, clast supported, well sorted, sub rounded, quartz rich sandstone, red zones of oxidation, some fine red silty matrix
EI37	EI22.2 Pannikan PRC022	237.6 m	Light to medium grey, coarse grained, sub angular to sub rounded sandstone, matrix supported, matrix a light grey very fine silt, some 0.5cm darker grey

APPENDIX B: DETAILED METHODOLOGY

Sampling and Sample Preparation

A total of 36 samples were collected from six cores from the Pepegoona, Pepegoona West and Pannikan U-deposits, with six samples collected across each core. The cores were chosen using Heathgate Resources company reports, to obtain an accurate representation of the deposits at Beverley North.

Sampling within cores was targeted to obtain an accurate representation of the mineralisation and its host-formation whilst optimising pyrite content where possible. Small samples (~4 x 4cm) were taken primarily from the ore zones; however representative samples were taken from the contacts with underlying and overlying formations, oxidised and reduced zones as well as un-mineralised sections.

Due to their unconsolidated nature, samples were kept frozen to retain competency until sample preparation could be carried out. Samples were prepared into one-inch polished ore blocks (Pontifex & Associates) and set in epoxy resin where necessary to maintain competency and make sample preparation possible.

Optical Microscopy (OM) & Scanning Electron Microscope (SEM)

A Nikon petrological microscope with magnification up to 50× was used in reflected light mode to identify pyrite, dominant U-bearing minerals and associated Fe-oxides, approximate their relative abundances and identify key relationships between minerals. Each sample was photographed using a mounted digital camera.

SEM work was subsequently carried out using a Phillips XL30 SEM instrument at Adelaide Microscopy, equipped with an energy dispersive X-ray spectrometer (EDAX) and back-scattered electron (BSE) detector. The SEM was operated at 20 eV accelerating voltage and spot size 4 on carbon coated samples. BSE imaging allowed observations of the previously

identified pyrite, U-bearing minerals and other minerals at the micro-scale. Particular emphasis was placed on variances in mineral morphologies, observable fine textures, mineral intergrowths, compositional zoning and inclusions. X-ray spectra were recorded for the identification of ambiguous minerals and for analysis of any minor element variation within pyrites or U-minerals.

Electron Probe Microanalysis (EPMA)

Quantitative compositional data for representative U-bearing phases, Fe-oxides and various morphological types of pyrite phases were obtained using a CAMECA SX-51 microprobe with wavelength-dispersive spectrometers at Adelaide Microscopy. The instrument was operated at an accelerating voltage of 20 kV and beam current of 40 nA. Work focussed on the trace element composition of the minerals with particular emphasis on areas of zonation. Typically 10-15 spots were taken per sample, dependent on observed mineral variation, consistency of results and time constraints.

Samples EI3, EI7, and EI15 were chosen for their high U-mineral content and the concentrations (wt%) within U-bearing phases were calculated for the following elements; F, Mg, Al, Si, P, K, Ca, Sc, Ti, Fe, Y, Zr, Nb, La, Ce, Pr, Nd, Sm, Eu, Gd, Tb, Dy, Ho, Er, Lu, Hf, Pb, Th and U.

Samples EI3, EI7, EI9, EI15, EI17, EI19, were chosen for their large and varied pyrite and Fe-oxide and the siderophile elements were analysed for Na, Mg, Al, Si, S, K. Ca, Ti, V, Cr, Mn, Fe, Co, Ni, Zn, Se, Zr, Nb, Mo, Ta, Th, U, Bi, Ag, Pb, Cu, Cd, Sb and As.

The standards, spectral lines and minimum detection limits for the calibration for the respective analyses are outlined by Table 1 and Table 2 below.

Table 1: Elements in U-bearing minerals analysis

Element	Standard	Line	Approximate mdl (wt%)
F	Fluorite	Kα	0.60
Mg	Almandine	Kα	0.07
Al	Almandine	Kα	0.04
Si	Almandine	Kα	0.04
P	Apatite	Kα	0.06
K	Sanidinie	Kα	0.03
Ca	Apatite	Kα	0.03
Sc	Scandium metal	Kα	0.02
Ti	Rutile	Kα	0.03
Fe	Almandine	Kα	0.06
Y	REE glass #1	Lα	0.11
Zr	Zircon	Lα	0.12
Nb	Niobium metal	Lα	0.07
La	REE glass #3	Lα	0.10
Ce	REE glass #2	Lα	0.10
Pr	REE glass #1	Lβ	0.25
Nd	Neodymium glass	Lβ	0.22
Sm	REE glass #3	Lβ	0.23
Eu	EuF_3	Lβ	0.28
Gd	REE glass #3	Lβ	0.23
Tb	Terbium metal	Lβ	0.70
Dy	REE glass #1	Lβ	0.23
Ho	Holium metal	Lβ	0.18
Er	REE glass #1	Lβ	0.25
Lu	LuF_3	Lα	0.10
Hf	Zircon	Mα	0.16
Pb	Lead glass	Mβ	0.09
Th	Huttonite	Mα	0.17
U	Uraninite	Mβ	0.15

NB: The REE glasses are silicates.

All standards supplied by Astimex except the REE glasses, uraninite, huttonite and Pb glass standards which are supplied by the University of Edinburgh

Table 2: Elements in Pyrite and Fe-(Ti)-oxide analyses

Element	Standard	Line	Approximate mdl (wt%)
Na	Albite	Kα	0.102
Mg	Almandine	Kα	0.05
Al	Almandine	Kα	0.0641
Si	Almandine	Kα	0.0288
S	Marcasite	Kα	0.12
K	Sanidine	Kα	0.0172
Ca	Wollastonite	Kα	0.0159
Ti	Rutile	Kα	0.0317
V	Vanadium metal	Kα	0.01
Cr	Pyrope Garnet	Kα	0.018
Mn	Rhodonite	Kα	0.041
Fe	Almandine	Kα	0.07
Co	Cobalt metal	Kα	0.0478
Ni	Pentlandite	Kα	0.052
Zn	Sphalerite	Kα	0.113
Se	Bismuth Selenide	Lα	0.093
Zr	Zircon	Lα	0.0919
Nb	Niobium metal	Lα	0.0619
Mo	Molybdenum metal	Lα	0.0823
Ta	Tantalum metal	Lα	0.116
Th	Huttonite	Mα	0.1135
U	UO_2	Mβ	0.1
Bi	Bismuth Selenide	Mα	0.175
Ag	Ag_2Te_3	Lα	0.112
Pb	Galena	Mα	0.173
Cu	Chalcopyrite	Kα	0.078
Cd	Cadmium metal	Lα	0.194
Sb	Stibnite Sb_2S_3	Lα	0.082
As	GaAs	Lα	0.21

Laser-Ablation Inductively-coupled Plasma Mass Spectrometry (LA-ICP-MS)

LA-ICP-MS spot analysis of pyrite was undertaken using the Agilent HP-7500 Quadrupole ICPMS instrument at Adelaide Microscopy. The instrument is equipped with a New Wave UP-213 Nd:YAG laser ablation system equipped with MeoLaser 213 software. Data reduction was performed using Glitter software (GEMOC 2005)

Polished samples with suitable grains of pyrite were ablated. Sample eligibility was determined by SEM and petrographical analysis, aiming to determine the presence of inclusions and other textures such as fractures or intergrowths that might affect the quality of the trace element data. Despite the attempt to determine the suitability of pyrite grains prior to LA-ICP-MS, the micron-scale inclusions invisible on the SEM may still have been present and thus data must be interpreted with this in mind, as discussed by Cook et al. (2011).
A total of 194 spots (on pyrite grains) were ablated, with the aim of collecting information from all morphologies and phases of pyrite. Spot analyses were made with a spot size diameter of 40 μm. The laser system was operated at pulse rates of 5 Hz, and 75% power level; laser energy was typically 6-9 J/cm-2, giving an ablation rate of approximately 1.5 μm/sec. Suitable pyrite grains were analysed for the following isotopes: ^{23}Na, ^{29}Si, ^{33}S,^{34}S, ^{43}Ca, ^{51}V, ^{52}Cr,^{55}Mn, ^{57}Fe, ^{60}Ni, ^{65}Cu, ^{66}Zn, ^{69}Ga, ^{75}As, ^{82}Se, ^{95}Mo, ^{107}Ag, ^{111}Cd, ^{115}In, ^{118}Sn, ^{121}Sb, ^{125}Te, ^{137}Ba,^{184}W, ^{193}Ir, ^{197}Au, ^{202}Hg, ^{205}Tl, ^{208}Pb, ^{209}Bi. The method used, labelled *RH-Chall*, undertook a total analysis time for each sample of 90 seconds (30 second measurement of background with the laser off, and a 60 second analysis with the laser on).

Calibration was performed using the Mass-1 trace element standard created by the National Institute of Standards, Gainsburg US (Wilson *et al.* 2002). The raw analytical data for each spot analysis is plotted as a line graph and the integration times for background and sample signal selected. The counts are then corrected for instrument drift (standards were run after each 5 unknown samples). Data reduction was undertaken using Glitter software (GEMOC 2005) and used Iron as the internal standard for pyrite. Data was converted to concentration values (ppm) using the known Fe values.

LA-ICP-MS Element Mapping

LA-ICP-MS mapping of approximately 0.5 cm^2 areas of pyrite was conducted using a Resonetics M-50-LR 193-nm Excimer laser microprobe coupled to an Agilent 7700cx Quadrupole ICP-MS housed at Adelaide Microscopy, University of Adelaide. This new-generation laser system permits high spatial resolution matched by sensitivity of low (sub-ppm) element concentrations. Imaging was performed by ablating sets of parallel line rasters across the sample using a 5µm beams size, line spacing of 5 µm and 5 µm/s scan speed at a laser frequency of 10 Hz and 0.003 dwell time for all elements. Redeposition during mapping was minimised by pre-ablating each line prior to data collection. Identical rasters were done on standard MASS-1, at the start and end of each mapping run to correct for instrumental drift.

Images were compiled and processed using the program Iolite (e.g. Woodhead et al., 2007) developed by the Melbourne Isotope Group at Melbourne University (Paton *et al.* 2011). Iolite is an open source software package for processing ICP-MS data, and is an add-in for the data analysis program Igor developed by WaveMetrics.

Sulphur Isotope Analysis (SIMS)

The CAMECA IMS 1280 high resolution, multi-collector ion microprobe (CAMECA 2012), located at the Centre for Microscopy, Characterisation & Analysis (CMCA) at The University of Western Australia, was used to perform *in-situ* sulphur isotope analysis ($^{34}S/^{33}S$) of pyrites from the polished block samples.

Representative samples were chosen from petrographical, SEM and LA-ICP-MS trace element analysis. Samples were chosen to be representative of all deposits, different horizons and differing morphological pyrite types.

Samples were prepared by cutting small (< 5 mm^2) portions of the polished ore blocks and mounting them in epoxy resin with Son Std. Three to four samples were used in each mount and the pyrite grain mounts were Au-coated (~50 nm) before analysis was carried out.

The grains of Son standard which were cast in the centre of each sample mount were measured five times initially to account for instrument drift, and then in at least two spots before and after every ~8-10 sample analyses. The standard deviations of the Son standard analyses are equal to $\pm$ 0.13 %.

The method used had a total running time of three minutes and 15 seconds, with the acquisition time being two minutes and 53 seconds. A spot size was 10 µm and impact energy of 20,000 V was used, resulting in an average sample emission of ~0.73 µA.

Raw measured $^{34}S/^{32}S$ and $^{33}S/^{32}S$ ratios were converted to the delta notation of $\delta^{34}S$ and $\delta^{33}S$ respectively by normalising to Vienna Cañon Diablo Troilite values;

$(^{34}S/^{32}S)_{VCDT} = 0.044163$ and $^{33}S/^{32}S_{VCDT} = 0.00015368$ (Ding *et al.* 2001, Kita *et al.* 2011).

Drift correction was applied to collected data in Microsoft excel where regression was significant.

APPENDIX C: LA-ICP-MS TRACE ELEMENT DATA FOR PYRITE

Significant elevations (ppm) were observed in tabulated elements from 194 spot analyses on 19 samples. Na, Cu, Zn, Ga, Ag, Cd, In, Sn, Te, Ir, Au, Hg, Pb and Bi are excluded from the table as trace element concentrations rarely exceed the minimum detection limits (mdl).

		V	Cr	Mn	Co	Ni	As	Se	Mo	Sb	Ba	W	Tl
EI1 (Pepegoona, PRC012, 216.3 m)													
1	Euhedral & Cubic	47	14	152	9.1	15	323	107	30	3.9	271	59	243
2	Euhedral & Cubic	19	14	97	186	172	574	33	34	15	2523	44	174
3	Framboidal	75	28	265	5.8	13	276	54	30	5.9	877	121	213
4	Cement	2082	1317	251	835	1401	1054	152	435	83	16517	2568	236
5	Veined, Infill & Overgrowth	8.4	3.5	434	154	161	539	285	25	47	393	10	154
	mean	**446**	**275**	**240**	**238**	**352**	**553**	**126**	**111**	**31**	**4116**	**561**	**204**
EI 2 (Pepegoona, PRC012, 247.02 m)													
1	Veined, Infill & Overgrowth	1.1	<1.06	24	0.3	0.7	11	<1.91	0.6	0.4	133	1.6	0.7
2	Veined, Infill & Overgrowth	1.7	<0.90	6.6	4.8	7.3	27	1.9	1.9	1.2	178	2.4	1
3	Veined, Infill & Overgrowth	3.9	2.3	9	1.5	5.9	137	<1.87	3.8	1.9	179	5.9	5.3
4	Veined, Infill & Overgrowth	19	6.6	11	0.5	1.3	168	<2.07	4.9	2	300	41	11
5	Veined, Infill & Overgrowth	14	4.4	16	0.4	0.9	202	<2.43	4.7	1.5	276	26	8
6	Euhedral & Cubic	1.4	<0.94	27	<0.12	<0.29	4.7	<1.97	0.9	0.8	204	3.6	0.6
7	Veined, Infill & Overgrowth	19	7.2	18	2.3	5.3	571	<2.41	15	5.4	311	36	25
8	Cement	13	3.2	6.8	1	1.6	68	2.4	5.4	1.3	329	28	4.5
9	Veined, Infill & Overgrowth	9.6	4.1	8.9	0.3	1.4	192	2.4	4.9	1.4	242	22	6
10	Euhedral & Cubic	1	<0.78	4.7	0.1	0.7	10	<1.70	1.5	0.3	163	2.4	0.8
	mean	**8.4**	**4.6**	**13**	**1.2**	**2.8**	**139**	**2.2**	**4.4**	**1.6**	**232**	**17**	**6.3**
EI3 (Pepegoona, PRC013, 201.7 m)													
1	Euhedral & Cubic	1462	127	23	159	207	16896	233	261	649	1340	1337	1155
2	Euhedral & Cubic	1060	<****	31	231	348	16903	305	249	556	1076	978	1214
3	Framboidal	3354	78	180	635	780	4960	493	232	446	1552	2953	273
4	Euhedral & Cubic	942	359	153	286	292	16048	519	222	648	415	827	1025
5	Euhedral & Cubic	1697	1308	62	488	515	9777	944	181	545	840	1574	711
6	Euhedral & Cubic	793	<6.00	24	271	264	13283	191	188	616	294	693	1173
7	Euhedral & Cubic	1648	<7.00	117	343	571	2773	863	260	241	3429	1361	186
8	Euhedral & Cubic	32	<1.94	3.7	190	75	11051	467	107	445	15	15	779
9	Euhedral & Cubic	3853	<12.67	109	591	760	15333	340	351	869	1885	3300	1100
10	Euhedral & Cubic	818	9.2	18	230	279	13885	255	202	618	281	664	1337
	mean	**1566**	**376**	**72**	**342**	**409**	**12091**	**461**	**225**	**563**	**1113**	**1370**	**895**

		V	Cr	Mn	Co	Ni	As	Se	Mo	Sb	Ba	W	Tl
EI4 (Pepegoona, PRC013, 204 m)													
1	Framboidal	139	<23.07	22	175	65	303	44	32	5.2	12403	86	42
2	Framboidal	37	<2.27	13	66	24	287	20	11	1.9	81	16	27
3	Framboidal	69	42	25	185	97	333	35	37	5	212	77	43
4	Framboidal	74	28	46	69	46	176	18	17	2.6	1249	208	24
5	Framboidal	533	437	335	269	344	271	103	90	10	14473	761	41
	mean	**170**	**169**	**88**	**153**	**115**	**274**	**44**	**37**	**5**	**5684**	**229**	**35**
EI6 (Pepegoona, PRC015, 203.9 m)													
1	Euhedral & Cubic	3.1	375	4.3	164	350	1157	319	123	29	231	5.5	32
2	Framboidal	106	234	8.2	76	45	817	85	38	3.7	432	50	11
3	Framboidal	33	116	2.8	176	60	922	53	32	3.4	172	8.7	37
4	Framboidal	111	50	2.5	132	56	969	70	24	2.8	22	5	26
5	Framboidal	23	59	2.2	167	70	1098	42	15	1.6	21	1.5	38
6	Framboidal	33	<6.96	2.7	181	73	1102	58	19	2.9	447	3.7	39
7	Framboidal	221	14	5.3	161	87	1259	173	62	10	232	31	47
8	Framboidal	30	3.7	2	157	65	1135	59	25	6.2	65	3.8	33
9	Framboidal	153	7	4.8	11	20	298	105	33	2	432	22	62
10	Framboidal	16	<1.50	2	169	71	1158	42	17	4.5	8.4	1.7	39
	mean	**73**	**107**	**3.7**	**139**	**90**	**991**	**101**	**39**	**6.6**	**206**	**13**	**36**
EI7 (Pepegoona, PRC015, 219.2 m)													
1	Framboidal	83	5	85	2721	2109	3646	35	108	69	190	3	384
2	Framboidal	1134	4	25	400	229	12436	16	72	631	460	688	528
3	Framboidal	816	3	23	659	407	5287	15	38	185	190	468	239
4	Cement	152302	454	8228	12085	12122	57295	482	2576	12523	30589	125202	1521
5	Cement	30	3	56	585	405	659	4	10	4	400	1	366
6	Euhedral & Cubic	23	2	37	571	359	1857	<8.17	19	17	170	5	130
7	Framboidal	80	3	75	2486	1715	2585	52	47	63	412	5	442
8	Framboidal	837	9	44	478	397	3209	36	26	194	986	567	196
	mean	**19413**	**60**	**1072**	**2498**	**2218**	**10872**	**91**	**362**	**1711**	**4175**	**15867**	**476**
EI8 (Pepegoona, PRC015, 222.6 m)													
1	Euhedral & Cubic	4.8	<2.16	4.2	37	68	1499	<1.65	180	4.9	6.3	0.9	3.5
2	Euhedral & Cubic	1.2	<1.74	5.3	4.6	22	882	<1.50	30	0.3	16	0.2	14
3	Euhedral & Cubic	19	3.6	15	291	253	1244	6	147	15	188	2.6	57
4	Euhedral & Cubic	1.6	<1.30	6.3	4.5	10	788	4	35	0.4	31	0.6	17
5	Euhedral & Cubic	7.6	<1.92	6.2	108	137	1921	3	287	9.2	186	0.6	11
6	Euhedral & Cubic	5.1	10	5.1	4.2	29	177	3.9	44	0.8	25	1.2	4.3
7	Cement	2.4	4.4	10	17	22	148	2.8	25	0.6	27	0.9	5.9
8	Euhedral & Cubic	130	16	32	40	91	237	3.4	221	5.3	57	8.2	5.8
9	Cement	3.2	2.3	5.9	3.4	30	359	2.8	25	0.7	29	1.1	11
10	Euhedral & Cubic	54	16	6.6	14	51	252	2.9	116	2.6	32	2.8	7.4
11	Framboidal	114	12	7.7	105	135	251	5.1	126	6.1	75	3.7	17
12	Euhedral & Cubic	1.8	1.4	6.1	3.5	33	498	3.8	26	1.2	22	0.5	27
13	Framboidal	229	31	12	106	138	408	<7.36	488	9.4	1625	5.2	14

		V	Cr	Mn	Co	Ni	As	Se	Mo	Sb	Ba	W	Tl
14	Cement	2.1	2.3	5.5	0.6	6.4	140	3	16	0.3	22	0.7	7.2
15	Cement	6.4	4.2	19	44	61	210	7.5	56	4.7	26	0.7	35
16	Cement	49	13	11	44	45	272	2.9	134	4.6	51	4.2	5.2
	mean	**39**	**10**	**10**	**52**	**71**	**580**	**3.9**	**122**	**4.1**	**151**	**2.1**	**15**
EI9 (Pepegoona, PRC014, 231.3 m)													
1	Cement	1.2	<1.88	5.3	1	6.5	3.8	<4.68	293	0.3	148	2.9	0.8
2	Cement	0.3	<1.92	3.2	20	52	92	<5.06	4	2	8.9	0.3	22
3	Veined, Infill & Overgrowth	3.2	4.1	21	88	95	230	14	6.2	3.7	37	1.4	35
4	Cement	1.7	<1.60	5.6	5	10	2.4	<4.31	112	0.1	230	2.6	1.1
5	Euhedral & Cubic	1.3	<1.68	4.2	0.3	0.5	4.2	<4.62	153	0.2	178	2.3	0.1
6	Cement	1.3	<1.60	3.6	0.2	1	7.1	<4.11	191	0.1	199	3.4	0
7	Veined, Infill & Overgrowth	2	1.9	3.4	23	98	1953	51	126	107	222	3	50
8	Veined, Infill & Overgrowth	1	<1.59	5.5	125	111	1026	24	87	17	110	1.3	48
9	Cement	0.6	<1.46	7.6	0.7	1.4	67	<4.21	107	4	171	1.7	2.3
10	Veined, Infill & Overgrowth	0.6	<1.66	7	77	71	366	10	16	2.5	17	1	116
11	Cement	0.5	<1.58	141	16	153	383	20	252	126	27	0.5	130
12	Cement	1.2	<1.58	3.7	37	57	32	<4.39	131	0.8	64	1.4	12
13	Cement	2	<1.50	2.6	6.6	77	162	<4.45	86	4.8	219	3.4	6
14	Cement	1.1	<1.36	4.7	3.1	107	43	<3.94	183	17	171	2	7.1
15	Euhedral & Cubic	1.1	<1.50	5.2	<0.123	0.4	2.1	<4.19	86	0	119	1.8	0
	mean	**1.3**	**3**	**14.9**	**29**	**56**	**292**	**24**	**122**	**19**	**128**	**1.9**	**29**
EI11 (Pepegoona West, PRC023, 253 m)													
1	Cement	5.7	<0.67	3.5	16	2.2	126	189	106	47	55	6.6	27
2	Cement	5.4	<0.74	4.5	21	2.9	22	149	504	0.5	82	10	1
3	Cement	53	<0.70	3.9	41	7.7	296	1228	448	64	68	38	20
4	Euhedral & Cubic	14	<0.66	4.7	14	2.1	137	350	279	21	84	10	5.8
5	Cement	87	<0.70	5	260	29	176	15424	345	7.4	100	97	8.9
6	Cement	69	<0.67	4.7	61	8.3	241	533	552	99	80	65	21
7	Veined, Infill & Overgrowth	147	1.7	6.6	70	12	403	679	300	13	125	121	11
8	Veined, Infill & Overgrowth	487	4	2.4	179	28	863	1348	32	40	147	466	14
9	Veined, Infill & Overgrowth	185	<0.76	1.4	38	8.7	371	848	10	19	56	182	4.9
10	Veined, Infill & Overgrowth	64	<0.75	7.5	30	5.6	474	260	260	6	128	66	6.2
11	Cement	20	1.1	8.3	31	4.2	154	180	293	2.9	62	12	3.3
12	Euhedral & Cubic	16	0.7	8.2	20	4	491	282	105	127	67	7.7	76
13	Veined, Infill & Overgrowth	182	1.8	14	81	24	1268	627	72	110	86	131	80
14	Cement	32	0.6	7.4	10	2.5	930	92	83	57	68	26	88
15	Cement	2.1	0.9	10	0.6	<0.186	359	8.7	170	4.5	65	5.9	15
16	Cement	3.6	0.9	7.4	74	18	217	172	635	42	288	5.1	18
17	Euhedral & Cubic	0.8	1.1	10	5.2	1.4	248	14	214	1.6	66	4.1	5.5

		V	Cr	Mn	Co	Ni	As	Se	Mo	Sb	Ba	W	Tl
18	Euhedral & Cubic	84	4.4	10	170	37	405	830	470	60	130	39	35
19	Euhedral & Cubic	4.6	0.7	13	11	1.7	391	631	186	85	52	4.1	70
20	Euhedral & Cubic	0.4	0.4	10	0.3	0.2	300	23	177	69	56	2.5	64
21	Cement	181	2.1	5.3	410	46	347	7985	935	7.1	73	118	14
22	Cement	6.1	2.2	8.1	16	4	1301	247	91	688	86	7.6	136
23	Cement	3.9	1	7.1	15	2.2	176	208	357	30	87	4.8	6.8
24	Veined, Infill & Overgrowth	172	5.8	13	178	51	418	36432	48	15	77	135	22
25	Veined, Infill & Overgrowth	47	0.7	2.9	17	3.4	139	120	2.6	3.9	13	23	1.4
26	Veined, Infill & Overgrowth	124	1.4	8.7	38	18	329	385	337	15	85	112	10
	mean	**77**	**1.7**	**7.2**	**70**	**13**	**407**	**2663**	**270**	**63**	**88**	**65**	**29**
EI12 (Pepegoona West, PRC023, 257.2 m)													
1	Cement	0.1	<3.20	18	3	5.3	24	<1.25	0.6	2.7	12	0.2	1.7
2	Veined, Infill & Overgrowth	1.8	<2.65	57	69	119	223	4	14	38	365	1.8	38
3	Framboidal	5.7	<2.07	49	63	171	184	1.2	3.5	7.6	256	2.3	86
4	Cement	1.2	<1.76	35	39	69	81	<1.14	9.1	3.6	382	2.4	10
5	Cement	3.6	<1.67	126	236	306	153	2.7	24	18	163	2.3	49
6	Veined, Infill & Overgrowth	2.1	2.4	50	262	699	450	1.4	43	31	388	1.9	94
7	Veined, Infill & Overgrowth	1.8	1.6	47	129	310	219	2.6	23	56	359	2.2	47
8	Cement	1.3	<0.72	10	6.1	26	73	<1.05	1.6	7	31	1.1	18
9	Cement	1.7	<0.85	148	43	54	229	12	34	103	230	1.1	62
10	Veined, Infill & Overgrowth	0.9	<0.68	187	217	312	205	9.1	20	45	56	1.1	31
	mean	**2**	**2**	**73**	**107**	**207**	**184**	**4.7**	**17**	**31**	**224**	**1.6**	**44**
EI13 (Pepegoona West, PRC023, 269.1 m)													
1	Cement	0.6	<1.37	1.3	2.1	31	219	<4.12	25	0.3	20	0	4.5
2	Cement	0.5	<1.30	1.2	9	8.3	84	<3.85	2.4	0.1	12	0	6.6
3	Cement	1.9	<1.46	32	1.2	7.7	368	<4.59	1.4	0.6	65	0.3	297
4	Cement	0.6	<1.45	1.5	27	25	602	<4.36	16	2.8	28	1.3	5.4
5	Cement	0.7	<1.37	1.3	0.2	1.2	92	<3.99	6.3	0.1	25	0.2	4.3
6	Cement	0.9	<1.44	3.9	29	45	143	<4.20	4.3	0.8	67	0.4	23
7	Cement	0.5	<1.44	2.4	42	64	150	<4.23	7.5	2.1	25	0.2	21
8	Cement	0.6	<1.41	5.5	48	65	220	<4.22	3.2	1	40	0.2	41
9	Cement	1	<1.39	1.7	10	16	25	<3.96	2.1	0.3	87	0.1	6.6
10	Cement	10.7	5	12	79	141	235	<6.39	10	2.5	1468	1	46
	mean	**1.8**	**5**	**6.3**	**25**	**40**	**214**	**<mdl**	**7.9**	**1.1**	**184**	**0.4**	**45**
EI14 (Pannikan, PRC021, 222.5m)													
1	Framboidal	48	<18.10	23	48	36	197	<54.69	32	1.9	290	171	28
2	Framboidal	81	<107.93	55	56	306	254	<311.19	41	2.9	1982	418	22
3	Euhedral & Cubic	150	<569.04	<153.44	281	1566	<290.74	<1828.02	43	9.2	23443	673	18
4	Framboidal	640	228	140	164	128	359	<85.79	667	15	11957	788	53
5	Framboidal	54	43	18	190	86	227	55	64	3.2	10404	185	44
6	Framboidal	82	114	23	141	118	86	<132.42	37	3.4	2912	101	22

		V	Cr	Mn	Co	Ni	As	Se	Mo	Sb	Ba	W	Tl
7	Framboidal	43	15	27	111	45	234	<45.77	26	4.8	794	150	32
8	Framboidal	50	16	15	70	35	264	55	41	2.4	413	253	32
	mean	**143**	**83**	**43**	**133**	**290**	**232**	**55**	**119**	**5.3**	**6524**	**342**	**31**
EI15 (Pannikan, PRC021, 260.4 m)													
1	Cement	1	<0.88	22	2.8	37	64	<2.06	0.3	0.1	75	0.1	486
2	Cement	1.1	<0.75	27	6.7	48	71	<2.03	0.4	0.1	83	0.1	529
3	Cement	1.4	<0.76	18	502	635	229	7.9	1.7	0.4	101	1.7	309
4	Euhedral & Cubic	0.8	<0.61	15	4.4	73	69	<1.81	0.4	0.1	57	0.1	285
5	Euhedral & Cubic	4.7	1.5	27	809	820	550	6.3	52	1.2	170	227	489
6	Cement	94	3.9	25	3949	3233	321	58	59	4.2	127	89	431
7	Cement	10	1.5	24	326	217	130	<1.56	8.1	0.3	86	23	424
8	Framboidal	1.8	0.7	20	66	162	67	1.7	1.5	0.2	69	4.2	367
9	Cement	1.3	0.7	19	3.3	53	123	<1.36	0.6	0.1	105	0.2	369
10	Cement	1.5	0.7	17	18	41	25	1.5	0.4	0.1	72	0.2	464
	mean	**12**	**1.5**	**21**	**569**	**532**	**165**	**15**	**12**	**0.7**	**95**	**35**	**415**
EI16 (Pannikan, PRC022, 228.1 m)													
1	Cement	19	7.7	22	13	7.9	18	<1.35	34	0.4	50	16	22
2	Cement	5.3	2.3	12	2.2	1.3	12	1.3	122	0.2	39	1.7	21
3	Cement	7	0.1	89	17	12	22	2.2	31	0.5	66	2.5	33
4	Cement	11	<****	16	8.8	7	39	6.5	225	0.7	63	2.1	59
5	Cement	1	2.2	12	11	3.5	17	2.4	22	0.2	142	1	11
6	Framboidal	59	<****	109	5.2	16	32	28	7.2	2.8	166	35	109
7	Framboidal	47	128	104	22	34	23	22	7.9	2.4	610	49	93
8	Framboidal	11	11	170	3.5	7.3	29	19	4.8	3.1	60	5.5	140
9	Cement	25	8.3	42	174	106	31	4.5	60	1.2	295	23	22
10	Cement	16	1	21	136	77	51	<1.47	22	0.6	416	20	37
	mean	**20**	**20**	**60**	**39**	**27**	**27**	**11**	**54**	**1.2**	**191**	**15**	**55**
EI17 (Pannikan, PRC022, 244.18m)													
1	Cement	1.5	<3.03	1356	0.2	1.3	156	1736	52	0.4	45	1	17
2	Cement	1	<1.68	939	100	503	496	1598	109	4.2	54	0.6	97
3	Cement	11	12	700	7.6	20	183	1071	77	1	207	2.5	11
4	Cement	6.1	<1.40	779	19	21	239	984	67	1.3	234	1.5	66
5	Cement	37	30	1135	61	71	329	1067	71	0.9	131	11	232
	mean	**11**	**21**	**982**	**38**	**123**	**281**	**1291**	**75**	**1.6**	**134**	**3.4**	**84**
EI18 (Pannikan, PRC022, 263.5 m)													
1	Veined, Infill & Overgrowth	0.5	<19.10	5.6	0.1	0.4	5.8	<3.04	0.4	0	8.2	0.3	0.2
2	Framboidal	44	109	6.5	1.8	4.4	62	<2.29	3.1	0.5	201	23	5.5
3	Euhedral & Cubic	4.1	<3.13	45	0.8	0.9	65	<2.53	1.3	0.2	62	4.5	0.7
4	Cement	32	29	7.3	8.3	15	79	6.5	3.6	1.3	236	28	5.3
5	Cement	11	6	15	1.9	20	69	<1.99	2.4	0.3	151	8.8	2.5
6	Veined, Infill & Overgrowth	1.2	<0.64	6.9	<0.101	0.3	5.5	<1.75	0.1	<0.0240	32	0.6	0.1
7	Euhedral & Cubic	0.8	<0.57	151	0.1	1.8	0.5	<1.61	<0.05	0	12	0.5	0.4

		V	Cr	Mn	Co	Ni	As	Se	Mo	Sb	Ba	W	Tl
									9				
8	Cement	9.2	1.4	28	1.6	5.1	3.7	<1.76	0	<0.028	50	2.5	0.1
9	Cement	19	10	87	5	52	87	1.9	3.9	0.2	224	11	6.1
10	Cement	1.1	<0.42	4.9	0.6	1.9	4.6	<1.39	0.3	<0.023	17	0.8	0.1
	mean	**12**	**31**	**36**	**2.3**	**10**	**38**	**4.2**	**1.7**	**0.4**	**99**	**8.1**	**2.1**
EI19 (Pannikan, PRC022, 265.4 m)													
1	Cement	<0.032	237	2.5	2.2	13	238	2.7	7	4.7	5.1	<0.033	6.1
2	Cement	1.2	<46.05	4.8	1.2	6.8	287	4.8	7.7	5.1	627	0.1	16
3	Cement	0.1	<12.45	2.6	1.9	10	266	2.4	7.3	3.8	13	<0.038	7.3
4	Cement	0.5	<5.51	4	3.7	18	341	5.3	6.5	5.5	172	<0.032	8.6
5	Cement	0	<3.69	2.8	3.2	16	239	8.6	4.9	5.9	6.7	<0.028	7.6
6	Cement	0.2	<0.97	6.2	6.5	34	584	23	7.1	17	57	<0.028	50
7	Cement	1.4	<0.95	10	2.2	10	260	9	6.6	4.7	151	0.2	7.2
8	Cement	5.5	1	11	3.1	10	412	3.7	16	4.4	268	0.7	18
9	Cement	1.1	<0.71	11	1.1	6.3	293	3	7.4	4.2	70	<0.027	7.1
10	Cement	4.5	1.6	47	6	31	608	10	9.1	11	153	0.2	12
	mean	**1.6**	**80**	**10**	**3.1**	**15**	**353**	**7.2**	**8**	**6.7**	**152**	**0.3**	**14**
EI 20 (Pannikan, PRC022, 264.4 m)													
1	Euhedral & Cubic	3.1	1.2	13	1.8	6.2	35	<3.26	2.1	0.2	75	2.2	0.5
2	Euhedral & Cubic	5.7	2	16	1.3	4.8	69	<3.42	3.9	0.1	74	6.9	0.4
3	Euhedral & Cubic	0.8	<0.54	12	0.1	0.4	1.1	<3.37	<0.136	0	33	2	0
4	Euhedral & Cubic	3.3	1.7	37	1	2.5	46	<3.64	5	0.1	55	4.1	0.7
5	Euhedral & Cubic	1.9	0.8	13	0.7	1.6	20	<3.65	0.6	0.1	47	1.9	0.2
6	Veined, Infill & Overgrowth	33	10.8	161	38	108	93	<4.65	40	0.7	461	13	4.3
7	Cement	11	3.6	112	2	30	69	<3.68	20	0.2	106	5	2
8	Euhedral & Cubic	0.7	<0.47	96	0.4	1.9	6.9	3.2	0.2	<0.047	18	2	0.3
9	Euhedral & Cubic	4.6	2	103	1	6.5	9	<3.10	0.9	<0.050	76	3.8	0.9
10	Euhedral & Cubic	2.5	3.1	11	2.4	5.2	140	<2.99	5.3	0.1	68	2	0.9
	mean	**6.6**	**3.2**	**57**	**4.9**	**17**	**49**	**3.2**	**8.7**	**0.2**	**101**	**4.3**	**1**
EI 20B (Pannikan, PRC022, 264.4 m)													
1	Euhedral & Cubic	4.3	<0.88	4.5	4.5	7.4	19	<3.77	1.1	0.9	128	2.6	1.5
2	Euhedral & Cubic	0.9	<0.91	8	0.1	0.5	4.6	<3.57	<0.133	<0.049	44	1.6	0.2
3	Euhedral & Cubic	4.7	1	6.2	3	4.5	26	<3.92	<0.133	0.2	98	3.1	0.2
4	Euhedral & Cubic	1	<0.85	30	0.4	0.6	0.3	<3.38	<0.126	0.1	38	3	0.1
5	Veined, Infill & Overgrowth	1.5	<0.80	34	0.3	0.5	<0.34	<3.24	0.2	<0.041	35	1.8	0.1
6	Veined, Infill & Overgrowth	3.7	1.2	25	2.1	11	5.5	<3.14	2.3	0.1	62	2.4	0.2

		V	Cr	Mn	Co	Ni	As	Se	Mo	Sb	Ba	W	Tl
	mean	**2.7**	**1.1**	**18**	**1.7**	**4**	**11**		**1.2**	**0.3**	**68**	**2.4**	**0.4**

APPENDIX D: ELECTRON PROBE MICROANALYSIS (EPMA) RESULTS.

Electron probe microanalysis results are given for 2 sessions of pyrite analysis, U-bearing minerals, ilmenite, rutile and Fe-oxide minerals are outlined in Tables 1-6. Calibration standards and approximate minimum detection limits (mdl) are given in Appendix A.

Table 1: EPMA Analysis of Pyrite from session 1, showing largely stoichiometric pyrite.

Analysis No.	**EI15.5**	**EI15.7**	**EI15.8**	**EI15.9**	**EI15.11**	**EI15.12**	**EI15.13**	**EI15.14**	**EI15.15**	**EI15.17**	**EI15.19**	**EI15.20**	**EI15.21**	**EI3.8**	**EI3.9**	**EI3.14**	**EI7.1**
S (wt%)	52.82	52.19	52.54	52.46	52.55	50.72	50.73	52.56	53.27	50.16	49.76	52.22	51.58	47.31	45.18	47.69	48.99
Fe (wt%)	43.83	44.65	45.23	43.74	44.69	44.11	42.58	45.63	45.35	44.70	43.86	45.24	44.40	41.05	38.45	42.71	43.62
Co (wt%)	0.00	0.00	0.00	0.00	0.07	0.06	0.36	0.00	0.00	0.02	0.00	0.00	0.02	0.01	0.00	0.00	0.04
Ni (wt%)	0.02	0.00	0.01	0.04	0.03	0.00	0.00	0.00	0.00	0.00	0.01	0.01	0.03	0.04	0.01	0.00	0.07
Cu (wt%)	0.03	0.02	0.04	0.04	0.02	0.04	0.01	0.05	0.00	0.03	0.00	0.01	0.00	0.06	0.06	0.05	0.04
Zn (wt%)	0.00	0.00	0.00	0.00	0.03	0.07	0.06	0.05	0.00	0.00	0.02	0.00	0.02	0.04	0.00	0.00	0.00
As (wt%)	0.05	0.07	0.08	0.09	0.00	0.06	0.12	0.09	0.07	0.05	0.00	0.05	0.05	1.58	1.50	0.09	0.02
Ag (wt%)	0.04	0.00	0.00	0.00	0.00	0.00	0.04	0.00	0.04	0.01	0.02	0.00	0.00	0.08	0.00	0.00	0.02
Cd (wt%)	0.00	0.01	0.00	0.11	0.00	0.01	0.00	0.00	0.00	0.00	0.00	0.00	0.01	0.00	0.00	0.00	0.00
Sb (wt%)	0.00	0.00	0.01	0.00	0.00	0.00	0.00	0.00	0.02	0.00	0.00	0.01	0.02	0.00	0.03	0.00	0.00
Pb (wt%)	0.17	0.16	0.17	0.14	0.12	0.01	0.01	0.11	0.10	0.06	0.00	0.19	0.12	0.17	0.12	0.04	0.15
Bi (wt%)	0.12	0.07	0.11	0.12	0.12	0.00	0.02	0.11	0.06	0.07	0.00	0.01	0.21	0.08	0.07	0.12	0.11
Total	**97.06**	**97.17**	**98.18**	**96.74**	**97.62**	**95.08**	**93.94**	**98.59**	**98.90**	**95.10**	**93.68**	**97.75**	**96.46**	**90.42**	**85.41**	**90.70**	**93.07**
Formula (to 3 atoms)																	
Fe	0.97	0.99	0.99	0.97	0.98	1.00	0.97	1.00	0.98	1.01	1.01	1.00	0.99	0.99	0.97	1.02	1.01
Co	0.00	0.00	0.00	0.00	0.00	0.00	0.01	0.00	0.00	0.00	0.00	0.00	0.00	0.00	0.00	0.00	0.00
Ni	0.00	0.00	0.00	0.00	0.00	0.00	0.00	0.00	0.00	0.00	0.00	0.00	0.00	0.00	0.00	0.00	0.00
Cu	0.00	0.00	0.00	0.00	0.00	0.00	0.00	0.00	0.00	0.00	0.00	0.00	0.00	0.00	0.00	0.00	0.00
Zn	0.00	0.00	0.00	0.00	0.00	0.00	0.00	0.00	0.00	0.00	0.00	0.00	0.00	0.00	0.00	0.00	0.00
Ag	0.00	0.00	0.00	0.00	0.00	0.00	0.00	0.00	0.00	0.00	0.00	0.00	0.00	0.00	0.00	0.00	0.00
Cd	0.00	0.00	0.00	0.00	0.00	0.00	0.00	0.00	0.00	0.00	0.00	0.00	0.00	0.00	0.00	0.00	0.00
Sb	0.00	0.00	0.00	0.00	0.00	0.00	0.00	0.00	0.00	0.00	0.00	0.00	0.00	0.00	0.00	0.00	0.00
Pb	0.00	0.00	0.00	0.00	0.00	0.00	0.00	0.00	0.00	0.00	0.00	0.00	0.00	0.00	0.00	0.00	0.00
Bi	0.00	0.00	0.00	0.00	0.00	0.00	0.00	0.00	0.00	0.00	0.00	0.00	0.00	0.00	0.00	0.00	0.00
Total	*0.97*	*0.99*	*0.99*	*0.97*	*0.99*	*1.00*	*0.98*	*1.00*	*0.98*	*1.02*	*1.01*	*1.00*	*0.99*	*0.99*	*0.98*	*1.02*	*1.02*
As	0.00	0.00	0.00	0.00	0.00	0.00	0.00	0.00	0.00	0.00	0.00	0.00	0.00	0.03	0.03	0.00	0.00
S	2.03	2.01	2.00	2.02	2.01	2.00	2.02	2.00	2.01	1.98	1.99	2.00	2.00	1.98	1.99	1.98	1.98
Total	*2.03*	*2.01*	*2.01*	*2.03*	*2.01*	*2.00*	*2.02*	*2.00*	*2.01*	*1.98*	*1.99*	*2.00*	*2.01*	*2.01*	*2.02*	*1.98*	*1.98*

Sum	**3.00**	**3.00**	**3.00**	**3.00**	**3.00**	**3.00**	**3.00**	**3.00**	**3.00**	**3.00**	**3.00**	**3.00**	**3.00**	**3.00**	**3.00**	**3.00**	**3.00**

Analysis No.	**EI7.2**	**EI7.3**	**EI7.4**	**EI7.5**	**EI7.7**	**EI7.8**	**EI7.9**	**EI7.10**	**EI7.11**	**EI7.12**	**EI7.13**	**EI7.14**	**EI9.2**	**EI9.3**	**EI9.5**	**EI9.6**	**EI9.9**
S (wt%)	49.02	52.72	52.99	52.88	52.55	52.79	52.50	52.91	52.40	51.94	52.97	45.70	51.94	53.55	53.07	53.05	53.21
Fe (wt%)	42.45	45.82	45.09	44.48	44.37	45.68	45.60	46.58	45.26	44.13	45.46	39.13	45.15	46.36	45.81	46.45	46.21
Co (wt%)	0.24	0.00	0.00	0.02	0.01	0.00	0.00	0.00	0.00	0.00	0.00	0.25	0.02	0.00	0.07	0.00	0.02
Ni (wt%)	0.17	0.04	0.01	0.05	0.01	0.00	0.02	0.00	0.01	0.01	0.00	0.11	0.04	0.47	0.14	0.00	0.03
Cu (wt%)	0.10	0.00	0.00	0.01	0.01	0.00	0.03	0.00	0.00	0.05	0.02	0.00	0.00	0.01	0.03	0.00	0.04
Zn (wt%)	0.00	0.03	0.01	0.06	0.01	0.08	0.00	0.07	0.03	0.00	0.02	0.02	0.02	0.00	0.00	0.00	0.02
As (wt%)	0.26	0.10	0.23	0.25	0.08	0.10	0.20	0.23	0.36	0.93	0.33	0.14	0.03	0.05	0.45	0.06	0.07
Ag (wt%)	0.05	0.00	0.02	0.00	0.00	0.05	0.00	0.05	0.11	0.09	0.06	0.00	0.00	0.03	0.00	0.05	0.02
Cd (wt%)	0.00	0.08	0.00	0.01	0.00	0.00	0.06	0.00	0.14	0.02	0.00	0.00	0.00	0.08	0.00	0.10	0.00
Sb (wt%)	0.00	0.05	0.00	0.02	0.00	0.00	0.02	0.00	0.00	0.02	0.01	0.00	0.00	0.00	0.01	0.00	0.00
Pb (wt%)	0.23	0.05	0.14	0.20	0.09	0.31	0.11	0.16	0.19	0.24	0.18	0.09	0.10	0.09	0.24	0.21	0.03
Bi (wt%)	0.10	0.20	0.15	0.15	0.25	0.13	0.13	0.29	0.02	0.15	0.12	0.12	0.13	0.15	0.09	0.08	0.17
Total	**92.61**	**99.09**	**98.63**	**98.13**	**97.40**	**99.14**	**98.66**	**100.29**	**98.53**	**97.58**	**99.18**	**85.55**	**97.42**	**100.79**	**99.91**	**99.98**	**99.82**
Formula (to 3 atoms)																	
Fe	0.99	1.00	0.98	0.97	0.98	0.99	1.00	1.00	0.99	0.98	0.99	0.98	1.00	0.99	0.99	1.00	1.00
Co	0.01	0.00	0.00	0.00	0.00	0.00	0.00	0.00	0.00	0.00	0.00	0.01	0.00	0.00	0.00	0.00	0.00
Ni	0.00	0.00	0.00	0.00	0.00	0.00	0.00	0.00	0.00	0.00	0.00	0.00	0.00	0.01	0.00	0.00	0.00
Cu	0.00	0.00	0.00	0.00	0.00	0.00	0.00	0.00	0.00	0.00	0.00	0.00	0.00	0.00	0.00	0.00	0.00
Zn	0.00	0.00	0.00	0.00	0.00	0.00	0.00	0.00	0.00	0.00	0.00	0.00	0.00	0.00	0.00	0.00	0.00
Ag	0.00	0.00	0.00	0.00	0.00	0.00	0.00	0.00	0.00	0.00	0.00	0.00	0.00	0.00	0.00	0.00	0.00
Cd	0.00	0.00	0.00	0.00	0.00	0.00	0.00	0.00	0.00	0.00	0.00	0.00	0.00	0.00	0.00	0.00	0.00
Sb	0.00	0.00	0.00	0.00	0.00	0.00	0.00	0.00	0.00	0.00	0.00	0.00	0.00	0.00	0.00	0.00	0.00
Pb	0.00	0.00	0.00	0.00	0.00	0.00	0.00	0.00	0.00	0.00	0.00	0.00	0.00	0.00	0.00	0.00	0.00
Bi	0.00	0.00	0.00	0.00	0.00	0.00	0.00	0.00	0.00	0.00	0.00	0.00	0.00	0.00	0.00	0.00	0.00
Total	*1.00*	*1.00*	*0.98*	*0.98*	*0.98*	*1.00*	*1.00*	*1.01*	*0.99*	*0.98*	*0.99*	*0.99*	*1.00*	*1.00*	*1.00*	*1.00*	*1.00*
As	0.00	0.00	0.00	0.00	0.00	0.00	0.00	0.00	0.01	0.02	0.01	0.00	0.00	0.00	0.01	0.00	0.00
S	1.99	2.00	2.01	2.02	2.02	2.00	2.00	1.99	2.00	2.00	2.00	2.00	2.00	2.00	2.00	1.99	2.00
Total	*2.00*	*2.00*	*2.02*	*2.02*	*2.02*	*2.00*	*2.00*	*1.99*	*2.00*	*2.02*	*2.01*	*2.01*	*2.00*	*2.00*	*2.00*	*1.99*	*2.00*
Sum	**3.00**	**3.00**	**3.00**	**3.00**	**3.00**	**3.00**	**3.00**	**3.00**	**3.00**	**3.00**	**3.00**	**3.00**	**3.00**	**3.00**	**3.00**	**3.00**	**3.00**

Analysis No.	**EI9.10**	**EI19.1**	**EI19.2**	**EI19.3**	**EI19.4**	**EI19.5**	**EI19.10**	**EI17.1**	**EI17.4**	**EI17.6**	**EI17.7**	**EI17.8**	**EI17.9**	**EI17.11**	**EI17.12**
S (wt%)	52.89	54.07	53.77	53.97	53.69	53.66	53.89	49.18	52.18	52.80	51.92	51.46	52.72	53.04	52.68
Fe (wt%)	46.29	46.61	47.13	46.84	46.89	46.94	46.83	41.04	45.08	46.46	45.36	45.62	45.47	46.86	45.99
Co (wt%)	0.00	0.01	0.01	0.01	0.00	0.00	0.00	0.01	0.00	0.00	0.00	0.00	0.00	0.00	0.00
Ni (wt%)	0.03	0.03	0.00	0.02	0.05	0.03	0.00	0.07	0.02	0.00	0.00	0.00	0.00	0.02	0.01

Cu (wt%)	0.03	0.00	0.00	0.00	0.00	0.03	0.00	0.34	0.08	0.03	0.03	0.00	0.03	0.02	0.03
Zn (wt%)	0.03	0.03	0.00	0.06	0.00	0.01	0.00	0.00	0.03	0.01	0.06	0.02	0.00	0.00	0.00
As (wt%)	0.08	0.10	0.09	0.10	0.06	0.12	0.10	0.10	0.04	0.01	0.08	0.02	0.00	0.03	0.08
Ag (wt%)	0.00	0.01	0.07	0.03	0.01	0.01	0.01	0.00	0.05	0.09	0.00	0.00	0.05	0.03	0.00
Cd (wt%)	0.00	0.03	0.00	0.00	0.03	0.02	0.00	0.00	0.00	0.00	0.07	0.11	0.00	0.03	0.00
Sb (wt%)	0.00	0.00	0.00	0.00	0.00	0.00	0.01	0.00	0.03	0.00	0.02	0.00	0.02	0.06	0.03
Pb (wt%)	0.13	0.23	0.23	0.22	0.21	0.18	0.14	0.22	0.08	0.19	0.11	0.17	0.25	0.11	0.15
Bi (wt%)	0.09	0.06	0.14	0.18	0.09	0.12	0.10	0.16	0.15	0.16	0.18	0.16	0.15	0.20	0.13
Total	**99.57**	**101.17**	**101.44**	**101.42**	**101.05**	**101.12**	**101.09**	**91.13**	**97.73**	**99.74**	**97.84**	**97.55**	**98.69**	**100.41**	**99.11**
Formula (to 3 atoms)															
Fe	1.00	0.99	1.00	1.00	1.00	1.00	1.00	0.97	0.99	1.01	1.00	1.01	0.99	1.01	1.00
Co	0.00	0.00	0.00	0.00	0.00	0.00	0.00	0.00	0.00	0.00	0.00	0.00	0.00	0.00	0.00
Ni	0.00	0.00	0.00	0.00	0.00	0.00	0.00	0.00	0.00	0.00	0.00	0.00	0.00	0.00	0.00
Cu	0.00	0.00	0.00	0.00	0.00	0.00	0.00	0.01	0.00	0.00	0.00	0.00	0.00	0.00	0.00
Zn	0.00	0.00	0.00	0.00	0.00	0.00	0.00	0.00	0.00	0.00	0.00	0.00	0.00	0.00	0.00
Ag	0.00	0.00	0.00	0.00	0.00	0.00	0.00	0.00	0.00	0.00	0.00	0.00	0.00	0.00	0.00
Cd	0.00	0.00	0.00	0.00	0.00	0.00	0.00	0.00	0.00	0.00	0.00	0.00	0.00	0.00	0.00
Sb	0.00	0.00	0.00	0.00	0.00	0.00	0.00	0.00	0.00	0.00	0.00	0.00	0.00	0.00	0.00
Pb	0.00	0.00	0.00	0.00	0.00	0.00	0.00	0.00	0.00	0.00	0.00	0.00	0.00	0.00	0.00
Bi	0.00	0.00	0.00	0.00	0.00	0.00	0.00	0.00	0.00	0.00	0.00	0.00	0.00	0.00	0.00
Total	*1.00*	*0.99*	*1.00*	*1.00*	*1.00*	*1.00*	*1.00*	*0.98*	*1.00*	*1.01*	*1.01*	*1.01*	*0.99*	*1.01*	*1.00*
As	0.00	0.00	0.00	0.00	0.00	0.00	0.00	0.00	0.00	0.00	0.00	0.00	0.00	0.00	0.00
S	1.99	2.00	1.99	2.00	2.00	1.99	2.00	2.02	2.00	1.99	1.99	1.99	2.00	1.99	2.00
Total	*1.99*	*2.01*	*1.99*	*2.00*	*2.00*	*2.00*	*2.00*	*2.02*	*2.00*	*1.99*	*2.00*	*1.99*	*2.00*	*1.99*	*2.00*
Sum	**3.00**	**3.00**	**3.00**	**3.00**	**3.00**	**3.00**	**3.00**	**3.00**	**3.00**	**3.00**	**3.00**	**3.00**	**3.00**	**3.00**	**3.00**

Table 2: EPMA Analysis of Pyrite from session 2, again showing largely stoichiometric pyrite.

Analysis No.	**EI15.1**	**EI15.2**	**EI15.4**	**EI15.5**	**EI15.6**	**EI15.10**	**EI2.1**	**EI2.2**	**EI2.4**	**EI2.8**	**EI2.9**	**EI2.10**	**EI2.12**	**EI2.15**	**EI2.19**	**EI1.2**
Na (wt%)	0.01	0.01	0.06	0.04	0.00	0.00	0.00	0.00	0.02	0.05	0.00	0.03	0.04	0.01	0.03	0.02
Mg (wt%)	0.00	0.00	0.00	0.00	0.00	0.00	0.00	0.00	0.00	0.00	0.00	0.00	0.00	0.00	0.00	0.01
Al (wt%)	0.03	0.00	0.00	0.16	0.00	0.00	0.00	0.00	0.14	0.01	0.00	0.00	0.02	0.10	0.50	0.01
Si (wt%)	0.01	0.00	0.07	0.16	0.02	0.00	0.00	0.11	0.17	0.02	0.11	0.02	0.01	0.83	2.77	0.06
Si (wt%)	52.18	52.38	50.29	47.33	51.67	52.54	52.80	52.15	52.39	52.76	52.44	52.30	52.55	51.16	47.88	51.70
K (wt%)	0.00	0.01	0.00	0.01	0.02	0.00	0.00	0.01	0.02	0.03	0.02	0.04	0.03	0.02	0.07	0.00
Ca (wt%)	0.01	0.01	0.01	0.01	0.00	0.00	0.01	0.00	0.01	0.01	0.01	0.01	0.00	0.00	0.01	0.01

Ti (wt%)	0.01	0.01	0.03	0.00	0.00	0.01	0.00	0.00	0.04	0.00	0.04	0.00	0.02	0.29	0.67	0.00
V (wt%)	0.00	0.00	0.03	0.00	0.02	0.00	0.01	0.01	0.02	0.02	0.00	0.00	0.03	0.00	0.00	0.00
Cr (wt%)	0.00	0.00	0.00	0.01	0.01	0.00	0.02	0.00	0.01	0.01	0.00	0.01	0.02	0.00	0.00	0.00
Mn (wt%)	0.00	0.00	0.00	0.01	0.00	0.00	0.00	0.00	0.00	0.00	0.00	0.03	0.03	0.00	0.00	0.00
Fe (wt%)	44.43	44.66	44.26	42.03	44.10	45.95	46.75	45.82	46.22	45.35	45.41	45.56	45.59	45.07	41.45	44.64
Co (wt%)	0.00	0.00	0.00	0.00	0.00	0.00	0.00	0.00	0.00	0.00	0.00	0.00	0.00	0.01	0.00	0.06
Ni (wt%)	0.05	0.07	0.01	0.03	0.01	0.00	0.01	0.02	0.04	0.00	0.04	0.00	0.00	0.00	0.02	0.06
Zn (wt%)	0.05	0.01	0.00	0.02	0.00	0.02	0.03	0.00	0.08	0.05	0.06	0.02	0.03	0.02	0.00	0.00
Se (wt%)	0.01	0.01	0.01	0.00	0.00	0.03	0.04	0.01	0.00	0.00	0.03	0.01	0.03	0.00	0.00	0.00
Zr (wt%)	0.00	0.00	0.01	0.00	0.00	0.00	0.05	0.00	0.00	0.06	0.00	0.00	0.02	0.01	0.02	0.00
Nb (wt%)	0.00	0.03	0.00	0.03	0.00	0.00	0.03	0.00	0.00	0.03	0.00	0.04	0.00	0.00	0.00	0.02
Mo (wt%)	0.61	0.72	0.58	0.52	0.57	0.65	0.65	0.67	0.58	0.70	0.75	0.76	0.65	0.54	0.58	0.74
Ta (wt%)	0.12	0.10	0.09	0.00	0.00	0.00	0.01	0.03	0.00	0.02	0.00	0.00	0.00	0.00	0.08	0.00
Th (wt%)	0.02	0.00	0.00	0.00	0.00	0.00	0.05	0.06	0.00	0.04	0.13	0.02	0.00	0.00	0.12	0.05
U (wt%)	0.11	0.00	0.00	0.07	0.00	0.00	0.00	0.00	0.00	0.01	0.00	0.00	0.00	0.00	0.00	0.10
Total	97.65	98.02	95.45	90.42	96.42	99.20	100.47	98.90	99.76	99.17	99.05	98.85	99.06	98.05	94.21	97.49
Formula (to 3 atoms)																
Na (wt%)	0.00	0.00	0.00	0.00	0.00	0.00	0.00	0.00	0.00	0.00	0.00	0.00	0.00	0.00	0.00	0.00
Mg (wt%)	0.00	0.00	0.00	0.00	0.00	0.00	0.00	0.00	0.00	0.00	0.00	0.00	0.00	0.00	0.00	0.00
Al (wt%)	0.00	0.00	0.00	0.01	0.00	0.00	0.00	0.00	0.01	0.00	0.00	0.00	0.00	0.00	0.02	0.00
Si (wt%)	0.00	0.00	0.00	0.01	0.00	0.00	0.00	0.00	0.01	0.00	0.00	0.00	0.00	0.04	0.12	0.00
K (wt%)	0.00	0.00	0.00	0.00	0.00	0.00	0.00	0.00	0.00	0.00	0.00	0.00	0.00	0.00	0.00	0.00
Ca (wt%)	0.00	0.00	0.00	0.00	0.00	0.00	0.00	0.00	0.00	0.00	0.00	0.00	0.00	0.00	0.00	0.00
Ti (wt%)	0.00	0.00	0.00	0.00	0.00	0.00	0.00	0.00	0.00	0.00	0.00	0.00	0.00	0.01	0.02	0.00
V (wt%)	0.00	0.00	0.00	0.00	0.00	0.00	0.00	0.00	0.00	0.00	0.00	0.00	0.00	0.00	0.00	0.00
Cr (wt%)	0.00	0.00	0.00	0.00	0.00	0.00	0.00	0.00	0.00	0.00	0.00	0.00	0.00	0.00	0.00	0.00
Mn (wt%)	0.00	0.00	0.00	0.00	0.00	0.00	0.00	0.00	0.00	0.00	0.00	0.00	0.00	0.00	0.00	0.00
Fe (wt%)	0.98	0.98	1.00	1.00	0.98	1.00	1.01	1.00	1.00	0.99	0.99	1.00	0.99	0.99	0.94	0.99
Co (wt%)	0.00	0.00	0.00	0.00	0.00	0.00	0.00	0.00	0.00	0.00	0.00	0.00	0.00	0.00	0.00	0.00
Ni (wt%)	0.00	0.00	0.00	0.00	0.00	0.00	0.00	0.00	0.00	0.00	0.00	0.00	0.00	0.00	0.00	0.00
Zn (wt%)	0.00	0.00	0.00	0.00	0.00	0.00	0.00	0.00	0.00	0.00	0.00	0.00	0.00	0.00	0.00	0.00
Se (wt%)	0.00	0.00	0.00	0.00	0.00	0.00	0.00	0.00	0.00	0.00	0.00	0.00	0.00	0.00	0.00	0.00
Zr (wt%)	0.00	0.00	0.00	0.00	0.00	0.00	0.00	0.00	0.00	0.00	0.00	0.00	0.00	0.00	0.00	0.00
Nb (wt%)	0.00	0.00	0.00	0.00	0.00	0.00	0.00	0.00	0.00	0.00	0.00	0.00	0.00	0.00	0.00	0.00
Mo (wt%)	0.01	0.01	0.01	0.01	0.01	0.01	0.01	0.01	0.01	0.01	0.01	0.01	0.01	0.01	0.01	0.01
Ta (wt%)	0.00	0.00	0.00	0.00	0.00	0.00	0.00	0.00	0.00	0.00	0.00	0.00	0.00	0.00	0.00	0.00
Th (wt%)	0.00	0.00	0.00	0.00	0.00	0.00	0.00	0.00	0.00	0.00	0.00	0.00	0.00	0.00	0.00	0.00
U (wt%)	0.00	0.00	0.00	0.00	0.00	0.00	0.00	0.00	0.00	0.00	0.00	0.00	0.00	0.00	0.00	0.00
Total	*0.99*	*0.99*	*1.02*	*1.03*	*0.99*	*1.01*	*1.02*	*1.02*	*1.03*	*1.00*	*1.01*	*1.01*	*1.01*	*1.05*	*1.12*	*1.01*
S	2.01	2.01	1.98	1.97	2.01	1.99	1.98	1.98	1.97	2.00	1.99	1.99	1.99	1.95	1.88	1.99

Total	*2.01*	*2.01*	*1.98*	*1.97*	*2.01*	*1.99*	*1.98*	*1.98*	*1.97*	*2.00*	*1.99*	*1.99*	*1.99*	*1.95*	*1.88*	*1.99*
Sum	3.00	3.00	3.00	3.00	3.00	3.00	3.00	3.00	3.00	3.00	3.00	3.00	3.00	3.00	3.00	3.00

Analysis No.	EI1.3	EI1.6	EI1.7	EI1.8	EI1.9	EI1.12	EI1.15	EI24.1	EI24.8	EI24.9	EI24.10	EI24.11	EI24.12	EI24.13	EI19.1	EI19.2
Na (wt%)	0.01	0.03	0.02	0.00	0.01	0.15	0.13	0.03	0.04	0.00	0.00	0.04	0.03	0.00	0.00	0.04
Mg (wt%)	0.00	0.00	0.00	0.00	0.00	0.00	0.00	0.00	0.00	0.00	0.00	0.00	0.00	0.00	0.00	0.00
Al (wt%)	0.01	0.05	0.00	0.01	0.00	0.00	0.00	0.36	0.05	0.03	0.01	0.05	0.00	0.04	0.00	0.00
Si (wt%)	0.02	0.04	0.05	0.09	0.03	0.05	0.01	0.83	0.08	0.05	0.07	0.06	0.10	0.21	0.00	0.00
Si (wt%)	52.16	51.74	53.36	52.51	52.34	50.05	51.34	50.66	50.63	52.45	51.02	50.64	50.20	50.00	53.11	53.08
K (wt%)	0.01	0.01	0.02	0.01	0.03	0.03	0.03	0.04	0.01	0.00	0.02	0.04	0.04	0.02	0.00	0.00
Ca (wt%)	0.00	0.02	0.00	0.01	0.01	0.01	0.02	0.04	0.03	0.01	0.02	0.03	0.02	0.03	0.01	0.00
Ti (wt%)	0.01	0.02	0.01	0.02	0.02	0.05	0.03	0.02	0.00	0.00	0.01	0.01	0.07	0.00	0.00	0.00
V (wt%)	0.01	0.00	0.01	0.01	0.00	0.00	0.00	0.01	0.00	0.00	0.02	0.00	0.00	0.01	0.00	0.00
Cr (wt%)	0.00	0.00	0.01	0.00	0.00	0.00	0.00	0.00	0.00	0.01	0.00	0.00	0.00	0.00	0.00	0.00
Mn (wt%)	0.00	0.00	0.02	0.01	0.00	0.02	0.04	0.01	0.01	0.01	0.00	0.00	0.00	0.00	0.01	0.00
Fe (wt%)	45.55	46.41	44.91	46.21	45.87	44.32	44.95	44.11	45.15	45.68	45.12	44.24	44.32	44.39	46.17	46.29
Co (wt%)	0.00	0.00	0.00	0.00	0.04	0.00	0.00	0.00	0.00	0.00	0.00	0.00	0.00	0.01	0.00	0.00
Ni (wt%)	0.01	0.00	0.00	0.00	0.08	0.01	0.02	0.00	0.04	0.00	0.01	0.01	0.01	0.02	0.00	0.01
Zn (wt%)	0.00	0.03	0.00	0.02	0.00	0.01	0.00	0.03	0.01	0.03	0.04	0.01	0.01	0.00	0.00	0.00
Se (wt%)	0.02	0.02	0.01	0.01	0.02	0.02	0.03	0.02	0.02	0.00	0.00	0.00	0.00	0.00	0.01	0.00
Zr (wt%)	0.00	0.00	0.00	0.00	0.00	0.00	0.00	0.03	0.00	0.00	0.00	0.00	0.00	0.00	0.01	0.05
Nb (wt%)	0.02	0.01	0.05	0.00	0.02	0.00	0.00	0.00	0.00	0.00	0.01	0.00	0.00	0.04	0.01	0.04
Mo (wt%)	0.62	0.67	0.70	0.74	0.60	0.61	0.69	0.69	0.65	0.70	0.70	0.54	0.60	0.66	0.70	0.75
Ta (wt%)	0.00	0.08	0.00	0.00	0.05	0.00	0.00	0.00	0.00	0.01	0.02	0.00	0.00	0.00	0.02	0.00
Th (wt%)	0.02	0.03	0.00	0.00	0.00	0.01	0.00	0.00	0.06	0.03	0.00	0.00	0.00	0.00	0.18	0.06
U (wt%)	0.04	0.00	0.00	0.00	0.00	0.03	0.00	0.00	0.00	0.04	0.00	0.07	0.00	0.00	0.00	0.00
Total	98.52	99.16	99.16	99.65	99.12	95.38	97.29	96.88	96.80	99.04	97.05	95.75	95.41	95.43	100.23	100.33
Formula (to 3 atoms)																
Na	0.00	0.00	0.00	0.00	0.00	0.01	0.01	0.00	0.00	0.00	0.00	0.00	0.00	0.00	0.00	0.00
Mg	0.00	0.00	0.00	0.00	0.00	0.00	0.00	0.00	0.00	0.00	0.00	0.00	0.00	0.00	0.00	0.00
Al	0.00	0.00	0.00	0.00	0.00	0.00	0.00	0.02	0.00	0.00	0.00	0.00	0.00	0.00	0.00	0.00
Si	0.00	0.00	0.00	0.00	0.00	0.00	0.00	0.04	0.00	0.00	0.00	0.00	0.00	0.01	0.00	0.00
K	0.00	0.00	0.00	0.00	0.00	0.00	0.00	0.00	0.00	0.00	0.00	0.00	0.00	0.00	0.00	0.00
Ca	0.00	0.00	0.00	0.00	0.00	0.00	0.00	0.00	0.00	0.00	0.00	0.00	0.00	0.00	0.00	0.00
Ti	0.00	0.00	0.00	0.00	0.00	0.00	0.00	0.00	0.00	0.00	0.00	0.00	0.00	0.00	0.00	0.00
V	0.00	0.00	0.00	0.00	0.00	0.00	0.00	0.00	0.00	0.00	0.00	0.00	0.00	0.00	0.00	0.00
Cr	0.00	0.00	0.00	0.00	0.00	0.00	0.00	0.00	0.00	0.00	0.00	0.00	0.00	0.00	0.00	0.00
Mn	0.00	0.00	0.00	0.00	0.00	0.00	0.00	0.00	0.00	0.00	0.00	0.00	0.00	0.00	0.00	0.00
Fe	1.00	1.01	0.97	1.00	1.00	1.00	1.00	0.98	1.01	1.00	1.01	1.00	1.00	1.01	1.00	1.00
Co	0.00	0.00	0.00	0.00	0.00	0.00	0.00	0.00	0.00	0.00	0.00	0.00	0.00	0.00	0.00	0.00
Ni	0.00	0.00	0.00	0.00	0.00	0.00	0.00	0.00	0.00	0.00	0.00	0.00	0.00	0.00	0.00	0.00
Zn	0.00	0.00	0.00	0.00	0.00	0.00	0.00	0.00	0.00	0.00	0.00	0.00	0.00	0.00	0.00	0.00
Se	0.00	0.00	0.00	0.00	0.00	0.00	0.00	0.00	0.00	0.00	0.00	0.00	0.00	0.00	0.00	0.00
Zr	0.00	0.00	0.00	0.00	0.00	0.00	0.00	0.00	0.00	0.00	0.00	0.00	0.00	0.00	0.00	0.00

Nb	0.00	0.00	0.00	0.00	0.00	0.00	0.00	0.00	0.00	0.00	0.00	0.00	0.00	0.00	0.00	0.00
Mo	0.01	0.01	0.01	0.01	0.01	0.01	0.01	0.01	0.01	0.01	0.01	0.01	0.01	0.01	0.01	0.01
Ta	0.00	0.00	0.00	0.00	0.00	0.00	0.00	0.00	0.00	0.00	0.00	0.00	0.00	0.00	0.00	0.00
Th	0.00	0.00	0.00	0.00	0.00	0.00	0.00	0.00	0.00	0.00	0.00	0.00	0.00	0.00	0.00	0.00
U	0.00	0.00	0.00	0.00	0.00	0.00	0.00	0.00	0.00	0.00	0.00	0.00	0.00	0.00	0.00	0.00
Total	*1.01*	*1.03*	*0.99*	*1.02*	*1.01*	*1.03*	*1.02*	*1.05*	*1.03*	*1.01*	*1.02*	*1.01*	*1.02*	*1.03*	*1.01*	*1.01*
S	1.99	1.97	2.01	1.98	1.99	1.97	1.98	1.95	1.97	1.99	1.98	1.99	1.98	1.97	1.99	1.99
Total	*1.99*	*1.97*	*2.01*	*1.98*	*1.99*	*1.97*	*1.98*	*1.95*	*1.97*	*1.99*	*1.98*	*1.99*	*1.98*	*1.97*	*1.99*	*1.99*
Sum	3.00	3.00	3.00	3.00	3.00	3.00	3.00	3.00	3.00	3.00	3.00	3.00	3.00	3.00	3.00	3.00

Analysis No.	EI19.3	EI19.4	EI19.5	EI19.9	EI19.10	EI19.11	EI16.1	EI16.2	EI16.3	EI16.4	EI16.6	EI16.11	EI16.12	EI5.1	EI5.2	EI5.5
Na (wt%)	0.00	0.00	0.02	0.00	0.03	0.20	0.04	0.00	0.00	0.02	0.00	0.00	0.01	0.03	0.04	0.04
Mg (wt%)	0.00	0.00	0.00	0.00	0.00	0.01	0.00	0.00	0.00	0.00	0.00	0.00	0.00	0.00	0.00	0.00
Al (wt%)	0.01	0.01	0.00	0.00	0.00	0.04	0.00	0.01	0.10	0.11	0.00	0.00	0.00	0.18	2.01	0.02
Si (wt%)	0.00	0.01	0.00	0.04	0.00	0.12	0.01	0.03	0.12	0.13	0.00	0.02	0.01	0.29	1.98	0.06
Si (wt%)	53.01	52.87	52.88	52.80	53.03	42.53	52.44	50.89	51.46	51.34	52.86	49.82	51.90	50.68	45.50	51.74
K (wt%)	0.01	0.00	0.01	0.02	0.02	0.27	0.01	0.01	0.02	0.01	0.00	0.01	0.01	0.02	0.03	0.01
Ca (wt%)	0.00	0.00	0.00	0.00	0.00	0.02	0.00	0.01	0.01	0.02	0.00	0.02	0.01	0.01	0.08	0.02
Ti (wt%)	0.01	0.00	0.00	0.01	0.00	0.01	0.01	0.00	0.04	0.01	0.00	0.04	0.01	0.01	0.02	0.12
V (wt%)	0.01	0.00	0.00	0.00	0.01	0.00	0.00	0.00	0.01	0.00	0.01	0.00	0.01	0.00	0.00	0.00
Cr (wt%)	0.00	0.00	0.00	0.01	0.00	0.00	0.00	0.00	0.00	0.01	0.01	0.00	0.00	0.00	0.00	0.00
Mn (wt%)	0.00	0.00	0.00	0.01	0.00	0.02	0.00	0.01	0.01	0.01	0.02	0.01	0.00	0.01	0.01	0.04
Fe (wt%)	46.48	45.99	46.55	46.66	46.65	38.34	46.32	45.41	45.89	46.06	46.52	45.98	46.49	44.57	40.30	45.03
Co (wt%)	0.00	0.00	0.00	0.00	0.00	0.00	0.00	0.00	0.00	0.00	0.00	0.00	0.00	0.00	0.00	0.00
Ni (wt%)	0.03	0.01	0.03	0.00	0.00	0.00	0.01	0.00	0.00	0.02	0.01	0.01	0.00	0.00	0.03	0.01
Zn (wt%)	0.00	0.00	0.00	0.01	0.00	0.00	0.00	0.03	0.00	0.03	0.00	0.02	0.02	0.01	0.01	0.00
Se (wt%)	0.00	0.00	0.00	0.02	0.05	0.03	0.02	0.02	0.04	0.00	0.00	0.00	0.00	0.02	0.02	0.00
Zr (wt%)	0.00	0.00	0.00	0.02	0.00	0.00	0.00	0.01	0.02	0.05	0.01	0.00	0.00	0.00	0.01	0.00
Nb (wt%)	0.04	0.02	0.00	0.00	0.03	0.01	0.00	0.00	0.00	0.00	0.00	0.02	0.00	0.00	0.00	0.01
Mo (wt%)	0.70	0.68	0.69	0.76	0.51	0.52	0.59	0.59	0.73	0.67	0.70	0.62	0.65	0.77	0.61	0.60
Ta (wt%)	0.03	0.00	0.00	0.05	0.00	0.00	0.00	0.00	0.06	0.01	0.00	0.00	0.00	0.06	0.00	0.00
Th (wt%)	0.00	0.01	0.01	0.12	0.12	0.01	0.01	0.00	0.00	0.02	0.00	0.00	0.05	0.00	0.00	0.07
U (wt%)	0.00	0.04	0.00	0.00	0.00	0.00	0.00	0.00	0.00	0.00	0.02	0.00	0.01	0.00	0.07	0.00
Total	100.32	99.63	100.20	100.52	100.44	82.14	99.46	97.00	98.52	98.52	100.18	96.56	99.19	96.65	90.73	97.76
Formula (to 3 atoms)																
Na	0.00	0.00	0.00	0.00	0.00	0.01	0.00	0.00	0.00	0.00	0.00	0.00	0.00	0.00	0.00	0.00
Mg	0.00	0.00	0.00	0.00	0.00	0.00	0.00	0.00	0.00	0.00	0.00	0.00	0.00	0.00	0.00	0.00
Al	0.00	0.00	0.00	0.00	0.00	0.00	0.00	0.00	0.00	0.00	0.00	0.00	0.00	0.01	0.10	0.00
Si	0.00	0.00	0.00	0.00	0.00	0.01	0.00	0.00	0.01	0.01	0.00	0.00	0.00	0.01	0.09	0.00
K	0.00	0.00	0.00	0.00	0.00	0.01	0.00	0.00	0.00	0.00	0.00	0.00	0.00	0.00	0.00	0.00
Ca	0.00	0.00	0.00	0.00	0.00	0.00	0.00	0.00	0.00	0.00	0.00	0.00	0.00	0.00	0.00	0.00
Ti	0.00	0.00	0.00	0.00	0.00	0.00	0.00	0.00	0.00	0.00	0.00	0.00	0.00	0.00	0.00	0.00
V	0.00	0.00	0.00	0.00	0.00	0.00	0.00	0.00	0.00	0.00	0.00	0.00	0.00	0.00	0.00	0.00
Cr	0.00	0.00	0.00	0.00	0.00	0.00	0.00	0.00	0.00	0.00	0.00	0.00	0.00	0.00	0.00	0.00
Mn	0.00	0.00	0.00	0.00	0.00	0.00	0.00	0.00	0.00	0.00	0.00	0.00	0.00	0.00	0.00	0.00
Fe	1.00	1.00	1.00	1.00	1.00	1.01	1.01	1.01	1.01	1.01	1.00	1.03	1.02	0.99	0.94	0.99
Co	0.00	0.00	0.00	0.00	0.00	0.00	0.00	0.00	0.00	0.00	0.00	0.00	0.00	0.00	0.00	0.00
Ni	0.00	0.00	0.00	0.00	0.00	0.00	0.00	0.00	0.00	0.00	0.00	0.00	0.00	0.00	0.00	0.00
Zn	0.00	0.00	0.00	0.00	0.00	0.00	0.00	0.00	0.00	0.00	0.00	0.00	0.00	0.00	0.00	0.00
Se	0.00	0.00	0.00	0.00	0.00	0.00	0.00	0.00	0.00	0.00	0.00	0.00	0.00	0.00	0.00	0.00
Zr	0.00	0.00	0.00	0.00	0.00	0.00	0.00	0.00	0.00	0.00	0.00	0.00	0.00	0.00	0.00	0.00

Nb	0.00	0.00	0.00	0.00	0.00	0.00	0.00	0.00	0.00	0.00	0.00	0.00	0.00	0.00	0.00	0.00
Mo	0.01	0.01	0.01	0.01	0.01	0.01	0.01	0.01	0.01	0.01	0.01	0.01	0.01	0.01	0.01	0.01
Ta	0.00	0.00	0.00	0.00	0.00	0.00	0.00	0.00	0.00	0.00	0.00	0.00	0.00	0.00	0.00	0.00
Th	0.00	0.00	0.00	0.00	0.00	0.00	0.00	0.00	0.00	0.00	0.00	0.00	0.00	0.00	0.00	0.00
U	0.00	0.00	0.00	0.00	0.00	0.00	0.00	0.00	0.00	0.00	0.00	0.00	0.00	0.00	0.00	0.00
Total	*1.01*	*1.01*	*1.01*	*1.02*	*1.01*	*1.05*	*1.02*	*1.02*	*1.03*	*1.04*	*1.01*	*1.05*	*1.03*	*1.03*	*1.15*	*1.01*
S	1.99	1.99	1.99	1.98	1.99	1.95	1.98	1.98	1.97	1.96	1.99	1.95	1.97	1.97	1.85	1.99
Total	*1.99*	*1.99*	*1.99*	*1.98*	*1.99*	*1.95*	*1.98*	*1.98*	*1.97*	*1.96*	*1.99*	*1.95*	*1.97*	*1.97*	*1.85*	*1.99*
Sum	3.00	3.00	3.00	3.00	3.00	3.00	3.00	3.00	3.00	3.00	3.00	3.00	3.00	3.00	3.00	3.00

Analysis No.	EI5.6	EI5.8	EI8.1	EI8.2	EI8.4	EI8.5	EI8.6	EI12.2	EI12.3	EI12.4	EI12.5	EI12.6	EI12.7	EI12.9	EI12.10	EI12.12
Na (wt%)	0.00	0.04	0.00	0.00	0.00	0.00	0.03	0.03	0.02	0.00	0.00	0.00	0.01	0.00	0.00	0.00
Mg (wt%)	0.00	0.00	0.00	0.00	0.00	0.00	0.00	0.00	0.00	0.00	0.00	0.01	0.00	0.00	0.00	0.00
Al (wt%)	0.87	0.02	0.00	0.89	0.00	0.00	0.00	0.10	0.00	2.07	0.00	2.09	0.00	0.00	0.15	3.24
Si (wt%)	0.89	0.03	0.02	0.98	0.01	0.01	0.00	0.16	0.02	2.18	0.01	2.34	0.01	0.00	0.17	3.12
Si (wt%)	48.20	52.05	51.95	46.61	52.06	52.32	52.33	51.33	51.70	47.14	51.70	46.75	51.75	52.30	51.01	43.90
K (wt%)	0.02	0.02	0.00	0.01	0.00	0.00	0.01	0.01	0.02	0.02	0.01	0.01	0.00	0.00	0.00	0.00
Ca (wt%)	0.06	0.00	0.00	0.01	0.00	0.00	0.00	0.01	0.00	0.01	0.01	0.01	0.00	0.02	0.03	0.02
Ti (wt%)	0.06	0.00	0.01	0.01	0.00	0.01	0.00	0.00	0.00	0.00	0.01	0.02	0.01	0.01	0.01	0.00
V (wt%)	0.01	0.01	0.00	0.00	0.00	0.00	0.00	0.00	0.01	0.02	0.00	0.00	0.01	0.00	0.00	0.00
Cr (wt%)	0.00	0.00	0.00	0.00	0.00	0.00	0.00	0.00	0.00	0.00	0.00	0.00	0.00	0.00	0.00	0.00
Mn (wt%)	0.04	0.01	0.00	0.00	0.02	0.00	0.00	0.00	0.00	0.00	0.00	0.01	0.02	0.00	0.00	0.02
Fe (wt%)	42.89	45.96	45.63	41.26	46.10	46.22	46.07	45.65	46.86	41.43	45.92	39.82	46.36	46.40	44.76	39.06
Co (wt%)	0.01	0.00	0.00	0.00	0.00	0.00	0.00	0.00	0.00	0.00	0.00	0.05	0.00	0.00	0.00	0.00
Ni (wt%)	0.03	0.01	0.01	0.03	0.02	0.03	0.02	0.01	0.03	0.07	0.05	0.26	0.02	0.01	0.02	0.09
Zn (wt%)	0.03	0.00	0.04	0.00	0.00	0.00	0.00	0.00	0.00	0.01	0.01	0.00	0.00	0.01	0.00	0.01
Se (wt%)	0.02	0.01	0.00	0.00	0.00	0.00	0.05	0.03	0.04	0.00	0.00	0.06	0.00	0.01	0.01	0.01
Zr (wt%)	0.07	0.01	0.08	0.00	0.01	0.02	0.04	0.00	0.03	0.03	0.04	0.02	0.03	0.01	0.00	0.04
Nb (wt%)	0.02	0.02	0.00	0.00	0.00	0.00	0.03	0.00	0.00	0.00	0.02	0.00	0.00	0.04	0.00	0.00
Mo (wt%)	0.59	0.76	0.67	0.71	0.67	0.70	0.67	0.60	0.70	0.55	0.59	0.63	0.56	0.64	0.70	0.51
Ta (wt%)	0.05	0.03	0.02	0.02	0.00	0.02	0.05	0.00	0.02	0.00	0.01	0.00	0.00	0.03	0.00	0.00
Th (wt%)	0.00	0.00	0.00	0.03	0.00	0.08	0.03	0.00	0.03	0.00	0.01	0.00	0.02	0.02	0.08	0.03
U (wt%)	0.00	0.00	0.00	0.00	0.07	0.00	0.00	0.00	0.05	0.00	0.00	0.00	0.06	0.00	0.02	0.00
Total	93.86	98.98	98.43	90.58	98.97	99.42	99.33	97.94	99.53	93.53	98.38	92.10	98.85	99.51	96.96	90.06
Formula (to 3 atoms)																
Na	0.00	0.00	0.00	0.00	0.00	0.00	0.00	0.00	0.00	0.00	0.00	0.00	0.00	0.00	0.00	0.00
Mg	0.00	0.00	0.00	0.00	0.00	0.00	0.00	0.00	0.00	0.00	0.00	0.00	0.00	0.00	0.00	0.00
Al	0.04	0.00	0.00	0.04	0.00	0.00	0.00	0.00	0.00	0.10	0.00	0.10	0.00	0.00	0.01	0.16
Si	0.04	0.00	0.00	0.05	0.00	0.00	0.00	0.01	0.00	0.10	0.00	0.11	0.00	0.00	0.01	0.14
K	0.00	0.00	0.00	0.00	0.00	0.00	0.00	0.00	0.00	0.00	0.00	0.00	0.00	0.00	0.00	0.00
Ca	0.00	0.00	0.00	0.00	0.00	0.00	0.00	0.00	0.00	0.00	0.00	0.00	0.00	0.00	0.00	0.00
Ti	0.00	0.00	0.00	0.00	0.00	0.00	0.00	0.00	0.00	0.00	0.00	0.00	0.00	0.00	0.00	0.00
V	0.00	0.00	0.00	0.00	0.00	0.00	0.00	0.00	0.00	0.00	0.00	0.00	0.00	0.00	0.00	0.00
Cr	0.00	0.00	0.00	0.00	0.00	0.00	0.00	0.00	0.00	0.00	0.00	0.00	0.00	0.00	0.00	0.00
Mn	0.00	0.00	0.00	0.00	0.00	0.00	0.00	0.00	0.00	0.00	0.00	0.00	0.00	0.00	0.00	0.00
Fe	0.98	1.00	1.00	0.98	1.01	1.01	1.00	1.01	1.02	0.94	1.01	0.91	1.02	1.01	1.00	0.91
Co	0.00	0.00	0.00	0.00	0.00	0.00	0.00	0.00	0.00	0.00	0.00	0.00	0.00	0.00	0.00	0.00
Ni	0.00	0.00	0.00	0.00	0.00	0.00	0.00	0.00	0.00	0.00	0.00	0.01	0.00	0.00	0.00	0.00
Zn	0.00	0.00	0.00	0.00	0.00	0.00	0.00	0.00	0.00	0.00	0.00	0.00	0.00	0.00	0.00	0.00
Se	0.00	0.00	0.00	0.00	0.00	0.00	0.00	0.00	0.00	0.00	0.00	0.00	0.00	0.00	0.00	0.00
Zr	0.00	0.00	0.00	0.00	0.00	0.00	0.00	0.00	0.00	0.00	0.00	0.00	0.00	0.00	0.00	0.00

Nb	0.00	0.00	0.00	0.00	0.00	0.00	0.00	0.00	0.00	0.00	0.00	0.00	0.00	0.00	0.00	0.00
Mo	0.01	0.01	0.01	0.01	0.01	0.01	0.01	0.01	0.01	0.01	0.01	0.01	0.01	0.01	0.01	0.01
Ta	0.00	0.00	0.00	0.00	0.00	0.00	0.00	0.00	0.00	0.00	0.00	0.00	0.00	0.00	0.00	0.00
Th	0.00	0.00	0.00	0.00	0.00	0.00	0.00	0.00	0.00	0.00	0.00	0.00	0.00	0.00	0.00	0.00
U	0.00	0.00	0.00	0.00	0.00	0.00	0.00	0.00	0.00	0.00	0.00	0.00	0.00	0.00	0.00	0.00
Total	*1.08*	*1.02*	*1.01*	*1.08*	*1.02*	*1.02*	*1.02*	*1.03*	*1.04*	*1.14*	*1.02*	*1.14*	*1.03*	*1.02*	*1.02*	*1.22*
S	1.92	1.98	1.99	1.92	1.98	1.98	1.98	1.97	1.96	1.86	1.98	1.86	1.97	1.98	1.98	1.78
Total	*1.92*	*1.98*	*1.99*	*1.92*	*1.98*	*1.98*	*1.98*	*1.97*	*1.96*	*1.86*	*1.98*	*1.86*	*1.97*	*1.98*	*1.98*	*1.78*
Sum	3.00	3.00	3.00	3.00	3.00	3.00	3.00	3.00	3.00	3.00	3.00	3.00	3.00	3.00	3.00	3.00

Analysis No.	EI12.14	EI12.15	EI8.8	EI8.9	EI8.11	EI8.12	EI8.13	EI8.14	EI8.15	EI8.16	EI8.17	EI8.18	EI6.18	EI6.19	EI6.20	EI5.12
Na (wt%)	0.03	0.00	0.00	0.02	0.02	0.03	0.04	0.00	0.00	0.00	0.00	0.00	0.00	0.02	0.02	0.00
Mg (wt%)	0.00	0.00	0.00	0.00	0.00	0.00	0.00	0.00	0.00	0.00	0.00	0.00	0.00	0.00	0.00	0.00
Al (wt%)	0.00	0.11	0.71	0.89	0.00	0.00	0.01	0.00	0.00	0.84	0.00	0.00	0.00	0.21	1.02	0.00
Si (wt%)	0.00	0.13	0.58	1.00	0.00	0.09	0.01	0.01	0.04	0.91	0.03	0.27	0.01	0.47	1.30	0.00
Si (wt%)	51.70	52.22	50.80	49.86	51.83	52.91	52.27	52.42	52.43	50.11	52.18	51.42	52.79	50.12	47.57	51.85
K (wt%)	0.01	0.00	0.01	0.02	0.02	0.00	0.03	0.00	0.02	0.02	0.02	0.01	0.02	0.02	0.02	0.02
Ca (wt%)	0.00	0.00	0.01	0.01	0.00	0.00	0.00	0.00	0.00	0.00	0.00	0.00	0.00	0.00	0.00	0.01
Ti (wt%)	0.00	0.00	0.00	0.01	0.00	0.00	0.02	0.00	0.00	0.00	0.01	0.03	0.00	0.02	0.06	0.01
V (wt%)	0.00	0.02	0.01	0.01	0.00	0.00	0.00	0.00	0.00	0.00	0.00	0.00	0.00	0.00	0.02	0.01
Cr (wt%)	0.00	0.01	0.00	0.00	0.00	0.00	0.00	0.01	0.00	0.00	0.00	0.00	0.01	0.00	0.00	0.00
Mn (wt%)	0.02	0.00	0.01	0.01	0.00	0.00	0.00	0.00	0.00	0.01	0.02	0.00	0.00	0.02	0.00	0.01
Fe (wt%)	46.07	46.20	44.34	43.25	45.24	46.12	45.68	45.83	45.52	43.56	46.01	44.80	46.35	42.87	40.06	45.86
Co (wt%)	0.00	0.00	0.01	0.00	0.00	0.00	0.00	0.00	0.02	0.05	0.00	0.00	0.00	0.00	0.00	0.00
Ni (wt%)	0.02	0.05	0.03	0.06	0.00	0.01	0.01	0.01	0.00	0.04	0.01	0.02	0.00	0.00	0.02	0.01
Zn (wt%)	0.03	0.00	0.04	0.00	0.00	0.06	0.05	0.00	0.03	0.00	0.00	0.00	0.01	0.00	0.00	0.00
Se (wt%)	0.02	0.00	0.00	0.02	0.00	0.02	0.03	0.00	0.00	0.00	0.05	0.02	0.00	0.00	0.00	0.01
Zr (wt%)	0.01	0.00	0.02	0.00	0.00	0.00	0.00	0.00	0.00	0.00	0.04	0.02	0.00	0.00	0.02	0.01
Nb (wt%)	0.00	0.00	0.00	0.03	0.03	0.01	0.00	0.00	0.00	0.02	0.01	0.00	0.00	0.00	0.00	0.01
Mo (wt%)	0.61	0.56	0.72	0.59	0.67	0.69	0.77	0.63	0.72	0.76	0.66	0.65	0.61	0.65	0.58	0.69
Ta (wt%)	0.05	0.03	0.00	0.00	0.05	0.00	0.09	0.03	0.00	0.02	0.04	0.00	0.00	0.00	0.00	0.02
Th (wt%)	0.02	0.00	0.00	0.00	0.09	0.09	0.06	0.06	0.01	0.00	0.00	0.04	0.01	0.00	0.00	0.00
U (wt%)	0.00	0.00	0.06	0.01	0.00	0.00	0.00	0.00	0.00	0.00	0.04	0.03	0.04	0.00	0.02	0.00
Total	98.59	99.34	97.35	95.82	97.97	100.05	99.09	99.01	98.82	96.34	99.12	97.31	99.84	94.40	90.69	98.54
Formula (to 3 atoms)																
Na	0.00	0.00	0.00	0.00	0.00	0.00	0.00	0.00	0.00	0.00	0.00	0.00	0.00	0.00	0.00	0.00
Mg	0.00	0.00	0.00	0.00	0.00	0.00	0.00	0.00	0.00	0.00	0.00	0.00	0.00	0.00	0.00	0.00
Al	0.00	0.01	0.03	0.04	0.00	0.00	0.00	0.00	0.00	0.04	0.00	0.00	0.00	0.01	0.05	0.00
Si	0.00	0.01	0.03	0.04	0.00	0.00	0.00	0.00	0.00	0.04	0.00	0.01	0.00	0.02	0.06	0.00
K	0.00	0.00	0.00	0.00	0.00	0.00	0.00	0.00	0.00	0.00	0.00	0.00	0.00	0.00	0.00	0.00
Ca	0.00	0.00	0.00	0.00	0.00	0.00	0.00	0.00	0.00	0.00	0.00	0.00	0.00	0.00	0.00	0.00
Ti	0.00	0.00	0.00	0.00	0.00	0.00	0.00	0.00	0.00	0.00	0.00	0.00	0.00	0.00	0.00	0.00
V	0.00	0.00	0.00	0.00	0.00	0.00	0.00	0.00	0.00	0.00	0.00	0.00	0.00	0.00	0.00	0.00
Cr	0.00	0.00	0.00	0.00	0.00	0.00	0.00	0.00	0.00	0.00	0.00	0.00	0.00	0.00	0.00	0.00
Mn	0.00	0.00	0.00	0.00	0.00	0.00	0.00	0.00	0.00	0.00	0.00	0.00	0.00	0.00	0.00	0.00
Fe	1.01	1.00	0.98	0.96	1.00	1.00	1.00	1.00	0.99	0.97	1.00	0.99	1.00	0.97	0.94	1.01
Co	0.00	0.00	0.00	0.00	0.00	0.00	0.00	0.00	0.00	0.00	0.00	0.00	0.00	0.00	0.00	0.00
Ni	0.00	0.00	0.00	0.00	0.00	0.00	0.00	0.00	0.00	0.00	0.00	0.00	0.00	0.00	0.00	0.00
Zn	0.00	0.00	0.00	0.00	0.00	0.00	0.00	0.00	0.00	0.00	0.00	0.00	0.00	0.00	0.00	0.00
Se	0.00	0.00	0.00	0.00	0.00	0.00	0.00	0.00	0.00	0.00	0.00	0.00	0.00	0.00	0.00	0.00
Zr	0.00	0.00	0.00	0.00	0.00	0.00	0.00	0.00	0.00	0.00	0.00	0.00	0.00	0.00	0.00	0.00

Nb	0.00	0.00	0.00	0.00	0.00	0.00	0.00	0.00	0.00	0.00	0.00	0.00	0.00	0.00	0.00	0.00
Mo	0.01	0.01	0.01	0.01	0.01	0.01	0.01	0.01	0.01	0.01	0.01	0.01	0.01	0.01	0.01	0.01
Ta	0.00	0.00	0.00	0.00	0.00	0.00	0.00	0.00	0.00	0.00	0.00	0.00	0.00	0.00	0.00	0.00
Th	0.00	0.00	0.00	0.00	0.00	0.00	0.00	0.00	0.00	0.00	0.00	0.00	0.00	0.00	0.00	0.00
U	0.00	0.00	0.00	0.00	0.00	0.00	0.00	0.00	0.00	0.00	0.00	0.00	0.00	0.00	0.00	0.00
Total	*1.02*	*1.02*	*1.05*	*1.06*	*1.01*	*1.01*	*1.01*	*1.01*	*1.01*	*1.06*	*1.02*	*1.02*	*1.01*	*1.02*	*1.06*	*1.02*
S	1.98	1.98	1.95	1.94	1.99	1.99	1.99	1.99	1.99	1.94	1.98	1.98	1.99	1.98	1.94	1.98
Total	*1.98*	*1.98*	*1.95*	*1.94*	*1.99*	*1.99*	*1.99*	*1.99*	*1.99*	*1.94*	*1.98*	*1.98*	*1.99*	*1.98*	*1.94*	*1.98*
Sum	3.00	3.00	3.00	3.00	3.00	3.00	3.00	3.00	3.00	3.00	3.00	3.00	3.00	3.00	3.00	3.00

Analysis No.	EI11.2	EI11.3	EI11.4	EI11.5	EI11.7	EI11.9	EI11.10	EI11.11	EI31.6	EI7.4	EI7.5	EI17.1
Na (wt%)	0.02	0.00	0.03	0.00	0.06	0.00	0.02	0.01	0.00	0.00	0.01	0.01
Mg (wt%)	0.00	0.00	0.00	0.00	0.02	0.00	0.00	0.00	0.00	0.00	0.00	0.00
Al (wt%)	0.05	0.00	0.00	0.00	0.15	0.00	0.00	0.04	0.18	0.00	0.02	0.01
Si (wt%)	0.05	0.02	0.01	0.01	1.18	0.01	0.11	0.22	0.26	0.00	0.00	0.05
Si (wt%)	47.63	50.64	51.03	50.92	41.88	51.00	47.36	43.31	51.18	52.28	52.30	52.36
K (wt%)	0.01	0.01	0.01	0.01	0.05	0.00	0.00	0.00	0.02	0.01	0.00	0.00
Ca (wt%)	0.01	0.00	0.00	0.00	0.03	0.01	0.08	0.01	0.02	0.01	0.01	0.00
Ti (wt%)	0.00	0.01	0.01	0.01	0.02	0.00	0.01	0.00	0.35	0.00	0.00	0.00
V (wt%)	0.02	0.00	0.00	0.03	0.00	0.00	0.00	0.05	0.00	0.01	0.00	0.02
Cr (wt%)	0.00	0.00	0.00	0.00	0.00	0.00	0.00	0.00	0.00	0.00	0.01	0.00
Mn (wt%)	0.01	0.00	0.00	0.02	0.00	0.00	0.00	0.01	0.02	0.01	0.00	0.01
Fe (wt%)	43.93	44.71	43.84	44.87	34.96	45.51	42.67	45.35	44.02	45.13	46.32	45.30
Co (wt%)	0.05	0.00	0.00	0.00	0.06	0.00	0.05	0.04	0.00	0.00	0.00	0.00
Ni (wt%)	0.00	0.01	0.00	0.02	0.03	0.00	0.01	0.00	0.02	0.01	0.04	0.05
Zn (wt%)	0.00	0.00	0.01	0.00	0.02	0.00	0.00	0.01	0.00	0.04	0.01	0.00
Se (wt%)	3.79	0.00	0.01	0.03	21.08	0.03	0.26	0.54	0.00	0.00	0.00	0.05
Zr (wt%)	0.01	0.02	0.00	0.00	0.00	0.00	0.02	0.04	0.00	0.00	0.02	0.04
Nb (wt%)	0.04	0.00	0.01	0.01	0.00	0.01	0.00	0.01	0.00	0.02	0.02	0.02
Mo (wt%)	0.63	0.70	0.74	0.79	0.52	0.70	0.51	0.56	0.66	0.74	0.60	0.66
Ta (wt%)	0.00	0.01	0.02	0.03	0.09	0.00	0.00	0.00	0.00	0.00	0.05	0.00
Th (wt%)	0.00	0.00	0.00	0.05	0.06	0.00	0.00	0.02	0.01	0.10	0.06	0.00
U (wt%)	0.06	0.00	0.00	0.02	0.00	0.00	0.00	0.04	0.13	0.02	0.00	0.00
Total	96.33	96.13	95.72	96.81	100.22	97.28	91.12	90.25	96.89	98.39	99.47	98.58
Formula (to 3 atoms)												
Na	0.00	0.00	0.00	0.00	0.00	0.00	0.00	0.00	0.00	0.00	0.00	0.00
Mg	0.00	0.00	0.00	0.00	0.00	0.00	0.00	0.00	0.00	0.00	0.00	0.00
Al	0.00	0.00	0.00	0.00	0.01	0.00	0.00	0.00	0.01	0.00	0.00	0.00
Si	0.00	0.00	0.00	0.00	0.06	0.00	0.01	0.01	0.01	0.00	0.00	0.00
K	0.00	0.00	0.00	0.00	0.00	0.00	0.00	0.00	0.00	0.00	0.00	0.00
Ca	0.00	0.00	0.00	0.00	0.00	0.00	0.00	0.00	0.00	0.00	0.00	0.00
Ti	0.00	0.00	0.00	0.00	0.00	0.00	0.00	0.00	0.01	0.00	0.00	0.00
V	0.00	0.00	0.00	0.00	0.00	0.00	0.00	0.00	0.00	0.00	0.00	0.00
Cr	0.00	0.00	0.00	0.00	0.00	0.00	0.00	0.00	0.00	0.00	0.00	0.00
Mn	0.00	0.00	0.00	0.00	0.00	0.00	0.00	0.00	0.00	0.00	0.00	0.00
Fe	1.01	1.01	0.99	1.00	0.83	1.01	1.02	1.11	0.98	0.99	1.01	0.99
Co	0.00	0.00	0.00	0.00	0.00	0.00	0.00	0.00	0.00	0.00	0.00	0.00
Ni	0.00	0.00	0.00	0.00	0.00	0.00	0.00	0.00	0.00	0.00	0.00	0.00
Zn	0.00	0.00	0.00	0.00	0.00	0.00	0.00	0.00	0.00	0.00	0.00	0.00
Se	0.06	0.00	0.00	0.00	0.35	0.00	0.00	0.01	0.00	0.00	0.00	0.00

Zr	0.00	0.00	0.00	0.00	0.00	0.00	0.00	0.00	0.00	0.00	0.00	0.00
Nb	0.00	0.00	0.00	0.00	0.00	0.00	0.00	0.00	0.00	0.00	0.00	0.00
Mo	0.01	0.01	0.01	0.01	0.01	0.01	0.01	0.01	0.01	0.01	0.01	0.01
Ta	0.00	0.00	0.00	0.00	0.00	0.00	0.00	0.00	0.00	0.00	0.00	0.00
Th	0.00	0.00	0.00	0.00	0.00	0.00	0.00	0.00	0.00	0.00	0.00	0.00
U	0.00	0.00	0.00	0.00	0.00	0.00	0.00	0.00	0.00	0.00	0.00	0.00
Total	*1.09*	*1.02*	*1.00*	*1.02*	*1.27*	*1.02*	*1.04*	*1.15*	*1.02*	*1.00*	*1.02*	*1.01*
S	1.91	1.98	2.00	1.98	1.73	1.98	1.96	1.85	1.98	2.00	1.98	1.99
Total	*1.91*	*1.98*	*2.00*	*1.98*	*1.73*	*1.98*	*1.96*	*1.85*	*1.98*	*2.00*	*1.98*	*1.99*
Sum	3.00	3.00	3.00	3.00	3.00	3.00	3.00	3.00	3.00	3.00	3.00	3.00

Table 3: EPMA analysis of uranium minerals. Totals commonly fell short of 100% due to the highly porous and inter-grown nature of U-bearing phases.

Analysis No.	EI15.1	EI15.2	EI15.7	EI15.8	EI15.10	EI3.3	EI3.4	EI3.5	EI3.8	EI3.9	EI3.10	EI7.2	EI7.3	EI7.4	EI7.5	EI7.6	EI7.8	EI7.9	EI7.10
CaO (wt%)	3.16	3.44	3.96	5.02	6.82	3.25	1.92	3.97	2.94	4.11	4.88	3.27	0.71	1.35	2.45	1.82	0.13	0.15	0.02
Y_2O_3 (wt%)	0.04	0.00	0.02	0.06	0.07	0.50	0.28	0.38	0.34	0.33	0.45	0.35	0.51	0.48	0.44	0.39	0.27	0.81	0.53
La_2O_3 (wt%)	0.07	0.00	0.04	0.06	0.06	0.13	0.08	0.01	0.08	0.08	0.00	0.12	0.05	0.06	0.08	0.03	0.04	0.12	0.14
Ce_2O^3 (wt%)	0.18	0.22	0.17	0.24	0.20	0.29	0.23	0.24	0.24	0.18	0.26	0.41	0.26	0.38	0.35	0.29	0.19	0.23	0.27
Nd_2O_3 (wt%)	0.09	0.05	0.01	0.01	0.13	0.07	0.12	0.17	0.17	0.20	0.10	0.24	0.06	0.22	0.14	0.24	0.00	0.11	0.00
Pr_2O_3 (wt%)	0.00	0.00	0.00	0.00	0.03	0.00	0.00	0.00	0.00	0.00	0.06	0.00	0.00	0.00	0.00	0.04	0.00	0.00	0.00
Sm_2O_3 (wt%)	0.00	0.03	0.01	0.00	0.03	0.11	0.03	0.00	0.05	0.01	0.00	0.04	0.05	0.00	0.10	0.00	0.00	0.00	0.00
Eu_2O_3 (wt%)	0.00	0.00	0.00	0.00	0.00	0.00	0.00	0.00	0.00	0.00	0.00	0.00	0.00	0.00	0.00	0.00	0.00	0.00	0.00
Gd_2O_3 (wt%)	0.08	0.00	0.00	0.00	0.00	0.15	0.09	0.11	0.15	0.13	0.09	0.08	0.01	0.08	0.00	0.00	0.00	0.06	0.06
Tb_2O_3 (wt%)	0.00	0.12	0.00	0.00	0.00	0.00	0.00	0.00	0.00	0.00	0.00	0.00	0.00	0.00	0.00	0.00	0.00	0.00	0.00
Dy_2O_3 (wt%)	0.00	0.01	0.00	0.00	0.00	0.04	0.19	0.09	0.00	0.00	0.17	0.00	0.01	0.03	0.00	0.02	0.06	0.05	0.11
Ho_2O_3 (wt%)	0.02	0.05	0.00	0.00	0.00	0.00	0.00	0.02	0.01	0.00	0.00	0.00	0.08	0.05	0.01	0.00	0.00	0.09	0.05
Er_2O_3 (wt%)	0.00	0.01	0.00	0.03	0.00	0.14	0.08	0.10	0.08	0.04	0.00	0.05	0.02	0.00	0.00	0.02	0.00	0.03	0.00
Lu_2O_3 (wt%)	0.02	0.00	0.00	0.00	0.00	0.03	0.01	0.00	0.00	0.31	0.49	0.06	0.03	0.00	0.01	0.01	0.05	0.03	0.03
Sc_2O_3 (wt%)	0.00	0.00	0.00	0.00	0.00	0.05	0.04	0.03	0.05	0.03	0.05	0.00	0.01	0.00	0.00	0.00	0.00	0.00	0.00
ZrO_2 (wt%)	0.00	0.03	0.00	0.00	0.00	0.00	0.00	0.00	0.00	0.05	0.01	0.00	0.00	0.05	0.00	0.00	0.01	0.03	0.00
HfO_2 (wt%)	0.13	0.03	0.21	0.07	0.01	0.05	0.31	0.08	0.28	0.03	0.02	0.10	0.02	0.11	0.10	0.11	0.20	0.00	0.07
PbO (wt%)	0.00	0.00	0.00	0.00	0.00	0.00	0.02	0.00	0.00	0.00	0.04	0.04	0.03	0.06	0.00	0.03	0.01	0.00	0.00
Nb_2O_5 (wt%)	0.00	0.00	0.03	0.00	0.00	0.03	0.02	0.00	0.00	0.00	0.00	0.00	0.06	0.02	0.01	0.02	0.01	0.00	0.01
K_2O (wt%)	0.30	0.32	0.44	0.32	0.34	0.29	0.36	0.29	0.27	0.24	0.43	0.31	0.27	0.22	0.25	0.24	0.28	0.21	0.15
ThO_2 (wt%)	0.05	0.00	0.00	0.00	0.00	0.01	0.00	0.00	0.00	0.00	0.01	0.00	0.00	0.11	0.02	0.04	0.02	0.00	0.00
UO_2 (wt%)	74.40	68.24	72.57	78.18	77.18	71.85	59.04	70.78	63.65	58.92	72.08	77.97	64.79	71.13	71.64	72.61	68.46	60.72	59.39
FeO (wt%)	0.09	0.76	0.01	1.17	2.95	2.91	0.34	0.60	4.63	7.26	2.83	2.14	2.72	4.39	1.19	5.07	2.51	7.39	4.94
TiO_2 (wt%)	0.02	0.05	0.09	0.08	0.06	0.05	0.09	0.24	0.18	0.16	0.21	1.41	1.32	6.30	1.35	2.53	0.17	0.18	0.16
MgO (wt%)	0.11	0.09	0.09	0.08	0.13	0.09	0.09	0.10	0.08	0.07	0.09	0.14	0.23	0.13	0.11	0.15	0.11	0.21	0.15
SiO_2 (wt%)	4.08	1.23	7.85	1.96	0.43	1.49	9.38	1.99	8.92	0.70	0.52	3.67	0.77	3.92	3.39	3.91	6.93	0.00	3.34
$Al2O_3$ (wt%)	3.66	0.65	6.19	0.55	0.05	0.13	5.89	0.15	0.17	0.11	0.07	2.68	0.62	2.94	2.29	2.77	5.64	0.16	0.26
P_2O_5 (wt%)	0.75	0.81	1.03	1.60	0.93	0.81	0.50	0.63	0.57	0.46	0.61	0.47	0.71	0.70	0.41	0.64	0.12	0.29	0.27
F (wt%)	0.62	0.45	0.00	1.29	0.00	0.79	0.59	0.91	0.80	0.93	1.01	1.19	0.35	0.90	0.95	1.02	0.53	0.40	0.26
Total	**87.87**	**76.61**	**92.71**	**90.74**	**89.42**	**83.25**	**79.71**	**80.89**	**83.67**	**74.36**	**84.48**	**94.76**	**73.71**	**93.64**	**85.29**	**91.99**	**85.73**	**71.29**	**70.20**

Table 4: EPMA analysis of Ilmenite.

Analysis No.	EI36.1a	EI36.1	EI36.2	EI36.6	EI36.7	EI36.8	EI2.5	EI2.6	EI2.7	EI2.11	EI2.20	EI1.13	EI1.14	EI1.16	EI1.20	EI24.6
O (wt%)	34.47	34.08	34.08	34.82	34.36	34.23	34.72	34.93	36.06	35.35	34.77	34.68	34.35	34.30	33.68	38.75
Na (wt%)	0.04	0.06	0.17	0.07	0.09	0.07	0.12	0.14	0.01	0.13	0.05	0.05	0.05	0.07	0.05	0.02
Mg (wt%)	0.32	0.35	0.13	0.12	0.09	0.12	0.03	0.34	2.19	0.13	0.04	0.12	0.08	0.20	0.12	0.00
Al (wt%)	0.00	0.00	0.22	0.07	0.19	0.09	0.14	0.55	0.00	0.00	0.05	0.23	0.15	0.14	0.19	0.00
Si (wt%)	0.17	0.18	0.34	0.28	0.35	0.22	0.18	0.23	0.02	0.11	0.12	0.33	0.21	0.16	0.21	6.10
Si (wt%)	0.01	0.00	0.03	0.02	0.02	0.00	0.71	4.40	0.17	0.40	0.46	0.43	0.56	0.55	0.52	0.05
K (wt%)	0.00	0.00	0.02	0.02	0.02	0.01	0.04	0.03	0.02	0.01	0.01	0.01	0.01	0.03	0.00	0.04
Ca (wt%)	0.08	0.10	0.21	0.16	0.24	0.13	0.09	0.07	0.01	0.02	0.03	0.04	0.03	0.01	0.05	0.08
Ti (wt%)	36.87	37.22	38.99	39.21	40.93	37.88	39.84	36.34	27.60	39.85	38.62	43.27	40.65	40.63	40.41	46.02
V (wt%)	0.00	0.00	0.00	0.00	0.00	0.00	0.00	0.00	0.00	0.00	0.00	0.00	0.00	0.00	0.00	0.00
Cr (wt%)	0.07	0.06	0.02	0.02	0.05	0.03	0.03	0.04	0.00	0.03	0.04	0.06	0.05	0.02	0.04	0.01
Mn (wt%)	0.17	0.13	1.97	1.98	0.75	2.31	1.74	0.13	0.85	0.58	1.34	0.89	1.15	0.80	0.77	0.07
Fe (wt%)	21.25	19.87	13.45	15.50	12.98	16.01	13.65	11.72	35.92	17.79	17.06	8.44	12.06	12.72	11.48	2.01
Co (wt%)	0.00	0.00	0.05	0.04	0.00	0.00	0.01	0.00	0.00	0.00	0.00	0.01	0.01	0.02	0.01	0.00
Ni (wt%)	0.06	0.03	0.03	0.01	0.00	0.02	0.00	0.00	0.01	0.00	0.01	0.06	0.03	0.02	0.02	0.01
Zn (wt%)	0.09	0.17	0.26	0.19	0.27	0.18	0.02	0.02	0.02	0.04	0.00	0.17	0.12	0.07	0.12	0.01
Se (wt%)	0.00	0.00	0.00	0.02	0.00	0.00	0.06	0.00	0.00	0.00	0.06	0.02	0.01	0.06	0.00	0.02
Zr (wt%)	0.00	0.00	0.06	0.06	0.07	0.03	0.06	0.13	0.02	0.01	0.17	0.08	0.04	0.06	0.05	0.06
Nb (wt%)	0.06	0.00	0.08	0.14	0.05	0.11	0.00	0.03	0.03	0.00	0.05	0.11	0.00	0.06	0.10	0.04
Mo (wt%)	0.00	0.00	0.00	0.01	0.00	0.00	0.00	0.00	0.00	0.06	0.04	0.02	0.10	0.06	0.02	0.00
Ta (wt%)	0.00	0.00	0.00	0.00	0.00	0.00	0.03	0.00	0.01	0.06	0.07	0.03	0.00	0.02	0.04	0.00
Th (wt%)	0.01	0.04	0.03	0.05	0.00	0.03	0.01	0.00	0.03	0.00	0.00	0.25	0.10	0.08	0.14	0.02
U (wt%)	0.41	0.22	0.71	0.45	0.68	0.54	0.04	0.05	0.01	0.08	0.00	2.19	1.43	0.46	0.77	0.00
Total	**94.06**	**92.51**	**90.87**	**93.26**	**91.14**	**92.03**	**91.52**	**89.15**	**103.00**	**94.66**	**93.01**	**91.48**	**91.19**	**90.54**	**88.81**	**93.30**

Analysis No.	**EI24.7**	**EI34.1**	**EI34.2**	**EI34.5**	**EI34.6**	**EI34.8**	**EI34.10**	**EI16.5**	**EI16.13**	**EI12.1**	**EI12.8**	**EI8.10**	**EI8.21**	**EI8.24**	**EI12.16**	**EI12.17**
O (wt%)	38.49	34.72	34.41	33.76	32.51	33.34	34.14	34.34	35.32	35.55	36.93	33.91	33.91	34.97	34.94	33.97
Na (wt%)	0.02	0.05	0.02	0.04	0.03	0.01	0.08	0.18	0.21	0.23	0.21	0.05	0.41	0.19	0.10	0.07
Mg (wt%)	0.00	0.02	0.39	0.14	0.08	1.02	1.06	0.12	0.06	0.07	0.14	0.14	0.05	0.03	0.11	0.78
Al (wt%)	0.15	0.17	0.06	0.23	0.47	0.18	1.13	1.02	0.25	4.02	0.44	0.16	0.92	0.29	0.08	0.06
Si (wt%)	5.17	0.23	0.20	0.36	0.20	0.28	1.54	0.09	0.25	3.25	0.38	0.21	0.41	0.29	0.20	0.16
Si (wt%)	0.05	0.02	0.01	0.01	0.01	0.01	0.02	0.14	0.29	1.10	7.24	0.42	0.69	0.93	0.04	0.08
K (wt%)	0.08	0.03	0.01	0.01	0.01	0.01	0.06	0.06	0.03	0.10	0.15	0.02	0.09	0.04	0.02	0.01
Ca (wt%)	0.07	0.20	0.11	0.16	0.15	0.16	0.18	0.59	0.24	0.48	0.06	0.02	0.05	0.09	0.16	0.19
Ti (wt%)	47.76	44.95	39.39	38.53	40.19	40.34	36.65	46.26	42.69	37.17	34.97	38.17	37.88	47.29	40.87	39.73
V (wt%)	0.00	0.00	0.00	0.00	0.00	0.00	0.00	0.00	0.00	0.00	0.00	0.00	3.21	0.04	0.00	0.00
Cr (wt%)	0.00	0.06	0.02	0.04	0.03	0.09	0.04	0.05	0.04	0.03	0.05	0.04	0.09	0.04	0.06	0.03
Mn (wt%)	0.01	0.73	0.55	1.09	0.05	0.23	0.51	0.00	0.82	0.33	0.12	1.00	0.04	0.32	1.15	0.43
Fe (wt%)	0.96	8.36	16.52	15.20	11.19	11.47	13.27	2.35	11.77	3.61	11.41	15.63	9.27	3.11	14.49	14.15
Co (wt%)	0.00	0.00	0.00	0.00	0.00	0.00	0.01	0.00	0.02	0.00	0.04	0.02	0.04	0.00	0.00	0.01
Ni (wt%)	0.00	0.00	0.00	0.02	0.00	0.03	0.01	0.00	0.01	0.04	0.09	0.01	0.01	0.00	0.00	0.00
Zn (wt%)	0.02	0.01	0.04	0.03	0.00	0.04	0.03	0.03	0.03	0.07	0.01	0.03	0.09	0.03	0.00	0.06
Se (wt%)	0.03	0.02	0.03	0.01	0.03	0.01	0.03	0.03	0.00	0.06	0.01	0.04	0.00	0.04	0.07	0.02
Zr (wt%)	0.01	0.19	0.05	0.01	0.00	0.07	0.05	0.09	0.05	0.09	0.13	0.08	0.23	0.07	0.02	0.05
Nb (wt%)	0.04	0.01	0.01	0.00	0.02	0.00	0.03	0.50	0.04	0.00	0.06	0.11	0.10	0.02	0.08	0.05
Mo (wt%)	0.00	0.00	0.00	0.01	0.00	0.00	0.00	0.22	0.40	0.00	0.08	0.11	0.26	0.14	0.09	0.00
Ta (wt%)	0.00	0.00	0.01	0.00	0.01	0.00	0.00	0.05	0.00	0.00	0.02	0.02	0.00	0.00	0.03	0.00
Th (wt%)	0.08	0.12	0.08	0.10	0.00	0.14	0.01	0.03	0.05	0.06	0.23	0.03	0.05	0.06	0.09	0.20
U (wt%)	0.00	0.08	0.05	0.04	0.00	0.00	0.00	3.77	0.45	1.12	0.91	0.24	0.67	0.38	0.59	0.32
Total	**92.92**	**89.95**	**91.99**	**89.79**	**84.98**	**87.43**	**88.83**	**89.92**	**93.00**	**87.38**	**93.68**	**90.43**	**88.47**	**88.38**	**93.19**	**90.39**

Analysis No.	**EI28.5**	**EI31.1**	**EI31.2**	**EI31.3**	**EI31.4**	**EI31.5**	**EI17.2**	**EI17.3**	**EI17.4**
O (wt%)	33.46	35.11	35.41	35.15	34.58	33.74	34.35	38.19	35.52
Na (wt%)	0.15	0.08	0.04	0.14	0.10	0.07	0.09	0.02	0.05
Mg (wt%)	0.05	0.60	0.02	0.09	0.86	0.60	0.55	0.03	0.03
Al (wt%)	0.02	0.15	0.00	0.51	0.45	0.66	0.14	0.47	0.19
Si (wt%)	0.33	0.21	0.16	0.43	0.45	0.46	0.18	0.46	2.74
Si (wt%)	0.06	0.33	0.40	0.59	0.26	0.10	1.00	6.41	0.35
K (wt%)	0.03	0.02	0.01	0.03	0.02	0.04	0.01	0.05	0.07
Ca (wt%)	0.14	0.18	0.17	0.29	0.25	0.30	0.03	0.06	0.07
Ti (wt%)	39.42	42.09	40.82	43.10	41.64	39.50	40.33	35.20	37.59
V (wt%)	0.00	0.00	0.00	0.00	0.00	0.00	0.00	0.00	0.00
Cr (wt%)	0.02	0.04	0.03	0.03	0.11	0.06	0.04	0.03	0.03
Mn (wt%)	0.79	0.43	0.52	0.44	0.20	0.46	0.18	1.39	0.79
Fe (wt%)	13.85	11.77	15.78	8.07	10.09	11.57	12.45	14.67	13.90
Co (wt%)	0.00	0.03	0.03	0.05	0.07	0.06	0.01	0.01	0.00
Ni (wt%)	0.00	0.01	0.01	0.00	0.05	0.04	0.06	0.01	0.01
Zn (wt%)	0.04	0.05	0.04	0.06	0.06	0.06	0.00	0.03	0.01
Se (wt%)	0.00	0.03	0.00	0.03	0.02	0.01	0.09	0.06	0.02
Zr (wt%)	0.01	0.14	0.02	0.00	0.09	0.10	0.08	0.01	0.00
Nb (wt%)	0.16	0.02	0.06	0.05	0.05	0.03	0.01	0.00	0.10
Mo (wt%)	0.02	0.71	0.53	0.60	0.26	0.07	0.12	0.20	0.42
Ta (wt%)	0.00	0.06	0.00	0.06	0.00	0.00	0.05	0.00	0.03
Th (wt%)	0.13	0.00	0.01	0.12	0.00	0.06	0.20	0.14	0.08
U (wt%)	0.00	0.88	0.92	4.18	1.30	1.52	0.32	0.26	0.25
Total	**88.67**	**92.92**	**94.97**	**94.01**	**90.92**	**89.49**	**90.27**	**97.69**	**92.25**

Table 5: EPMA analysis of Rutile

Analysis No.	EI36.10	EI15.11	EI2.18	EI2.22	EI1.1	EI1.5	EI1.10	EI1.17	EI1.18	EI1.19	EI24.3	EI24.5	EI34.4	EI34.9	EI34.11	EI16.7
O (wt%)	40.19	39.89	39.86	39.65	39.89	39.83	35.66	38.65	39.75	36.79	38.57	38.15	38.79	34.79	38.12	34.91
Na (wt%)	0.03	0.00	0.00	0.01	0.02	0.00	0.04	0.01	0.05	0.01	0.00	0.04	0.03	0.04	0.03	0.17
Mg (wt%)	0.00	0.00	0.00	0.00	0.00	0.00	0.00	0.00	0.00	0.01	0.00	0.00	0.01	0.05	0.01	0.09
Al (wt%)	0.00	0.00	0.00	0.00	0.00	0.00	1.77	0.00	0.00	0.63	0.00	1.14	0.13	0.32	0.05	1.02
Si (wt%)	0.11	0.00	0.00	0.03	0.00	0.01	1.82	0.49	0.19	0.23	0.24	1.31	0.61	0.28	0.71	0.12
Si (wt%)	0.00	0.09	0.06	0.02	0.03	0.00	0.22	0.06	0.00	0.59	0.00	0.03	0.00	0.02	0.00	0.42
K (wt%)	0.01	0.01	0.00	0.00	0.01	0.01	0.01	0.02	0.01	0.02	0.03	0.03	0.04	0.03	0.03	0.05
Ca (wt%)	0.04	0.02	0.01	0.00	0.01	0.00	0.04	0.01	0.04	0.07	0.12	0.05	0.17	0.31	0.20	0.88
Ti (wt%)	59.36	58.82	59.21	58.15	59.30	59.17	46.80	54.73	58.81	51.26	56.82	52.82	56.49	49.56	54.41	46.82
V (wt%)	0.00	0.00	0.00	0.00	0.00	0.00	0.00	0.00	0.00	0.00	0.00	0.00	0.00	0.00	0.00	0.00
Cr (wt%)	0.00	0.05	0.03	0.02	0.01	0.03	0.00	0.02	0.00	0.03	0.01	0.01	0.00	0.02	0.00	0.04
Mn (wt%)	0.01	0.00	0.00	0.01	0.00	0.00	0.01	0.01	0.01	0.00	0.00	0.01	0.03	0.00	0.02	0.02
Fe (wt%)	0.23	0.76	0.22	1.42	0.42	0.11	0.73	1.20	0.22	0.79	0.25	0.36	0.07	1.45	0.26	1.54
Co (wt%)	0.00	0.04	0.00	0.01	0.00	0.02	0.01	0.00	0.01	0.00	0.02	0.00	0.01	0.00	0.00	0.02
Ni (wt%)	0.00	0.00	0.00	0.02	0.02	0.00	0.00	0.01	0.01	0.01	0.00	0.01	0.03	0.00	0.00	0.01
Zn (wt%)	0.00	0.00	0.00	0.00	0.02	0.04	0.02	0.00	0.01	0.00	0.02	0.00	0.00	0.01	0.00	0.01
Se (wt%)	0.02	0.05	0.00	0.00	0.04	0.00	0.01	0.06	0.03	0.03	0.02	0.03	0.00	0.03	0.00	0.04
Zr (wt%)	0.55	0.03	0.19	0.00	0.05	0.08	0.09	0.04	0.21	0.22	0.16	0.21	0.16	0.53	1.75	0.11
Nb (wt%)	0.15	0.15	0.14	0.22	0.01	0.38	0.13	1.99	0.04	0.09	0.22	0.04	0.06	0.08	0.15	0.19
Mo (wt%)	0.04	0.00	0.00	0.01	0.01	0.00	0.07	0.00	0.00	0.00	0.00	0.00	0.00	0.00	0.00	1.69
Ta (wt%)	0.01	0.10	0.00	0.01	0.01	0.04	0.04	0.11	0.00	0.00	0.03	0.00	0.00	0.03	0.00	0.05
Th (wt%)	0.00	0.03	0.00	0.00	0.01	0.01	0.00	0.03	0.00	0.07	0.03	0.02	0.10	0.09	0.10	0.09
U (wt%)	0.00	0.10	0.04	0.11	0.00	0.05	0.39	0.00	0.00	4.44	0.00	0.00	0.00	0.06	0.02	1.91
Total	**100.75**	**100.14**	**99.76**	**99.68**	**99.83**	**99.79**	**87.84**	**97.45**	**99.40**	**95.30**	**96.54**	**94.28**	**96.72**	**87.68**	**95.86**	**90.21**

Analysis No.	**EI16.9**	**EI16.10**	**EI6.1**	**EI6.3**	**EI6.4**	**EI6.6**	**EI5.3**	**EI5.7**	**EI5.9**	**EI5.10**	**EI12.13**	**EI8.20**	**EI8.23**	**EI12.18**	**EI12.19**	**EI6.11**
O (wt%)	39.81	49.05	39.41	43.41	34.56	35.86	39.95	39.76	40.07	39.48	41.02	39.17	39.32	39.84	35.25	39.75
Na (wt%)	0.02	0.02	0.01	0.01	0.06	0.07	0.00	0.00	0.00	0.00	0.00	0.02	0.07	0.01	0.11	0.00
Mg (wt%)	0.00	0.01	0.00	0.00	0.02	0.01	0.00	0.00	0.00	0.00	0.00	0.00	0.00	0.00	0.06	0.00
Al (wt%)	0.00	0.04	0.00	0.00	0.01	0.60	0.00	0.00	0.00	0.00	0.00	0.00	3.51	0.00	0.99	0.00
Si (wt%)	0.21	32.81	0.26	7.39	0.21	0.59	0.03	0.01	0.01	0.06	0.01	0.33	3.85	0.08	0.35	0.08
Si (wt%)	0.00	0.08	0.00	0.01	0.22	0.12	0.05	0.02	0.05	0.15	2.96	0.01	0.34	0.00	0.15	0.00
K (wt%)	0.07	0.04	0.00	0.01	0.01	0.02	0.00	0.00	0.00	0.01	0.01	0.01	0.03	0.01	0.04	0.00
Ca (wt%)	0.03	0.08	0.01	0.01	0.06	0.13	0.02	0.01	0.00	0.01	0.02	0.13	0.13	0.01	0.29	0.01
Ti (wt%)	58.98	16.96	57.36	52.02	50.24	51.07	59.26	59.26	59.16	58.14	54.94	57.71	46.07	58.97	48.90	59.02
V (wt%)	0.00	0.00	0.00	0.00	0.00	0.00	0.00	0.00	0.00	0.00	0.00	0.00	0.00	0.00	0.00	0.00
Cr (wt%)	0.01	0.00	0.00	0.00	0.03	0.00	0.00	0.00	0.00	0.01	0.00	0.00	0.01	0.00	0.02	0.02
Mn (wt%)	0.00	0.02	0.02	0.00	0.02	0.11	0.00	0.00	0.00	0.01	0.02	0.01	0.02	0.00	0.02	0.00
Fe (wt%)	0.03	0.22	0.76	0.21	0.66	0.35	0.35	0.21	0.66	0.61	2.97	0.26	1.13	0.49	1.66	0.12
Co (wt%)	0.00	0.01	0.00	0.00	0.00	0.02	0.00	0.00	0.01	0.01	0.00	0.00	0.01	0.00	0.00	0.00
Ni (wt%)	0.00	0.02	0.00	0.00	0.00	0.02	0.01	0.00	0.01	0.00	0.02	0.00	0.00	0.00	0.01	0.00
Zn (wt%)	0.00	0.08	0.00	0.00	0.02	0.01	0.01	0.00	0.00	0.03	0.00	0.00	0.03	0.01	0.01	0.00
Se (wt%)	0.06	0.00	0.00	0.03	0.00	0.02	0.04	0.00	0.02	0.01	0.05	0.01	0.03	0.00	0.05	0.04
Zr (wt%)	0.05	0.07	0.00	0.00	0.07	0.06	0.09	0.03	0.03	0.04	0.03	0.07	0.04	0.06	0.05	0.12
Nb (wt%)	0.16	0.01	0.95	0.21	0.23	0.06	0.11	0.04	0.42	0.23	0.03	0.04	0.08	0.21	0.29	0.24
Mo (wt%)	0.00	0.02	0.00	0.03	0.02	0.08	0.00	0.00	0.00	0.00	0.00	0.00	0.09	0.00	0.03	0.00
Ta (wt%)	0.02	0.00	0.15	0.04	0.01	0.00	0.05	0.00	0.00	0.02	0.00	0.00	0.00	0.00	0.05	0.00
Th (wt%)	0.05	0.02	0.00	0.00	0.09	0.00	0.05	0.00	0.03	0.04	0.02	0.03	0.00	0.01	0.09	0.00
U (wt%)	0.00	0.10	0.00	0.07	0.10	0.07	0.02	0.10	0.00	0.08	0.00	0.00	0.11	0.11	0.18	0.00
Total	**99.51**	**99.65**	**98.94**	**103.44**	**86.64**	**89.29**	**100.02**	**99.45**	**100.46**	**98.93**	**102.10**	**97.81**	**94.87**	**99.81**	**88.59**	**99.42**

Analysis No.	**EI6.12**	**EI6.13**	**EI6.14**	**EI6.15**	**EI6.16**	**EI6.17**	**EI5.11**	**EI26.1**	**EI26.2**	**EI26.3**	**EI26.4**	**EI26.5**	**EI26.6**	**EI31.7**
O (wt%)	39.57	39.20	35.25	39.62	39.62	38.36	39.68	39.94	39.04	39.67	39.08	38.14	39.23	39.42
Na (wt%)	0.00	0.01	0.78	0.00	0.03	0.01	0.05	0.02	0.00	0.01	0.01	0.09	0.00	0.01
Mg (wt%)	0.00	0.05	0.04	0.00	0.00	0.00	0.00	0.00	0.00	0.00	0.00	0.01	0.00	0.00
Al (wt%)	0.00	0.12	0.82	0.00	0.00	0.00	0.00	0.00	0.00	0.00	0.00	0.00	0.00	0.05
Si (wt%)	0.25	0.68	0.17	0.30	0.08	0.85	0.20	0.08	0.19	0.05	0.06	0.09	0.00	0.42
Si (wt%)	0.01	0.01	0.39	0.02	0.00	0.04	0.06	0.01	0.00	0.00	0.00	0.15	0.00	0.01
K (wt%)	0.01	0.12	0.07	0.01	0.01	0.01	0.01	0.01	0.00	0.00	0.01	0.05	0.01	0.04
Ca (wt%)	0.01	0.05	0.08	0.02	0.03	0.06	0.06	0.01	0.05	0.00	0.00	0.06	0.00	0.07
Ti (wt%)	57.85	56.67	48.33	58.63	58.76	55.52	58.35	59.09	56.36	58.96	57.53	55.33	56.50	57.65
V (wt%)	0.00	0.00	0.00	0.00	0.00	0.00	0.00	0.00	0.00	0.00	0.00	0.00	0.00	0.00
Cr (wt%)	0.02	0.00	0.03	0.00	0.00	0.01	0.01	0.00	0.00	0.01	0.11	0.03	0.00	0.00
Mn (wt%)	0.05	0.02	0.00	0.00	0.00	0.00	0.00	0.00	0.00	0.00	0.00	0.03	0.01	0.02
Fe (wt%)	1.01	0.17	2.00	0.11	0.20	0.30	0.42	0.44	2.26	0.41	0.52	0.41	1.15	0.30
Co (wt%)	0.00	0.00	0.04	0.01	0.02	0.00	0.01	0.00	0.00	0.00	0.00	0.00	0.01	0.00
Ni (wt%)	0.00	0.00	0.00	0.00	0.01	0.02	0.00	0.01	0.02	0.00	0.00	0.01	0.01	0.02
Zn (wt%)	0.02	0.00	0.02	0.00	0.00	0.02	0.02	0.00	0.00	0.02	0.03	0.03	0.04	0.00
Se (wt%)	0.00	0.02	0.02	0.00	0.06	0.00	0.04	0.01	0.03	0.02	0.02	0.03	0.00	0.00
Zr (wt%)	0.05	0.06	0.25	0.00	0.16	0.04	0.00	0.01	0.23	0.00	0.00	1.16	0.00	0.35
Nb (wt%)	0.26	0.53	0.06	0.08	0.08	0.11	0.38	0.26	0.14	0.06	0.65	0.09	2.14	0.10
Mo (wt%)	0.00	0.00	0.05	0.00	0.00	0.00	0.00	0.00	0.00	0.00	0.00	0.00	0.04	0.00
Ta (wt%)	0.07	0.10	0.00	0.00	0.12	0.07	0.02	0.04	0.02	0.00	0.00	0.02	0.10	0.04
Th (wt%)	0.00	0.00	0.16	0.00	0.03	0.05	0.01	0.08	0.00	0.00	0.00	0.08	0.09	0.00
U (wt%)	0.02	0.02	1.91	0.01	0.00	0.00	0.00	0.18	0.06	0.00	0.00	1.29	0.00	0.16
Total	**99.21**	**97.83**	**90.48**	**98.81**	**99.21**	**95.49**	**99.31**	**100.18**	**98.41**	**99.21**	**98.02**	**97.09**	**99.34**	**98.65**

Table 6: EPMA analysis of Fe-oxide minerals

Analysis No.	EI36.3	EI36.9	EI36.9	EI8.19	EI28.2	EI28.3	EI28.4
O (wt%)	25.63	25.69	25.69	26.66	26.61	34.36	24.95
Na (wt%)	0.17	0.20	0.20	0.37	0.12	0.32	0.36
Mg (wt%)	0.27	0.43	0.43	0.17	0.18	0.27	0.27
Al (wt%)	1.28	1.22	1.22	1.14	0.05	0.64	0.27
Si (wt%)	2.40	1.95	1.95	1.67	1.00	15.66	0.95
S (wt%)	0.09	0.04	0.04	2.19	0.05	0.25	0.06
K (wt%)	0.00	0.01	0.01	0.06	0.01	0.05	0.08
Ca (wt%)	0.55	0.47	0.47	0.06	0.09	0.17	0.09
Ti (wt%)	0.15	0.52	0.52	0.00	0.04	0.17	0.25
V (wt%)	0.14	0.12	0.12	0.03	0.32	0.50	0.42
Cr (wt%)	0.00	0.00	0.00	0.00	0.01	0.01	0.01
Mn (wt%)	0.09	0.02	0.02	0.02	0.04	0.04	0.04
Fe (wt%)	48.52	49.28	49.28	49.02	57.93	34.49	52.83
Co (wt%)	0.00	0.00	0.00	0.06	0.00	0.01	0.00
Ni (wt%)	0.00	0.04	0.04	0.09	0.05	0.03	0.02
Zn (wt%)	0.25	0.24	0.24	0.02	0.02	0.07	0.02
Se (wt%)	0.10	0.09	0.09	0.01	0.03	0.05	0.05
Zr (wt%)	0.00	0.00	0.00	0.00	0.00	0.00	0.00
Nb (wt%)	0.00	0.00	0.00	0.00	0.00	0.00	0.02
Mo (wt%)	0.06	0.16	0.16	0.25	0.00	0.01	0.04
Ta (wt%)	0.00	0.07	0.07	0.00	0.00	0.00	0.00
Th (wt%)	0.05	0.05	0.05	0.04	0.00	0.02	0.00
U (wt%)	0.07	0.00	0.00	0.34	0.00	0.00	0.00
Total	**79.81**	**80.61**	**80.61**	**82.18**	**86.57**	**87.13**	**80.73**

APPENDIX E: LA-ICP-MS ELEMENT MAP OF SAMPLE EI8

LA-ICP-MS element maps for pyrite cement which displayed oscillatory zonation on optical and BSE images (Figure 5b). Weak gradational chemical zonation is observable throughout the element maps. Element enrichment is primarily associated at grain margins with only Mn and Tl displaying extensive enrichment within the core of the grains. The lack of distinct element zonation is perhaps a factor of the resolution of the element mapping relative to the fine oscillatory zonation observed.

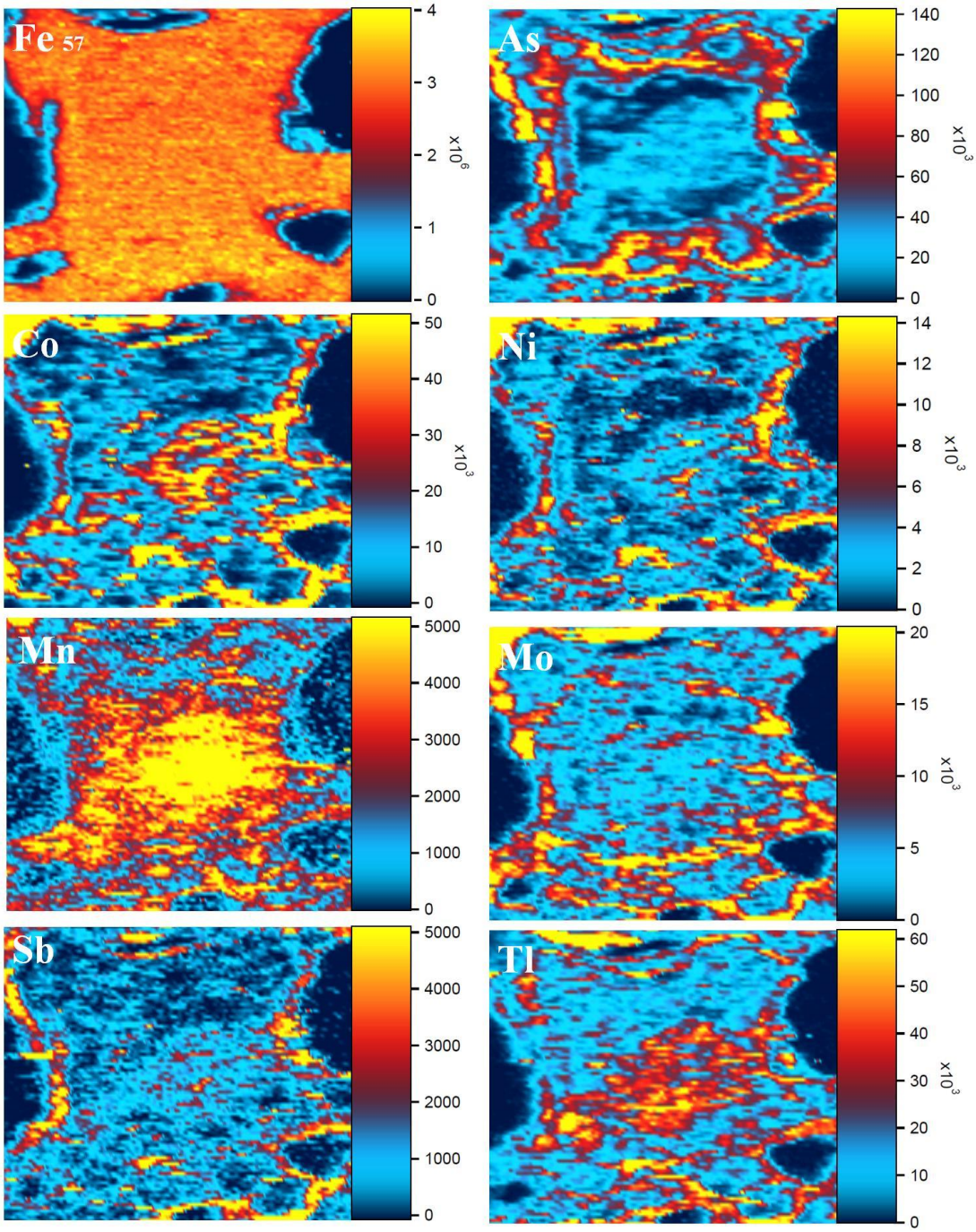

APPENDIX F: Sulphur isotope analysis dataset

The high-spatial resolution of the *in-situ* sulphur isotope microanalysis allowed each analyses to analysed in the context of pyrite morphology and inter-granular spatial distribution. The irregularity of both inter- and intra- granular data from these analyses means that, without in-depth sulphur isotope mapping to delineate chemical patterns, limited interpretations can be made of the spatial data. The full sulphur isotope data set in the context of pyrite morphology is displayed in Table 1, and displayed in Figure 1.

Table 1: Sulphur isotopic compositions

	Sample No.	Pyrite Morphology	Analysis No.	δ^{33}_{CDT}	Uncertainty	2s	δ^{34}_{CDT}	Uncertainty	2s
Pepegoona	EI3	Framboidal	1	-21.85	0.11	0.21	-42.17	0.14	0.27
		Framboidal	2	-22.16	0.14	0.27	-43.02	0.16	0.32
		Framboidal	3	-22.59	0.14	0.28	-43.87	0.16	0.32
		Framboidal	4	-21.80	0.09	0.19	-42.29	0.11	0.21
		Framboidal	5	-22.35	0.09	0.19	-43.53	0.11	0.22
		Framboidal	8	-21.96	0.10	0.20	-42.43	0.12	0.24
		Framboidal	9	-22.17	0.14	0.29	-42.93	0.14	0.28
		Framboidal	10	-22.02	0.11	0.21	-42.60	0.11	0.22
		Framboidal	11	-21.83	0.12	0.24	-42.23	0.16	0.31
		Framboidal	12	-22.72	0.11	0.21	-43.71	0.11	0.22
			mean (n=10)	**-22.14**	**0.11**	**0.23**	**-42.88**	**0.13**	**0.26**
	EI7	Framboidal	1	-16.32	0.17	0.34	-31.75	0.19	0.38
		Framboidal	2	-17.47	0.14	0.28	-34.11	0.13	0.26
		Framboidal	3	-15.35	0.17	0.34	-29.87	0.21	0.41
		Framboidal	4	-16.30	0.12	0.23	-31.79	0.08	0.16
			mean (n=4)	**-16.36**	**0.15**	**0.30**	**-31.88**	**0.15**	**0.30**
Pepegoona West	EI11	Cement (assoc with native Se)	1	15.65	0.16	0.31	30.72	0.13	0.25
		Cement (assoc with native Se)	2	14.90	0.11	0.22	28.85	0.14	0.28
		Cement (assoc	3	15.21	0.11	0.22	29.24	0.15	0.29

Sample No.	Pyrite Morphology	Analysis No.	δ^{33}_{CDT}	Uncertainty	2s	δ^{34}_{CDT}	Uncertainty	2s
	with native Se)							
	Cement (assoc with native Se)	4	16.55	0.08	0.16	32.10	0.07	0.15
	Cement (assoc with native Se)	5	16.05	0.12	0.25	31.01	0.14	0.28
	Cement (assoc with native Se)	6	15.43	0.10	0.20	30.15	0.13	0.26
	Cement (assoc with native Se)	7	16.67	0.12	0.23	32.40	0.12	0.24
	Cement (assoc with native Se)	8	15.66	0.09	0.18	30.33	0.14	0.27
	Cement (assoc with native Se)	9	14.31	0.09	0.19	28.07	0.13	0.26
	Cement (assoc with native Se)	10	14.52	0.12	0.25	28.35	0.12	0.24
	Cement (assoc with native Se)	11	14.51	0.14	0.27	28.39	0.20	0.40
	Cement (assoc with native Se)	12	15.48	0.12	0.25	30.17	0.14	0.27
	Cement (assoc with native Se)	13	13.46	0.10	0.20	25.97	0.07	0.14
	Cement (assoc with native Se)	14	13.46	0.15	0.30	26.15	0.18	0.35
	Cement (assoc with native Se)	15	15.69	0.10	0.19	30.50	0.13	0.27
	Cement (assoc with native Se)	16	14.93	0.18	0.36	28.87	0.27	0.53
		mean (n=16)	**15.16**	**0.12**	**0.24**	**29.45**	**0.14**	**0.28**
	Porous Cement	1	3.27	0.15	0.29	5.73	0.18	0.36
	Porous Cement	2	1.04	0.13	0.25	1.76	0.14	0.27
	Porous Cement	3	-0.28	0.13	0.26	-1.32	0.14	0.28
EI12	Porous Cement	4	12.54	0.08	0.17	24.12	0.12	0.24
	Porous Cement	5	12.55	0.14	0.28	24.31	0.14	0.28
	Anhedral	6	13.86	0.13	0.25	27.01	0.14	0.27
	Anhedral	7	13.55	0.13	0.26	26.41	0.14	0.28

	Sample No.	Pyrite Morphology	Analysis No.	δ^{33}_{CDT}	Uncertainty	2s	δ^{34}_{CDT}	Uncertainty	2s
		Porous Cement	8	12.92	0.13	0.27	25.02	0.13	0.27
		Porous Cement	9	11.80	0.12	0.24	22.92	0.13	0.27
		Porous Cement	10	10.87	0.12	0.23	21.02	0.12	0.24
		Porous Cement	11	13.59	0.12	0.23	26.27	0.13	0.26
		Porous Cement	12	9.99	0.10	0.21	19.02	0.12	0.23
		Porous Cement	13	7.50	0.10	0.19	14.46	0.13	0.27
		Porous Cement	14	8.13	0.14	0.28	15.57	0.13	0.26
		Porous Cement	15	-1.91	0.11	0.23	-3.77	0.13	0.25
		Porous Cement	16	-1.40	0.15	0.30	-3.40	0.13	0.27
		Porous Cement	17	-7.17	0.12	0.24	-14.00	0.12	0.23
		Porous Cement	18	-7.54	0.13	0.27	-14.95	0.14	0.29
		Porous Cement	19	-0.40	0.13	0.26	-0.99	0.12	0.23
		Porous Cement	20	-0.11	0.13	0.27	-0.57	0.13	0.27
			mean (n=20)	**5.64**	**0.12**	**0.25**	**10.73**	**0.13**	**0.27**
Pannikan	**EI15**	Cement	1	**13.22**	0.10	0.20	**25.61**	0.11	0.23
		Cement	2	**-5.10**	0.09	0.18	**-10.23**	0.13	0.26
		Cement	3	**-20.72**	0.10	0.19	**-40.18**	0.11	0.23
		Cement	4	**-0.93**	0.10	0.20	**-2.17**	0.18	0.36
		Cement	5	**-15.65**	0.11	0.21	**-30.50**	0.14	0.28
		Anhedral	6	**-9.85**	0.17	0.34	**-19.90**	0.34	0.68
		Anhedral	7	**0.59**	0.14	0.28	**0.74**	0.19	0.38
		Anhedral	8	**13.66**	0.12	0.24	**26.28**	0.14	0.28
		Cement	9	**0.96**	0.10	0.20	**1.29**	0.13	0.26
		Framboidal	12	**-8.86**	0.21	0.43	**-18.33**	0.08	0.15
			mean (n=10)	**-3.27**	**0.12**	**0.25**	**-6.74**	**0.16**	**0.31**
	EI19	Massive Cement	1	**-2.35**	0.10	0.20	**-4.59**	0.11	0.22
		Massive Cement	2	**-2.49**	0.07	0.15	**-5.07**	0.11	0.22
		Massive Cement	3	**-1.68**	0.10	0.20	**-3.68**	0.11	0.21
		Massive Cement	4	**-2.22**	0.12	0.24	**-4.46**	0.12	0.24
		Massive Cement	5	**-2.15**	0.07	0.14	**-4.18**	0.12	0.23
		Massive Cement	6	**-2.06**	0.09	0.17	**-4.07**	0.10	0.20
		Massive Cement	7	**-2.36**	0.08	0.16	**-4.61**	0.12	0.25
		Massive Cement	8	**-2.20**	0.07	0.14	**-4.56**	0.11	0.22
		Massive Cement	9	**-2.31**	0.10	0.20	**-4.63**	0.11	0.21
		Massive Cement	10	**-2.31**	0.09	0.18	**-4.63**	0.11	0.22

Sample No.	Pyrite Morphology	Analysis No.	δ^{33}_{CDT}	Uncertainty	2s	δ^{34}_{CDT}	Uncertainty	2s
	Massive Cement	11	**-2.43**	0.11	0.23	**-4.90**	0.11	0.22
	Massive Cement	12	**-2.44**	0.09	0.18	**-4.70**	0.10	0.21
	Massive Cement	13	**-2.25**	0.08	0.17	**-4.78**	0.10	0.21
	Massive Cement	14	**-2.44**	0.10	0.20	**-4.75**	0.11	0.22
		mean (n=14)	**-2.26**	**0.09**	**0.18**	**-4.54**	**0.11**	**0.22**
EI20	Cubic	1	**5.09**	0.15	0.29	**9.40**	0.21	0.42
	Overgrowth	2	**0.55**	0.10	0.20	**0.53**	0.11	0.22
	Cubic	3	**10.26**	0.15	0.30	**19.98**	0.06	0.11
	Overgrowth	4	**5.61**	0.16	0.32	**10.85**	0.27	0.53
	Cubic	5	**11.29**	0.08	0.16	**21.68**	0.06	0.13
	Cubic	6	**11.46**	0.12	0.23	**22.18**	0.15	0.31
	Euhedral	7	**6.86**	0.10	0.20	**13.02**	0.05	0.11
	Euhedral	8	**10.65**	0.08	0.16	**20.55**	0.12	0.24
	Overgrowth	9	**10.57**	0.13	0.26	**20.21**	0.14	0.27
	Overgrowth	10	**10.82**	0.11	0.22	**20.66**	0.15	0.30
	Euhedral	11	**11.31**	0.09	0.18	**21.91**	0.10	0.21
	Euhedral	12	**5.59**	0.08	0.16	**11.01**	0.09	0.17
	Overgrowth	14	**11.39**	0.09	0.17	**21.92**	0.11	0.23
	Cubic	15	**-0.34**	0.11	0.21	**-0.90**	0.06	0.13
	Overgrowth	17	**3.51**	0.09	0.18	**6.37**	0.07	0.14
	Overgrowth	18	**7.31**	0.10	0.20	**13.94**	0.14	0.28
	Overgrowth	19	**6.50**	0.10	0.19	**12.39**	0.13	0.26
	Overgrowth	20	**-5.82**	0.22	0.44	**-11.62**	0.20	0.41
	Overgrowth	21	**8.20**	0.10	0.19	**16.18**	0.12	0.23
	Overgrowth	22	**6.96**	0.07	0.15	**13.29**	0.09	0.17
		mean (n=20)	**6.89**	**0.11**	**0.22**	**13.18**	**0.12**	**0.24**

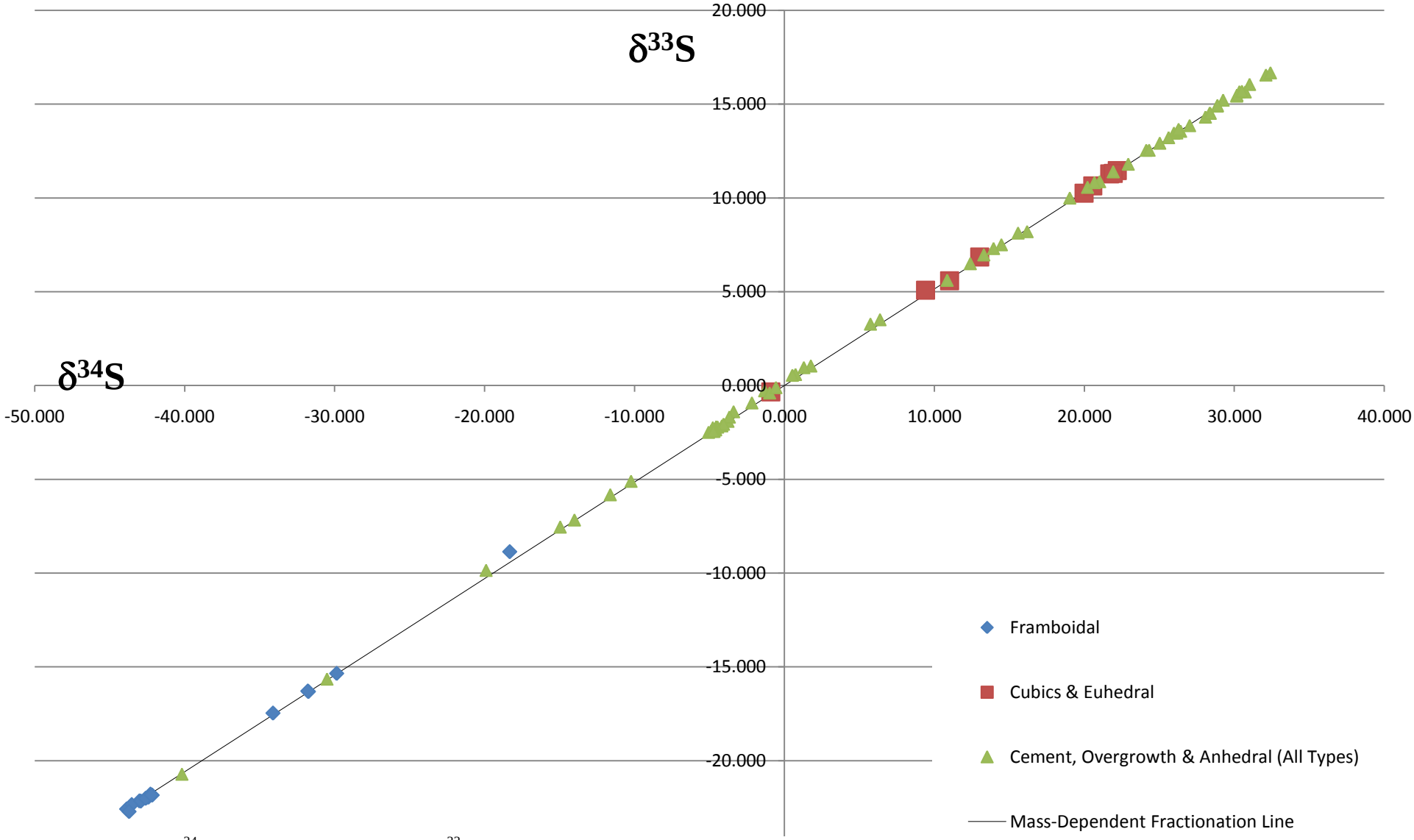

Figure 1: Recorded $\delta^{34}S$ values are displayed against $\delta^{33}S$ values for each individual analysis. Analyses are displayed by pyrite morphology and display the strong association of framboidal pyrite with discrete highly depleted $\delta^{34}S$ populations. These depletions are indicative of a biogenic sulphur source. Other pyrite morphologies display varied enrichments of $\delta^{34}S$, which point to progressive $\delta^{34}S$ enrichment of hydrothermal fluids during protracted pyrite crystallisation in an open system.